

Attachment of engineered silver nanoparticles to collector
surfaces - A batch sorption study using model and
environmental surfaces.

By

Priya Mary Abraham (MSc.)

From Kerala, India

Accepted Dissertation thesis for the partial fulfilment of the requirements for a
Doctor of Natural Sciences
Fachbereich 7: Natur- und Umweltwissenschaften
Universität Koblenz-Landau

Thesis Examiners:

Prof. Dr. Gabriele E. Schaumann (Universität Koblenz-Landau, Germany)

Dr. David Britt (Utah State University, USA)

Date of the oral examination: 16-01-2015

Declaration

I hereby declare that I autonomously conducted the work shown in this Ph.D thesis entitled “Attachment of engineered silver nanoparticles in the environment - A batch sorption study using model and environmental surfaces”. All used assistances and involved contributors are clearly declared.

This thesis has never been submitted elsewhere for an exam, as thesis or for evaluation in a similar context; to any department of this university or any scientific institution.

Place, Date

Signature

The following part of this thesis is published.

Chapter 2 has been published:

P.M.Abraham, S. Barnikol, T. Baumann, M. Kuehn, N.Ivleva, G.E. Schaumann. Interaction of silver nanoparticles with environmental and model surfaces. Environmental Science Technology 2013, 47 (10): 5083-5091.

My own contribution towards the chapter 2 is 75%.

My own contribution towards chapter 3 is 80 %

My own contribution towards chapter 4 is 90 %

Acknowledgements

First and foremost, I would like to extend my sincere gratitude to my supervisor Prof. Dr. Gabriele E. Schaumann for giving me an opportunity to work in this exciting field of science. Her encouragement, inspiration, passion for science, excellent guidance and constant support throughout my PhD, helped me to make this thesis possible.

This study was supported by the German ministry for Education, Science, and Culture of Rheinland-Pfalz (MBWWK) and the German Research foundation (DFG, Research unit INTERNANO). I express my gratitude to them.

I am highly thankful to current and previous colleagues in the department of environmental and soil chemistry for their help and scientific discussions. Special thanks to Ms. Sandra Barnikol, Dr. Doerte Diehl, Dr. Jette Schwarz, Dr. Yamuna Kunhi Mouvenchery, Dr. George Matreveli, Dr. Jiri Kucerik and Mrs. Angelika Holderle for all the help and support.

I would also like to thank my family for all the mental support they gave me during this time. My husband Rev. Levin Koshy Mallasseril was constantly there to support me in all the situations. Needless to say, this would not have been possible for me without my family.

To the Almighty Lord,
Who strengthened me to fulfill my venture.

Table of contents

1. Introduction -----	11
1.1. Introduction and background -----	12
1.2. Engineered silver nanoparticles: Properties, Production and Applications-----	13
1.3. Fate of silver nanoparticles in the environment-----	15
1.4. Objectives and working hypothesis-----	19
1.5. Structure of the thesis-----	20
2. Sorption of silver nanoparticles to environmental and model surfaces----	22
2.1. Abstract-----	23
2.2. Introduction-----	23
2.3. Materials and Methods-----	27
2.4. Results and Discussion-----	30
2.5. Supporting information-----	44
3. Effect of humic acid on the sorption of bare and citrate coated silver nanoparticles to environmental and model surfaces-----	58
3.1. Abstract-----	59
3.2. Introduction-----	60
3.3. Materials and Methods-----	62
3.4. Result and Discussion-----	66
3.5. Conclusion-----	82

3.6. Supporting Information-----	84
4. Chemical force microscopy –A promising tool to analyze nanoparticle surface modifications-----	98
4.1. Abstract-----	99
4.2. Introduction-----	99
4.3. Materials and methods-----	103
4.4. Results and Discussion-----	108
4.5. Conclusion-----	121
5. General conclusions and outlook-----	123
5.1. Observations and conclusions-----	124
5.2. Open questions for future research-----	125
6. References-----	127
7. Annex I-----	138

Abstract

A fundamental understanding of attachment of engineered nanoparticles to environmental surfaces is essential for the prediction of nanoparticle fate and transport in the environment. The present work investigates the attachment of non-coated silver nanoparticles and citrate coated silver nanoparticles to different model surfaces and environmental surfaces in the presence and absence of humic acid. Batch sorption experiments were used for this investigation. The objective of this thesis was to investigate how silver nanoparticles interact with surfaces having different chemical functional groups. The effect of presence of HA, on the particle-surface interactions was also investigated.

In the absence of humic acid, nanoparticle-surface interactions or attachment was influenced by the chemical nature of the interacting surfaces. On the other hand, in the presence of humic acid, nanoparticle-surface attachment was influenced by the specific surface area of the sorbent surfaces. The sorption of non-coated silver nanoparticles and citrate coated nanoparticles to all the surfaces was nonlinear and best described by Langmuir isotherm, indicating monolayer sorption of nanoparticles on to the surfaces. This can be explained as due to the blocking effect generated by the particle-particle repulsion. In the presence of humic acid, sorption of nanoparticles to the surfaces was linear. When the humic acid was present in the interacting medium, both the nanoparticles and surfaces were getting coated with humic acid and this masks the chemical functionalities of the surfaces. This leads to the change in particle-surface interactions, in the presence of humic acid. For the silver nanoparticle sorption from an unstable suspension, the sorption isotherms did not follow any classical sorption models, suggesting interplay between aggregation and sorption.

Citrate coated silver nanoparticles and humic acid coated silver nanoparticles showed a depression in sorption compared to the sorption of non-coated silver nanoparticles. In the

case of citrate coated silver nanoparticles the decrease in sorption can be explained by the more negative zeta potential of citrate coated nanoparticles compared to non-coated ones. For humic acid coated nanoparticles the sorption depression can be due to the steric hindrance caused by the free humic acid molecules which may coat the sorbent surface or due to the competition for sorption sites between the nanoparticle and free humic acid molecules present in the suspension. Thus nanoparticle surface chemistry is an important factor that determines the attachment of nanoparticles towards surfaces and it makes the characterization of nanoparticle surface an essential step in the study of their fate in the environment.

Another aim of this study was to introduce the potential of chemical force microscopy for nanoparticle surface characterization. With the use of this technique, it was possible to distinguish between bare silver nanoparticles, citrate coated silver nanoparticles, and humic acid coated silver nanoparticles. This was possible by measuring the adhesion forces between the nanoparticles and five different AFM probes having different chemical functionalization.

Zusammenfassung

Ein grundlegendes Verständnis der Anlagerung von künstlich hergestellten Nanopartikeln ist für die Prognose des Schicksals und Transports von Nanopartikeln in der Umwelt unerlässlich. In dieser Arbeit wurde die Anlagerung von unbedeckten und mit Citrat bedeckten Silbernanopartikeln an unterschiedliche Modell- und Umweltoberflächen in An- und Abwesenheit der Huminsäure untersucht. Für diese Untersuchungen wurden Sorptionsexperimente durchgeführt. Das Ziel dieser Arbeit ist es zu untersuchen, wie die Silbernanopartikel mit Oberflächen wechselwirken, die verschiedene chemische funktionelle Gruppen besitzen. Dabei wurde ebenfalls der Effekt der Huminsäure auf die Wechselwirkungen zwischen Partikel und Oberfläche untersucht.

Die Wechselwirkungen zwischen Nanopartikel und Oberfläche sind in Abwesenheit der Huminsäure wahrscheinlich durch die chemische Natur der wechselwirkenden Oberflächen beeinflusst. In Anwesenheit der Huminsäure wurde diese chemische Sensitivität gegen Anlagerung von Nanopartikeln nicht beobachtet und die Sorption war durch die spezifische Oberfläche von Sorbentien beeinflusst. Die Sorptionsisothermen wurden für die Sorption von Silbernanopartikeln an allen Oberflächen in Abwesenheit der Huminsäure durch Langmuir-Modell beschrieben. Das deutete auf Monoschicht-Sorption der Nanopartikel an Oberflächen hin. Das kann durch den bei der Partikel-Partikel-Abstoßung generierten blockierenden Effekt erklärt werden. In Anwesenheit der Huminsäure zeigten alle Sorptionsisothermen ein lineares Verhalten. Wenn die Huminsäure im Wechselwirkungsmedium vorhanden war, waren die Nanopartikel und Oberflächen mit Huminsäure bedeckt. Dadurch wird die chemische Funktionalität von Oberflächen maskiert. Das führt zu den Unterschieden zwischen Partikel-Oberfläche-Wechselwirkungen in An- und Abwesenheit der Huminsäure.

Die mit Citrat und Huminsäure bedeckten Silbernanopartikel zeigten eine Abnahme der Sorption an Oberflächen im Vergleich zu unbedeckten Silbernanopartikeln. Im Falle der mit Citrat bedeckten Silbernanopartikel kann die Abnahme der Sorption durch elektrostatische Kräfte erklärt werden, da diese Partikel ein mehr negatives Zetapotential zeigten. Die Sorptionsabnahme für die mit Huminsäure bedeckten Nanopartikel ist offensichtlich eine Folge der sterischen Behinderung, da es auf Grund der Sorption der Huminsäure an Oberflächen zur Konkurrenz zwischen Nanopartikeln und Huminsäuremolekülen für die Sorptionsplätze kommt. Durch die chemischen Eigenschaften der Nanopartikeloberfläche wird die Effizienz der Anlagerung an Oberflächen beeinflusst. Deswegen ist die Charakterisierung der Nanopartikeloberfläche ein wichtiger Schritt bei der Untersuchung des Schicksals von Nanopartikeln in der Umwelt.

Ein anderes Ziel dieser Arbeit ist es das Potential der chemischen Kraftmikroskopie für die Charakterisierung von Nanopartikeloberflächen mit chemischer Sensitivität zu zeigen. Durch die Anwendung dieser Methode war es möglich zwischen unbedeckten, mit Citrat und Huminsäure bedeckten Silbernanopartikeln zu unterscheiden. Das wurde durch die Messung der Adhäsionskräfte zwischen Nanopartikeln und fünf verschiedenen Atomkraftmikroskope-Spitzen mit unterschiedlichen chemischen Funktionalisierungen ermöglicht.

Chapter-1

Introduction

1.1 General Introduction and Background

Nanoscience and nanotechnology involve the synthesis, assembly, manipulation and application of engineered nanoparticles (Nagarajan 2008). Engineered nanoparticles (ENP) may be defined as any intentionally produced particles, that have a dimension from 1 to 100 nm, and having characteristic properties that differ from its bulk form (Auffan et al. 2009; Vert et al. 2012). Engineered nanoparticles are the fundamental building blocks for various nanotechnology applications (Nagarajan 2008) because of their (1) small size, which corresponds to large surface-to-volume ratio, (2) tailorable physical and chemical properties, which relate to size, shape, composition and coating, (3) unique target binding properties and (4) specific emissive, absorptive and light scattering properties (Rosi et al. 2005). Wide ranges of synthesis techniques have been developed to produce nanoparticles with desirable properties. These synthetic methods can be generalized into two main categories, top-down synthesis involving milling, photolithography, and electron beam lithography, and bottom-up synthesis involving chemical reactions, nucleation and growth processes, and physical and chemical vapor deposition methods (Pandey et al. 2011; Iqbal et al. 2012). Depending on chemical composition, nanoparticles can be carbon based materials like fullerenes and carbon nanotubes (Rao et al. 1996); metals like silver, gold, and iron; metal oxides like titanium dioxide, zinc oxide, and iron oxide; quantum dots like cadmium sulfide and cadmium selenide and polymer based materials like polystyrene and polyethyleneimine (Ju-Nam et al. 2008; Moreno-Vega et al. 2012), among which metallic nanoparticles are of particular interest because of their amenability of synthesis, ease of functionalization and ease of detection (Bönnemann et al. 2001).

The rapid development and expansion of nanotechnology make nanoindustry, one of the fastest growing industries in the history of mankind (LuxResearch 2008). Currently nanoparticles have significant impact on almost all industries and all areas of society.

Although the promise and potentials of nanotechnology to improve our quality of life seems unlimited and bright, its development will expose engineered nanoparticles to different environmental compartments (Gottschalk et al. 2013), where their possible impacts remain unknown. Hence the study of environmental implications of ENP, including fate, transport and toxicity is a major concern. The aggregation behavior and the surface properties of ENP are important factors that control their mobility and transport in aquatic and terrestrial environmental systems, which determine their attachment and interaction with environmental collector surfaces like biofilm, algae, plants, fungi, humic substances and soil sediments (Navarro et al. 2008). Interaction of ENP with natural organic matter is also an important point to consider since it alters the aggregation behavior and surface properties of ENP. There was always a gap in knowledge concerning the fate, transport and transformations of ENP in different environmental compartments, since there are a number of parameters and factors to be considered. Hence there is a critical need for pilot studies addressing fate and transport of ENP in the environment. In the same way, development of techniques for the detailed surface characterization of nanoparticles also needs a significant attention with regard to nanoparticle fate studies.

1.2 Engineered silver nanoparticles: Properties, production, and applications

Silver is a naturally occurring precious metal and has been used in a wide variety of applications like medicine, utensils, food containers, jewellery, coins, cloths, and building materials even from ancient civilizations. As the understanding of the material increased, its applications became far more sophisticated and today this metal is widely used in catalysis and electronic applications as well (Jiang et al. 2005; Takei et al. 2013).

Numerous methods have been developed for the synthesis of silver nanoparticles ($n\text{Ag}$) with different sizes, shapes, zeta potential, and surface coating. Some of the methods are:

(1) solution-phase synthesis technique using silver salt and any reducing agent to produce electrostatically stabilized silver nanoparticles (Mulfinger et al. 2007), (2) chemical reduction in the presence of capping agents to produce sterically stabilized nanoparticles (Song et al. 2009), (3) high temperature reduction in porous solid matrices (Wang et al. 2002), (4) vapor-phase deposition of silver onto a solid support (Zhao et al. 2002), (5) laser ablation of a metal target into a liquid suspension (Mafune et al. 2000), (6) photo reduction of Ag ions (Huang et al. 1996), and (7) electrolysis of an Ag salt solution (Zhu et al. 2000).

Miniaturization of silver into nano-dimensions makes it a candidate in applications that involve light because of its unique surface plasmon properties. Silver nanoparticles ($n\text{Ag}$) exhibit the highest efficiency of plasmon excitation among the other metal nanoparticles (Mulvaney 1996). Surface plasmons are collective electron oscillations in metal nanoparticle which can be excited by light (Klar et al. 1998). In metal nanoparticles, surface plasmons show a pronounced optical resonance in the visible or UV part of the spectrum and the resonance frequency of these oscillations are determined by the dielectric properties of the metal, the surrounding medium and the size and shape of the particle (Klar et al. 1998; Rycenga et al. 2011). Optical excitation of surface plasmons in silver nanoparticles is known to be the most efficient mechanism by which light interacts with matter (Evanoff et al. 2005). In addition silver is the only material whose plasmon resonance can be tuned to any wavelength in the visible spectrum (Evanoff et al. 2005; Rycenga et al. 2011). These superior performance of silver nanoparticles with respect to plasmonic properties make them a candidate in applications like biosensing, surface enhanced Raman scattering, and plasmon circuitry (Katrín et al. 2002; Ren et al. 2005; Xia et al. 2005; Jung et al. 2013). Moreover the optical properties makes $n\text{Ag}$ an easily characterizable nanomaterial and thus $n\text{Ag}$ is a suitable material for research topics as well.

Silver nanoparticles are also well known for their antibacterial (Sotiriou et al. 2010) fungicidal (Niazi et al. 2011), and antiviral (Lara et al. 2010) properties. Because of the antimicrobial properties, *n*Ag has been highly commercialized and it is found in a wide category of commercial products available in the market like food packaging materials, storage materials, water purificants, cloths, room sprays, detergents, washing machines, paints, lotions and soaps, surgical instruments, implantable devices, hygiene products, and bone cement (Benn et al. 2008; Kumar et al. 2008; Nadworny et al. 2008; Geranio et al. 2009; Nowack et al. 2011; Quadros et al. 2011; Walser et al. 2011). More and more products containing silver are getting added in to the market with advancements in its research and development.

1.3 Fate of Silver nanoparticles in the environment

The widespread application of *n*Ag in our daily life inevitably increases its exposure to environmental systems and living organisms. Increased release of such a powerful antimicrobial material into the environment will affect the bacterial colonies in natural system, thereby affecting nature's balance. There is also growing evidence that *n*Ag is highly toxic to mammalian cells (Wen et al. 2007), stem cells (Braydich-Stolle et al. 2005), brain cells (Grosse et al. 2013), and liver cells (Hussain et al. 2005) of higher order organisms. However it is still not clear, if nanoparticles themselves have some toxic effects or it's just because of the Ag ions released from the nanoparticles (Carlson et al. 2008; Bondarenko et al. 2013).

As the nanoparticles reach the environment, they can undergo transformations or aggregation which will determine their toxicity, fate, and transport (Levard et al. 2012). Hence to understand the mechanism behind the toxicity of nanoparticles, it is important to thoroughly analyze the physico-chemical properties of nanoparticles under relevant conditions.

1.3.1 Factors influencing fate and transport of *n*Ag

The fate and transport of *n*Ag in the environment is governed by a number of variables, such as particle size, surface charge, surface coatings and the surrounding environmental conditions including electrolyte composition, ionic strength, pH and presence of natural organic matter (NOM).

In the environmental compartments silver nanoparticles can get transformed by oxidation, dissolution, sulfidation, chlorination and regeneration (Yu et al. 2012). *n*Ag surface can be transformed to Ag₂O in high relative humidity conditions (oxidation), Ag⁺ ions can be released from *n*Ag surface depending on pH, temperature, ionic strength, and presence of dissolved oxygen (dissolution), nanosized Ag₂S can be formed by the reaction of *n*Ag or Ag⁺ with sulphur rich substances (sulfidation), AgCl can be formed in the presence of chloride ions (chlorination), and organic matter can reduce the silver ions released from *n*Ag, to small nanoparticles under natural sunlight (regeneration).

Once released into the environment, *n*Ag could undergo different pathways of transport. If the nanoparticles remain as individual particles in suspension and stay stable, they can be transported long distances. On the other hand, under favorable conditions resulting in particle-particle or particle-surface interactions, they are less likely to travel long distances (Yu et al. 2012). Particle-particle interactions and particle-surface interactions thus play a key role in controlling the aggregation, deposition and transport of *n*Ag (Petosa et al. 2010). These interactions have traditionally been described by Derjaguin-Landau-Verwey-Overbeek (DLVO) theory of colloidal stability, considering van der Waals and electrical double layer interactions. However, non DLVO interactions such as steric, magnetic and hydration forces also play an important role and thus to be considered (Petosa et al. 2010). Particle-particle or particle-surface interactions are termed favorable in the absence of repulsive interaction

energies, whereas these interactions are unfavorable when repulsive colloidal interactions predominates (Tufenkji et al. 2004). Colloid deposition or attachment under saturated conditions is commonly described in the literature by colloid filtration theory (Yao et al. 1971). This theory assumes that the colloids are irreversibly retained in the primary minimum of DLVO interaction energy profile as shown in figure 1 (Torkzaban et al. 2007). The huge energy barriers in this case will result in a firm attachment of nanoparticles on the surfaces. In contrast, for unfavorable conditions, where there is a prevailing repulsive electrostatic interaction between the particles and surfaces, the deposition or attachment will be occurring in secondary energy minimum (Redman et al. 2004). Thus, under unfavorable conditions, colloids can still get attached to the solid surfaces because of the presence of secondary minima at interaction distances greater than the location of energy barrier. In this case the attachment will be reversible and weak (Torkzaban et al. 2007).

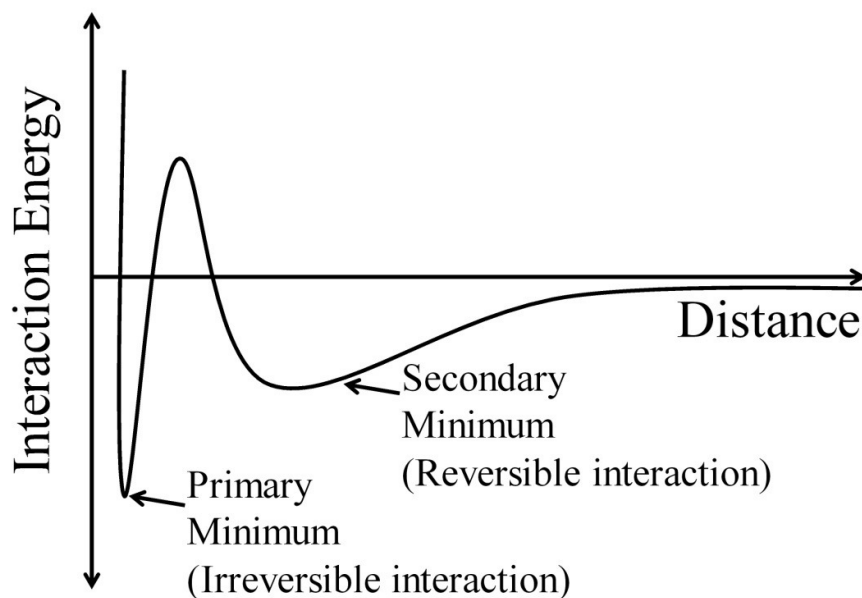


Figure 1: DLVO interaction energy profile showing primary and secondary minimum.

The attachment of particles in secondary minimum is sensitive to hydrodynamic shear and solution chemistry or the depth of the secondary minimum (Torkzaban et al. 2007).

Hydrodynamic shear forces may result in detachment of particles. As the ionic strength of the solution increases the depth of secondary minimum also increases (Torkzaban et al. 2007). Also, it has been shown in studies that the depth of secondary minimum increases with colloid size as a result of an enhancement in attractive van der Waals interactions. Kinetic studies of particle deposition and aggregation show its dependence on the height of energy barrier (Elimelech et al. 1995; Petosa et al. 2010). Particles having the ability to overcome the energy barrier will undergo aggregation, or surface deposition in a deep primary energy minimum. Smaller particles exhibit much lower energy barriers than micrometer sized particles (Elimelech et al. 1995). Thus nanoparticle size and aggregation behavior is also an important factor governing the deposition and transport.

Particle-surface interactions are also influenced by physical/chemical heterogeneities present on the collector surfaces such as surface roughness and geochemical heterogeneities (Petosa et al. 2010). There is evidence in the literature which shows that the inherent physical and chemical/charge heterogeneities of collector surfaces and nanoparticle surfaces can control particle deposition behavior under unfavorable conditions (Song et al. 1994; Tufenkji et al. 2004; Tufenkji et al. 2005). NOM, existing in environmental systems, is also a key factor influencing the fate of *nAg* by controlling the surface speciation and charge of nanoparticles (Navarro et al. 2008). NOM may attach to the nanoparticle surface physically or by electrostatic, hydrogen bonding and hydrophobic interactions (Xu et al. 2013). NOM can modify the collector surface properties by coating and it also has the capacity to influence the aggregation state of *nAg*, by steric or electrostatic stabilization. Thus, the presence of NOM in the environmental compartment also controls the nanoparticles fate and transport by influencing the particle size and surface chemistry.

1.4 Objectives and working hypothesis

Even though, the nanoparticle attachment and transport behavior in controlling fate and transport of silver nanoparticles is a widely discussed topic in recent years, there are still some detailed investigations needed to understand different factors controlling nanoparticle attachment. Fate and transport of nanoparticles in the environment will be determined by how the nanoparticles interact with themselves or with collector surfaces to get deposited or carried away.

Thus the objective of this study was to investigate the attachment of silver nanoparticles to different model and environmental surfaces and the factors involved in this attachment process. The nanoparticle-surface attachment was studied using batch sorption experiments and classical sorption models are used to describe the attachment under quasi equilibrium conditions. A set of five model surfaces with different functional groups, covering a wide range of intermolecular interactions were selected for the sorption experiment to study the dependence of collector surface chemistry on nanoparticle fate. Environmental surfaces having comparable chemical composition as model surfaces were also experimented the same way to see the consistency of the method in environmental point of view. Another objective of this study was to investigate the influence of organic matter present in the environment on nanoparticle-surface interactions both qualitatively and quantitatively. Physico-chemical properties of nanoparticles like surface charge, surface coating, particle size, and stability were also varied in experiments to understand the influence of respective parameters in nanoparticle-surface attachment and deposition. These physico-chemical properties of nanoparticles were characterized extensively using different characterization techniques like dynamic light scattering (DLS), UV-vis spectroscopy, fluorescent spectroscopy, surface enhanced Raman spectroscopy, Total organic carbon (TOC) measurements, inductively

coupled plasma mass spectrometry (ICP-MS), scanning electron microscopy (SEM), energy dispersive X-ray scattering (EDX), transmission electron microscopy (TEM), and atomic force microscopy (AFM). The potential of chemical force microscopy (CFM) to characterize nanoparticle surfaces is also proposed in the thesis.

The hypotheses followed in the thesis are:

- i. Nanoparticle-surface interactions can be described by classical sorption isotherms considering nanoparticles as sorbate and surfaces as sorbents.
- ii. Nanoparticle-surface interactions will include both DLVO interactions and electrostatic interactions. Thus the sorption will be sensitive to the chemical nature of the surfaces and zeta potential of the suspensions.
- iii. In the case of unstable suspensions, aggregation will overbalance sorption, resulting in a negligible sorption compared to the sorption of stable suspensions.
- iv. Presence of NOM in the environment will result in the attachment of NOM to both the nanoparticle and the sorbent surface. Hence particle-surface interactions will be governed by NOM- NOM interactions.
- v. Nanoparticle coating and size will also influence the sorption quantity because of the change in van der Waals and electrostatic forces accompanying the particle-surface interactions

1.5 Structure of the thesis

The thesis has three main chapters. Chapter 2 entitled ‘Sorption of silver nanoparticles to environmental and model surfaces’ includes the experimental results of batch sorption study conducted for the sorption of bare silver nanoparticles to the model surfaces and environmental surfaces. Hypothesis 1, 2 and 3 were checked in this chapter. The detailed

characterization of silver nanoparticles using a set of techniques is also included in the chapter.

Chapter 3 entitled ‘Effect of humic acid on the sorption of bare and citrate coated silver nanoparticles to environmental and model surfaces’, includes the experimental result for the sorption of bare and citrate coated nanoparticles on to the surfaces in the presence of humic acid (HA). Hypothesis 4 and 5 are checked in detail in this chapter. Nanoparticle- HA interactions, HA- surface interactions particle-surface interactions are considered and contribution of each interaction toward the particle sorption is discussed.

Chapter 4 entitled ‘Chemical Force Microscopy – A promising tool to analyze nanoparticle surface modifications’ is a method development chapter. This chapter includes characterization of all the nanoparticle suspensions used in the sorption studies, with chemical force microscopy. Detailed characterization of nanoparticle surface is very important when considering their environmental fate. Chemical force microscopy is an AFM based method with which we get chemical characteristics on the sample surface in nanometer resolution. Chemically modified AFM probes are used in this technique and in this study 5 different types of chemical modifications are used. Standardization of AFM probes for chemical sensitivity is also elucidated in this chapter.

Finally the conclusions of this study and recommendations for future work are summarized in chapter 5.

Chapter-2

Sorption of silver nanoparticles to environmental and model surfaces

Priya Mary Abraham¹, Sandra Barnikol¹, Thomas Baumann², Melanie Kuehn², Natalia P.

Ivleva² and Gabriele E Schauman¹

¹University of Koblenz-Landau, Institute of Environmental Sciences, Dept. Environmental and Soil Chemistry, Landau, Germany

²Technische Universität München, Institute of Hydrochemistry, Munich, Germany

2.1 Abstract

The fate of engineered nanoparticles in environmental systems is controlled by changes in colloidal stability and their interaction with different environmental surfaces. Little is known about nanoparticle-surface interactions on the basis of sorption isotherms under quasi-equilibrium conditions, although sorption isotherms are a valuable means of studying sorbate-sorbent interactions. We tested the extent to which the sorption of engineered silver nanoparticles (*nAg*) from stable and unstable suspensions to model (sorbents with specific chemical functional groups) and environmental (plant leaves and sand) surfaces can be described by classical sorption isotherms. Atomic force microscopy (AFM) and scanning electron microscopy (SEM) qualitative and quantitative analyses were also used to assess the morphology and nanomechanical parameters of the covered surfaces. The sorption of *nAg* from stable suspensions was non-linear and best described by the Langmuir isotherm. Langmuir coefficients varied with sorbent surface chemistry. For *nAg* sorption from an unstable suspension, the sorption isotherms did not follow any classical sorption models, suggesting interplay between aggregation and sorption. The validity of the Langmuir isotherm suggests monolayer sorption, which can be explained by the blocking effect due to electrostatic repulsion of individual nanoparticles. In unstable suspensions, aggregates are instead formed in suspension, formed on the surface and then sorbed, or formed in both ways.

2.2 Introduction

Engineered inorganic nanoparticles (EINP) are vital candidates for diverse novel and potential applications through their unique antimicrobial, electronic, optical and structural strength enhancement properties (Lee et al. 2010). EINPs are intentionally produced particles with at least one dimensional limit of 1 to 100 nm and which display special properties that differ from bulk material with the same chemical composition (Auffan et al. 2009, Hochella

et al. 2008). Silver nanoparticles (*nAg*) display antimicrobial properties (Sotiriou et al. 2010), leading to their use in fabrics, paints, personal care products, water filters, and other products (Lee et al. 2003, Jain et al. 2005, Kumar et al. 2008). Estimated global production of *nAg* is 500 tons per year and environmental concentration of *nAg* in soil and in water were predicted as 0.02 µg/kg and 0.03 µg/L, respectively (Mueller et al. 2008). Hence there is a chance of *nAg* entering wastewater streams and other aquatic environmental systems (Lin et al. 2011). There are also studies highlighting the mobility of *nAg* via food chains (Zhao et al. 2010, García-Alonso et al. 2011). Thus, a significant amount of the *nAg* entering the environment is also expected to reach organisms. Despite potential adverse effects there is still a lack of knowledge and it remains imperative to improve our current understanding of their environmental risk, transport and fate (Wijnhoven et al. 2009).

In aquatic environments and aquatic-terrestrial transition zones, the fate of EINPs is mainly determined by the nature of particle itself, hydrodynamic conditions, and the interaction of these particles with environmental surfaces such as leaves, organisms, and natural colloids (Petosa et al. 2010, Hahn et al. 2003, Badawy et al. 2010). EINPs can be immobilized via attachment to sessile environmental surfaces or sedimentation following homo- and heteroaggregation (Nowack et al. 2007, Klaine et al. 2008). They can also undergo chemical transformations such as oxidation, reduction, partial dissolution, hydrolysis, and biological degradation (Petosa et al. 2010).

To date, interactions between EINPs and surfaces have been investigated mainly in the context of nanoparticle transport in porous media using column experiments (Zhang et al. 2010, Song et al. 2011, Tufenkji et al. 2003, Ko et al. 2000). Another approach involves investigating nanoparticle deposition kinetics using a quartz crystal microbalance (Chen et al. 2006, Fatisson et al. 2009, Furman et al. 2013). Column scale experiments give indirect access to information such as attachment efficiency, deposition kinetics, aggregation kinetics,

and the retention of nanoparticles (Petosa et al. 2010). In these studies, silica gel (bare and coated with humic acid), glass beads (hydrophobic and hydrophilic), sand, and soil were used as sorbents (Petosa et al. 2010). It is known from experiments using non-invasive imaging techniques, that any heterogeneity of the sample translates into a change of the apparent sorption or filtration parameters (Baumann et al. 2005). Thus, the parameters derived from those experiments are likely ambiguous.

Surface chemistry also plays a significant role in nanoparticle attachment (Park et al. 2008). However, very few systematic studies (Lin et al. 2011, Marciano et al. 2008, Shateri Khalil-Abad et al. 2009) focus on the dependence of EINPs on the chemistry of the collector surface. Further studies focus on the sorption of molecules (Tsai et al. 2011) and metal ions (Song et al. 2011) to nanoparticles, describing the sorption using a Langmuir isotherm. Kinetic studies are available on the dynamic aspects of nanoparticle deposition based, for example, on the random sequential adsorption (RSA) model (Johnson et al. 1995). However, studies on the adsorption of nanoparticles to surfaces under quasi-equilibrium conditions are less frequently referenced in literature (Wagener et al. 2012). In a study investigating the Langmuir sorption of CdSe/ZnS quantum dots to model substrate, Park et al. expressed the need of future studies to assess the universality of this phenomenon (Park et al. 2008).

Interaction forces governing nanoparticle deposition and aggregation have been described by the DLVO (Derjaguin, Landau, Verwey, and Overbeek) theory of colloidal stability (Petosa et al. 2010, Verwey et al. 1948). In the current DLVO and extended DLVO conception, only van der Waals interactions are considered and a further extension of interaction theory includes the Lifshitz theory to account for Lewis acid-base interactions (Hoek et al. 2006, van Oss et al. 1993). Based on these models we can assume that under comparable electrostatic situations and in stable suspensions, nanoparticle-surface interactions are controlled mainly by their ability to interact via each intermolecular interaction type. A new model for colloid

transport eliminates the empirical concept of the attachment efficiency by splitting the colloid population into with different physico-chemical characteristics and therefore different sticking efficiency (Landkamer et al. 2013). This model, while ad hoc applicable to heterogeneous environmental particles, could benefit from a mechanistic description of the interaction between colloids and surfaces as presented in this study.

The analog in the interaction between organic chemicals and surfaces are polyparameter linear free energy relationship (pp-LFER) or linear solvation energy relationship (LSER) models (Abraham et al. 1987), which describe the partitioning of neutral chemicals between two phases by considering the energy contributions of the most important intermolecular interactions (Goss et al. 2001, Tuelp et al. 2008). Although nanoparticle-surface interactions are also subject to additional influences like electrostatic repulsion, electrostatic attraction, or steric repulsion – which are not yet directly integrated into the LFER model (Cho et al. 2004) – we expect that attractive interactions between nanoparticles and surfaces beyond electrostatic interactions will follow comparable patterns to those expected for intermolecular interactions.

The objective of this study was to assess whether the interaction of nanoparticles with surfaces can be described by classical sorption models and to what extent it depends on and varies with suspension stability. For this we investigated the attachment of *n*Ag from stable and unstable suspensions to model surfaces undergoing well-defined chemical interactions (Tuelp et al. 2008)³⁹, and environmental surfaces (glass beads, silica gel, quartz sand, leaf discs) from stable suspensions. The presence of nanoparticles on the sorbent surface was detected directly using adhesion-force measurements from AFM analyses. This technique is proposed as a tool to quantify the effective surface accessible to nanoparticles.

2.3 Materials and Methods

2.3.1 Preparation of the *n*Ag suspension.

The *n*Ag powder was purchased from io-li-tec (Ionic Liquid Technologies, Germany). They were produced using plasma-chemical vapor deposition (CVD). According to the manufacturer, their primary particle size was 35 nm. An aqueous nanoparticle suspension was prepared by following a standard protocol for preparing nanoparticle suspensions from dry powder using an ultrasonic processor without a stabilizing agent (Taurozzi et al. 2010).

2.3.2 Characterisation of *n*Ag

To confirm the existence of surface plasmon resonance, we recorded the UV/Vis spectrum of the *n*Ag suspension using a SPECORD 50 device (Analytic Jena, Germany). To obtain *n*Ag size information, dynamic light scattering (DLS, Beckman Coulter-Delsa Nano C, USA), AFM (Veeco Nanoscope V) and Transmission electron microscope (TEM, LEO 922 OMEGA) were employed. Samples for size and morphology analyses by AFM, were prepared by dipping a leaf disc of *Ficus benjamina* (see below) into a nanoparticle suspension and drying it overnight in a laminar flow cabinet (Spectec, Germany). Tapping-mode AFM images were taken using phosphorus-doped silicon probes with a force constant of 5 N/m and 125-169 kHz tapping frequency. TEM samples were prepared on a carbon coated copper grid by spraying the suspension using ultrasonic atomizer. To determine the fraction of dissolved Ag ions in a suspension, it was filtered using centrifugal ultrafiltration tubes with a 10 nm cut-off, as the particle size distribution did not show any particles smaller than 10 nm. Ag in filtered and unfiltered suspensions was determined using inductively coupled plasma-quadrupole mass spectroscopy (ICP-MS, Thermo Fisher Scientific, Germany) after digesting the *n*Ag with 5% HNO₃ for 24 hours, agitated at room temperature (Taurozzi et al. 2010). Our preliminary experiments showed that yields from this standard method differ by less than

0.5% from those of digestion methods with higher HNO₃ concentrations and with microwave extraction. To get information about the surface chemistry of nanoparticles, energy-dispersive X-ray (EDX, Bruker AXS Microanalysis, Germany) and surface-enhanced Raman spectroscopy (Horiba LabRAM HR Raman microscope, Japan) were used. For EDX measurements, samples were prepared by air drying 10 µL of *n*Ag suspension on aluminum discs. For Raman spectroscopy, samples were prepared by air drying 10 µL of *n*Ag suspension on a silicon wafer. We used a He-Ne excitation laser ($\lambda_0 = 632.8$ nm, power = 35 mW) to acquire Raman spectra. Wavelength calibration was accomplished using the first-order phonon band of pure silicon at 520 cm⁻¹ and by zero-order correction of the grating used through a 50x magnification objective. Raman spectra of nanoparticles were recorded within an exposure time of 1 second, through a 100x magnification objective.

2.3.3 Model surfaces for sorption studies

Following an idea of Tuelp and co-workers (Tuelp et al. 2008), who used column packing materials for HPLC systems to determine the LSER parameters for complex pesticides and pharmaceuticals, we worked with the following materials from YMC Europe GmbH: YMC*Gel Pro C18 RS (octadecane (C18) functional group), YMC*Gel Phenyl (phenyl (Ph) functional group), YMC*Gel Cyano (cyano (CN) functional group), and YMC*Gel Diol (diol (OH) functional group). In addition to these HPLC packing materials, we used silica gel (Carl Roth GmbH) and glass beads as model surfaces, and as simple representants of environmental surfaces with surface chemistry similar to that of the model materials, we used sand and leaf discs (*Ficus benjamina*, family: Moraceae). Five leaf discs with a diameter of 4 mm were used for the experiment. The surface areas of all surfaces were measured using BET (Autosorb 1-MP (Quantachrom), USA) by nitrogen physisorption. The surface charge was measured using a particle charge detector (PCD 02 Mütek, Germany). Sorbents were dispersed in water and titrated using an anionic polyelectrolyte (polydiallyl-

dimethylammonium chloride, 0.1 mmol L⁻¹), in an automatic titrator and the isoelectric point was detected via a PCD. The surface charge (Q_c) was evaluated from the amount of polyelectrolyte used until zero charge as

$$Q_c = \frac{V \cdot c}{w} \quad (1)$$

where V is the volume of polyelectrolyte added (L), c is the charge of polyelectrolyte (mol_cL⁻¹), and w is the sample amount (Kg). Table S1 (SI) shows the characteristic parameters of the sorbents.

2.3.4 Sorption experiments

Sorption experiments were carried out by adding specific amounts of sorbents to n Ag suspensions and agitating them at a speed of 15 rpm for 14 hours in an overhead shaker at 19°C. This duration was identified as sufficient for equilibrium conditions in preliminary experiments. Eight different initial concentrations of n Ag, ranging from 0 to 40 µg/L, were prepared for the sorption experiments. Higher n Ag concentrations were avoided to prevent homoaggregation of the particles (González et al. 2002). After agitation, the surfaces were separated by centrifugation using a speed of 1985 g (3500 rpm) for 20 min, which is low enough to avoid sedimentation of nanoparticles in the size range relevant for this study (Lentfer et al. 2003).⁴³ Concentrations of Ag in suspensions before and after sorption were measured using ICP-MS. In order to test, to which extent sorption of dissolved silver ions may contribute to the overall sorption, additional sorption experiments were done with a Ag⁺ solution, obtained by centrifugal filtration of a n Ag suspension with a filter cut-off of 10 nm as we aimed to evaluate the behavior of the Ag⁺ ions in exactly the same environment as the n Ag particles and there was no indication of particles smaller than 10 nm in any of our measurements (see below). Glass beads and silica gel surfaces before and after sorption were analyzed using the peak force quantitative nanomechanical mapping (PFQNM) AFM-based

method with antimony-doped silicon probes. AFM analysis was carried out using the PFQNM method to measure the adhesion force between the tip and the sample and to see if there is a difference in forces before and after sorption. After the sorption experiments, glass-bead and silica-gel sorbents were dried overnight in a laminar flow cabinet. Samples for AFM measurements were then prepared by fixing the sorbents on a glass slide using double-sided adhesive tape. The probe was calibrated prior to measurement; the tip radius was 5.18 nm and the spring constant was 17.68 N/m. To compare the adhesion force between the tip and the surface, adhesion forces corresponding to 262144 data points were taken from each image. After the sorption experiments, the leaf discs were analyzed using SEM (FEI Quanta, USA) in low vacuum mode with back-scattered detector.

2.4 Results and Discussion

2.4.1 Characterization of *n*Ag

The suspension was characterized for size and morphology by TEM and AFM (Figure 2). The AFM image indicates the presence of nanoparticles with sizes ranging from 40 nm to 170 nm. The phase image confirms the presence of nanoparticles, characterizing *n*Ag with a higher phase value (20°) than leaf surface (0°), thus indicating that Ag nanoparticles are harder than leaf surface.

Figure 2 shows two representative TEM images of the *n*Ag particles. In total, 6 TEM images with 32 particles were analysed with the following result: Particle sizes range from 13 nm to 160 nm and consist of 50 % aggregates (> 50 nm), 38% spherical primary particles (size $\sim 40 \pm 10$ nm) as well as small spherical particles in the size of 13-20 nm (12%). This corresponds to estimated mass percentages of 9.9 %, 89.9 % and 0.2 % of primary particles, aggregates and small particles, respectively.

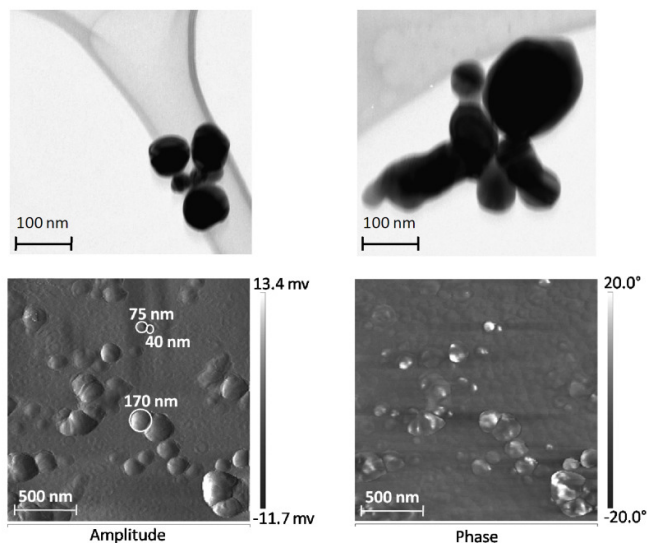


Figure 2: TEM image (above) of silver nanoparticles and AFM height, amplitude and phase images (below) of silver nanoparticles on terrestrial leaf surface. AFM scan area is 1.9 X 1.9 μm

UV/Vis absorption spectroscopy measurement displays a surface plasmon peak at a wavelength of 413 nm (SI Figure S1). For metal nanoparticles, the absorption maxima is controlled by the size, shape, and environment of particles and hence UV/Vis spectroscopy can be used as a complementary tool for structural and size characterization of nanoparticles in suspension (Noguez et al. 2007, Amendola et al. 2010). Previous studies report that a wavelength maximum (λ_{max}) around 420 nm corresponds to a particle size range of 35-60 nm (Mulfinger et al. 2007, Kamat et al. 1998). The measured peak maximum at 413 nm indicates that the nanoparticles in this study are on the smaller end of the reported sizes, which corresponds to the specification of the manufacturer, and our AFM and TEM measurements (Figure 2). The peak is rather broad (full width at half maximum, FWHM = 156.75 nm) indicating polydispersity and homoaggregation (Pillai et al. 2003, Taleb et al. 1997). There is a small shoulder peak at around 680 nm which can be attributed

to nonspherical particles, indicating that some nanoparticles in the suspension are ellipsoid (Rycenga et al. 2011). DLS studies indicated an average hydrodynamic diameter of 105.6 ± 5.2 nm (SI Figure S2), which also supports the presence of homoaggregates in the suspension. To test suspension stability for the planned sorption experiment duration, we conducted a time-dependent DLS measurement for 20 hours. During this time, the average diameter varied between 100 nm and 120 nm, with a non-significant but slightly decreasing trend (SI figure S3). The suspension was thus regarded as stable for the sorption experiment durations (14 hours). The zeta potential of the suspension was -44.31 mV and the pH was 6.4. In the stock *n*Ag suspension, 7.6% of the Ag passed through a filter with a cut-off of 10 nm (3000 Da) via centrifugal filtration and thus was regarded as dissolved Ag^+ as there was no indication of particles smaller than 10 nm in any of our measurements. Dissolution studies of bare *n*Ag with a primary particle size of 82 nm showed a 3% release of silver ions in natural surface water (Li et al. 2012), which is lower than the presented result. However, the silver-ion release rate depends on primary particle size (smaller size favors faster release), concentration, and environmental factors (Zhang et al. 2011). Size information from UV/Vis, DLS, and AFM thus correspond within the error ranges.

In order to analyze potential surface coatings of the silver nanoparticles SEM-EDX measurements were performed on nanoparticle aggregates (Figure S4) In addition to silver, the EDX analysis revealed a significant carbon signal (Figure S4B). Since the substrate also contributes to the EDX signal, further characterisation was performed with Raman microspectrometry. Raman spectra obtained from nanoparticles prepared on silicon wafers showed two small peaks at around 1350 cm^{-1} and 1580 cm^{-1} (SI Figure S5A) in addition to the characteristic peaks for bare silicon wafers (Figure S5B). These bands corresponds to D and G oscillations characteristic of carbon (Meyer et al. 2003) and are known to represent carbonaceous materials like graphite, soot, and carbon nanotubes (Zadezky et al. 2005, Wang

et al. 1990). Hence, the results indicate the presence of carbon on the nanoparticle surface, which may be a by-product of CVD synthesis (Yuan et al. 1995). No other capping agents were detected on silver nanoparticle surface.

2.4.2 Batch sorption study

Figure 3A shows an example of a sorption isotherm of $n\text{Ag}$, in this case for diol-functionalized surface. The shape of the sorption isotherms is qualitatively representative for all surfaces except leaf. Sorption isotherms for the $n\text{Ag}$ sorption to all other surfaces are shown in the supporting information (SI Figure S6). To rule out the effect and contribution of silver ions in the suspension on sorption behavior, we repeated the sorption experiment with an Ag^+ solution filtered from $n\text{Ag}$ suspension. Figure 3B shows an example of the difference in the sorption behavior of a $n\text{Ag}$ suspension and an Ag^+ solution, in this case for sorption onto diol-functionalized surface. For all other sorbents, see the supporting information (SI Figure S7). The results clearly show that the sorption of Ag^+ is negligible compared with $n\text{Ag}$ sorption.

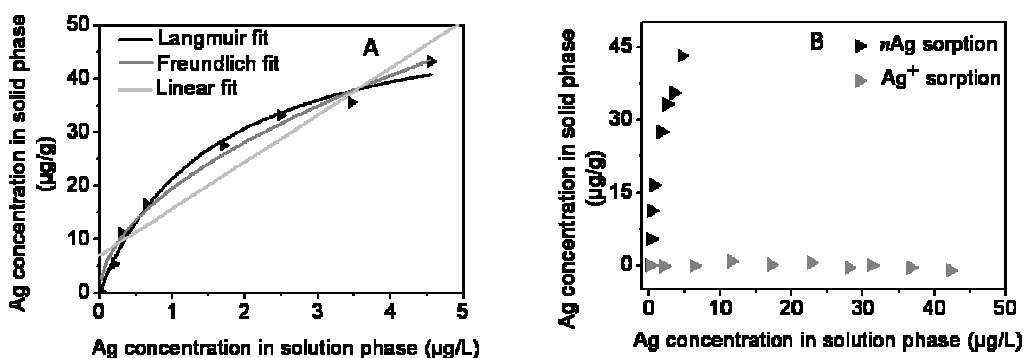


Figure 3. Representative sorption isotherm for sorption of silver nanoparticles to diol functionalized sorbent surface (A) and comparison for the sorption of silver ions and silver nanoparticles to diol functionalized sorbent surface (B).

To operationally describe sorption data and with the objective of deriving quantitative sorption parameters and testing their suitability, we tested to what extent classical sorption models can describe the attachment of $n\text{Ag}$ to the respective surfaces. We therefore tested linear sorption as well as Freundlich and Langmuir sorption isotherms:

Langmuir equation:
$$Q = \frac{K_L Q_{\max} c}{1 + K_L c} \quad (2)$$

Freundlich equation:
$$Q = K_F c^n \quad (3)$$

Q is the relative coverage, K_L is the Langmuir coefficient, K_F is the Freundlich coefficient, c is the concentration of sorbate in aqueous phase, Q_{\max} is the maximum amount adsorbed onto the sorbent, which for Langmuir adsorption would correspond to a monolayer, and n is the Freundlich exponent, which approaches 1 for linear sorption.

Figure 4 shows the sorption isotherm of $n\text{Ag}$ to the leaf discs. Here sorption is approximately linear. This can be explained by the hydrophobic wax film on leaf surface (Burton et al. 2006), which comprises aliphatic carbon chains. A comparable model is an octadecane-functionalized surface for which the Freundlich exponent displays a linear behavior. For leaf discs, linear sorption gives the slope as 3.26 L/g which is comparable to the slope for the near-linear sorption isotherm for $n\text{Ag}$ sorption to octadecane-functionalized sorbents (3.51 L/g). SEM image of leaf disc after $n\text{Ag}$ sorption show aggregates in some specific regions (SI Figure S8) that may be due to drying effect (Rabani et al. 2003), which would again underline the relatively low interactions between nanoparticles and surfaces, enabling their movement with the drying water front. Another explanation may be self assembly of nanoparticles driven by structural or constitutional features on certain areas of the leaf (Yin et al. 2001), or the formation of other colloids, e.g. silver chloride, on leaf surfaces since there can be chloride ions on the surface (Rogers et al. 2012).

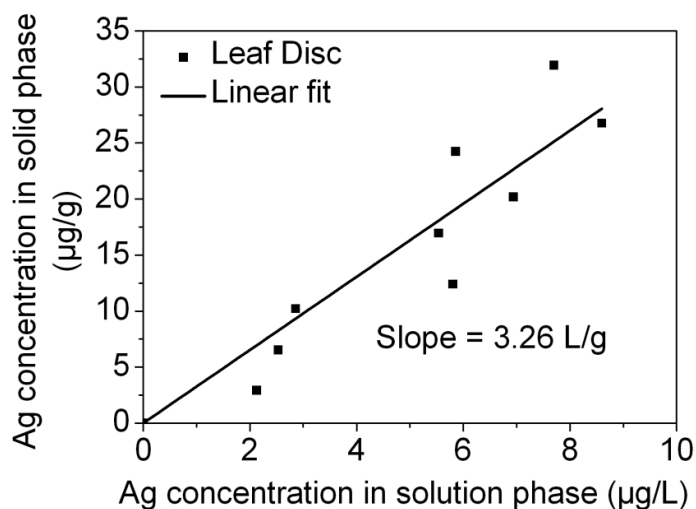


Figure 4. Sorption isotherm for the sorption of nAg on to leaf discs of the plant *Ficus Benjamina*.

2.4.3 Comparison of sorption models

The model assumptions in both isotherms differ significantly, reflecting different sorption mechanisms. The Freundlich isotherm was deduced under the assumption that sorption enthalpy is distributed heterogeneously on sorbent surfaces and increases with surface coverage. The Freundlich exponent can be described as an index of diversity of free energies associated with the sorption of nanoparticles to heterogeneous sorption sites on sorbents (Schwarzenbach et al. 2013). The Freundlich isotherm formally allows infinite coverage and thus unlimited sorption capacity (Adamson et al. 1997). In contrast, Langmuir adsorption is based on the assumption that adsorption takes place on fixed homogeneous adsorption sites of equal energy, forming a monolayer surface coverage (Xing et al. 1997). Both isotherms indicate that sorption becomes less favorable as sorbate concentrations increase, either due to the completion of a monolayer (Langmuir) or the occupation of sites with increasingly lower sorption enthalpy (Schwarzenbach et al. 2013).

Both sorption models describe experimental sorption with comparable fitting quality as demonstrated in Table S2 (SI) by the regression coefficient (R^2) and degree of freedom (Chi^2). Statistically, it is unclear which sorption model is more reasonable. Also, systematic deviations between the data and modeled isotherms were comparable for both models. Thus, as with many sorption isotherms of organic chemicals to NOM (Xing et al. 1997, Xing et al. 1996), the fitting quality does not allow the attribution of a Langmuir or Freundlich mechanism. Available sorption studies in the literature describe the sorption of silver nanoparticles to barium sulfate microparticle surface by Freundlich adsorption model (Wagener et al. 2012) and the sorption of CdSe/ZnS quantum dots to model substrates by Langmuir sorption model (Park et al. 2008).

The Freundlich coefficients (K_F) range from 8.4 ($\mu\text{g}^{(1-n)}\text{L}^n$)/g to 19.5 ($\mu\text{g}^{(1-n)}\text{L}^n$)/g (Table S2), and the Freundlich exponents n indicate a wide range of sorption curvature, ranging from near-linear sorption ($n = 0.96 \pm 0.15$) to strongly non-linear sorption up to $n = 0.53 \pm 0.04$ (Table S2). K_F and n vary in the order (Figures 4A and 4B):

K_F : Diol > Glass > Silica gel > Cyano > Sand > Phenyl > Octadecane

n : Octadecane > Phenyl > Cyano > Silica gel > Sand > Glass > Diol

From a chemical point of view, linearity would be expected for the lowest specific interactions between nanoparticles and the surface, and non-linearity is expected to increase with increasing binding strength and specificity (LeBoeuf et al. 1997, Chiou et al. 1998) or surface heterogeneity (Schwarzenbach et al. 2003). Assuming the least specific interactions for the alkyl and the phenyl surfaces and strongest ones for the most polar surfaces, it is in line with these prerequisites. Variation of K_F also follows this assumption by showing higher values for more polar diol-functionalized surfaces and lower values for the nonpolar octadecane- and phenyl-functionalized surfaces. However the sorption data are related to the

mass of the sorbent and all sorbents are expected to have a specific, but unknown, sorption capacity. Therefore, K_F as determined in this study cannot be used to obtain parameters describing nanoparticle-surface interactions unless the sorption capacity is known.

Assuming Langmuir-type sorption resulted in Langmuir coefficients ranging from close to zero ($K_L = 0.02 \pm 0.06$) L/g for the octadecane-functionalized surface up to ($K_L = 0.6 \pm 0.1$) L/g for the diol-functionalized surface. The parameters for maximum loading, Q_{max} range from $54.8 \pm 4.0 \mu\text{g/g}$ to $526.4 \pm 1757.5 \mu\text{g/g}$. Q_{max} , however, shows large errors for sorption to octadecane- and phenyl-functionalized surfaces. This uncertainty is due to the still weak curvature of the sorption isotherms (Figure 6A).

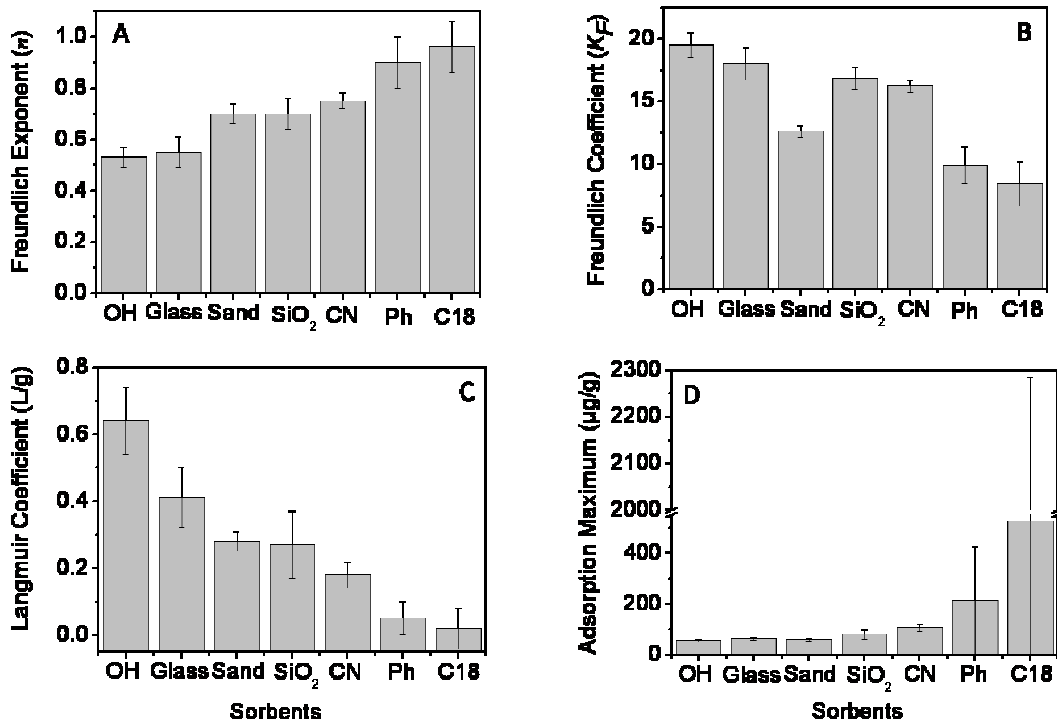


Figure 5. Freundlich exponents (A), Freundlich coefficients (B), Langmuir coefficient (C) and Langmuir adsorption maxima (D) for the sorption of silver nanoparticles onto the sorbents.

As shown in Figure 5C and 5D, K_L and Q_{max} vary in the order:

K_L : Diol > Glass > Sand > Silica gel > Cyano > Phenyl > Octadecane

Q_{max} : Octadecane > Phenyl > Cyano > Silica gel > Glass > Sand > Diol

Assuming a Langmuir type interaction, Q_{max} indicates the effective surface coverable by the nanoparticles, which is usually unknown and hard to describe. As expected, Q_{max} did not correlate with the BET surface area (SI Figure S9A). The functionalized surfaces in particular display only slight differences in BET surface area (SI Table S1) coinciding with significant changes in Q_{max} values (SI Table S2). This supports the assumption that BET surface area is not suitable as a descriptor of sorption capacity. It may be because a significant part of the BET surface area is located in pores not accessible by nanoparticles, or caused by nanoscale surface roughness. The additional lack of correlation between Q_{max} and sorbent surface roughness measured using AFM (SI Figure S9A) suggests that nanoscale surface roughness does not increase the effective space available for nanoparticle attachment which makes sense if the length scale of the surface roughness is smaller than the length scale of the particles. There was no correlation between sorbent surface charge and Q_{max} (data not shown), at least for the sorbents where we were able to measure the surface charge. This indicates that electrostatic forces did not play a major role in the sorption of nAg to the surfaces used in this study. An attempt to connect Q_{max} to the apparent geometrical surface area by considering the sorbents as spheres with smooth surfaces also failed. For example, Cyano-, phenyl-, and octadecane-functionalised surfaces (particle size 3 μm), have the same geometrical surface area ($0.8 \text{ m}^2 \text{ g}^{-1}$) but their Q_{max} varies by a factor of up to 5 (Table S2). Considering a debye radius of 1 μm around the 100 nm large particles, would lead to an occupied surface area of 1.5-7.5 $\text{cm}^2 \text{ g}^{-1}$, which would indicate an effective coverage of 2-11 % of the geometric surface area. This suggests that only part of the sorbent surface is involved in the nAg -surface

interaction observed in our study. This result nicely fits into the concept of attachment in non-uniform media under unfavorable conditions (Johnson et al. 2013). Thus, an independent approach to estimate the effectively coverable surface of the sorbents still needs to be developed and also needs to consider morphological heterogeneity of the sorbent surface.

Maximum particle coverage can also be estimated by extrapolating the particle deposition kinetics to infinite time (Adamczyk et al. 2009, Nattich-Rak et al. 2012, Ocwieja et al. 2011). Most of these studies use optical microscope and height information from AFM to study particle coverage on flat sorbent surfaces. This approach does not seem useful for real environmental systems because the surfaces display significant surface roughness on the order of a few nanometers. Below, we will discuss the suitability of using adhesion-force information from AFM to determine the effective surface area. Only with this information can the assumption of Langmuir sorption mechanisms ultimately be validated. Nevertheless, the Langmuir model allows the interaction parameter K_L and the capacity parameter Q_{max} to be separated. Therefore, we will keep to the Langmuir model when discussing specific interaction parameters, keeping in mind that the mechanism needs further validation.

Variation in the K_L value for different sorbents can be explained by their ability to undergo particular intermolecular interactions. Nonpolar sorbents (i.e. octadecane- and phenyl-functionalized sorbents) displayed the lowest K_L value and sorbents with polar groups undergoing H-donor/acceptor interactions displayed the highest K_L value. This is in line with expectations regarding intermolecular interaction (Li et al. 2012) under the assumption that nAg particles can undergo some H-donor/acceptor interactions. This may be due to the presence of carbonaceous or organic material in the nanoparticle surfaces as suggested from our Raman and EDX measurements. Furthermore, it has been reported, using SERS (surface-enhanced Raman scattering) and by a DFT (density functional theory) study of water on metal cathode of silver nanoparticles, that water molecules exist on the metal cathode with

HO-H---Ag hydrogen bonding interactions (Li et al. 2010). This confirms that even bare *n*Ag particles can undergo some H-acceptor interactions.

Figure 6 shows sorption data normalized to Q_{max} together with a fitted Langmuir isotherm. It is clear that with more polar diol-functionalized surfaces, more silver is adsorbed (79%) and with less polar sorbents, e.g. octadecane-functionalized (8%) and phenyl-functionalized (20%) surfaces, it is comparably less.

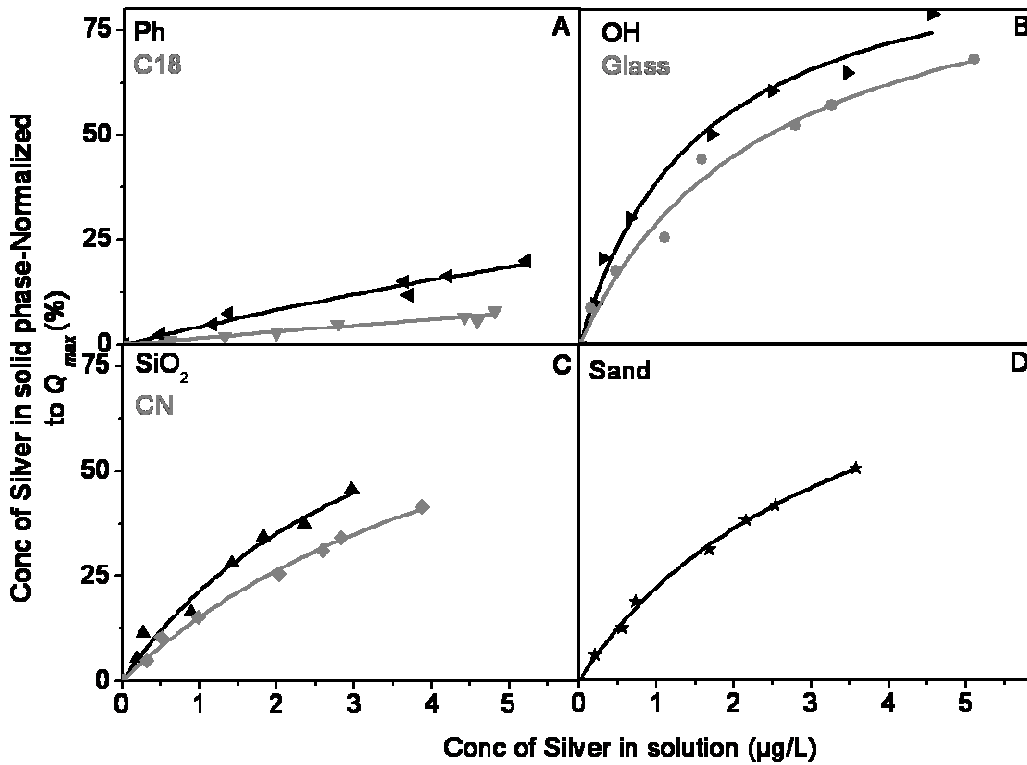


Figure 6. Langmuir sorption isotherms of silver nanoparticles on different sorbents.

Thus, although fitting quality is comparable for the Langmuir and Freundlich models, the application of the Langmuir model allows the direct separation of the effect of limited surface coverage and the effect of nanoparticle-surface interactions, each into a single sorption parameter. As long as sorption is ongoing from a stable suspension, the assumption of a

monolayer sorption is also reasonable as nanoparticle-nanoparticle interactions are effectively repulsive, inducing a blocking effect. This situation changes completely when investigating attachment to the same surface from less stable suspensions as demonstrated by a specific study in which the sorption of silver nanoparticles from unstable suspensions was investigated (hydrodynamic diameter growth rate: 14.3 nm/h, SI Figure S10). Here, sorption isotherms for all the sorbents were random points and did not follow any models (SI figure S11) indicating that nanoparticle-nanoparticle interactions outweigh nanoparticle-surface interactions.

2.4.4 Determination of the surface coverage in AFM images of μm -scale sections of sorbents.

Glass-bead and silica-gel surfaces before and after sorption with nanoparticles were analyzed using AFM. The chemically functionalized sorbent surfaces were not investigated due to the smaller grain size and difficulty in fixing them to a flat surface. Height images do not provide any information about the sorbed nanoparticles due to high surface roughness and sharp edges on the sorbents (SI Figure S12). However, the adhesion-force images obtained using PFQNM show clear differences between covered and uncovered surfaces (SI Figure S13 and S14). Adhesion-force values give information about the surface properties of the sample, including both chemical and material properties in nanometer scale (Cappella et al. 1999). As such, adhesion-force images can be used to explain changes in the material properties of a sample in nanometer resolution. The frequency distribution graph of adhesion force for uncovered glass beads and silica gel (black bars in Figure 7A and 7B) indicates adhesion forces ranging between 30 and 70 nN for glass-bead surfaces and between -10 and 30 nN for silica surfaces. Due to *n*Ag attachment, an increase in the number of data points with adhesion forces between 30 to 90 nN was observed for both surfaces. This range of adhesion forces was attributed to the presence of *n*Ag on the surface. We suggest determining surface

coverage by quantifying the increase in the percentage of data points in this force region. As the total area in the AFM image always has same total number of data points, the increase in this force region should correspond to nAg coverage. We found that the frequency of data points in this force region increased with measured coverage (data not shown), but as expected, a significantly higher number of images has to be taken and analyzed in order to directly quantify Q via AFM with reasonable certainty. Humidity also has a large effect on adhesion-force measurements (Fuji et al. 1999), hence PFQNM measurements have to be done in a humidity-controlled setup to obtain more quantitative results. Other challenges are the effects of sharp edges on adhesion force. Furthermore, reliability of such data always depends on the heterogeneity of surfaces and their force background pattern. For more heterogeneous surfaces, it may be advisable to combine adhesion-force measurements with other mechanical or material properties.

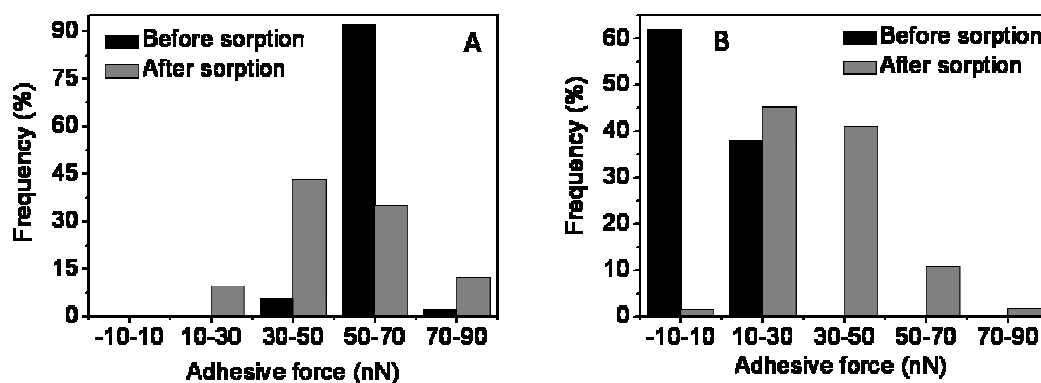


Figure 7. Frequency distribution of adhesion force between the AFM tip and glass bead surface (A) and silica gel surface (B), before and after sorption. 262144 data points in an image were taken to plot the frequency distribution.

In summary, the results show that nanoparticle attachment to sorbents depends on sorbent-sorbate intermolecular interactions that can be analyzed by investigating nanoparticle

sorption to a set of model surfaces undergoing well-known interactions under quasi-equilibrium conditions if the suspension is stable. In this case, Langmuir sorption isotherms allow the determination of both a nanoparticle-surface interaction parameter and a maximum surface coverage. The observation that nanoparticle attachment is limited to a maximum coverage could be explained by the blocking effect due to electrostatic repulsion or, as suggested by the low percentage of covered geometric surface, by preferential attachment of the particles to physically or chemically more favorable sites

The extension of this sorption study to environmental surfaces showed that *n*Ag sorption to leaves is comparable to sorption to the octadecane surface, and sorption to sand is comparable to sorption to glass and silica gel. This can be explained through chemical intermolecular interactions. The observation that environmental surfaces behaved in similar ways to sorbents undergoing comparable intermolecular interactions demonstrates the transferability of our approach to more complex surfaces. The set of Langmuir coefficients further suggests that *n*Ag may undergo H-bond acceptor interactions. This could be due to the binding of some organic compounds to part of the *n*Ag surface.

The results of our study thus help to understand particle-surface interactions on the basis of sorption isotherms under quasi-equilibrium conditions and for stable suspensions. This approach will help in assessing the fate of stable nanoparticle suspensions in the environment. To gain a more general understanding about the fate of EINPs in environmental systems, a larger set of stable and unstable suspensions and nanoparticles with different coatings must be investigated.

2.5 Supporting Information

Table S1: Characteristic parameters of Sorbents.

Table S2: Langmuir and Freundlich parameters for the sorption of silver nanoparticles to the sorbents and statistical parameters for fitting

Figure S1. UV/VIS absorption spectra of silver nanoparticle suspension.

Figure S2. Intensity-weighted hydrodynamic size distribution of the *n*Ag suspension obtained by dynamic light scattering.

Figure S3. Time dependent particle size of silver nanoparticle suspension.

Figure S4. SEM images of silver nanoparticles prepared Aluminium disc (A) substrate, showing the point where EDX measurements has been done (marked with black ring) and EDX spectra (B).

Figure S5. Raman spectra of silver nanoparticles deposited on a silicon wafer substrate (A) and of a blank silicon wafer substrate (B)

Figure S6. Sorption isotherms for the sorption of silver nanoparticles to different sorbent surfaces.

Figure S7. Comparison showing the sorption isotherms for the sorption of silver nanosuspension and ionic silver solution onto different sorbent surfaces.

Figure S8. ESEM image of leaf disc after sorption showing silver nanoparticle.

Figure S9. Variation of Q_{max} with surface roughness and BET surface area of the sorbents.

Figure S10. Time dependant size measurement of silver nanoparticle suspension, which is prepared by bath sonication of nano silver powder and without further filtration. This shows that the particle size is increasing with time.

Figure S11. Sorption isotherms for the sorption of unstable silver nanoparticles to different sorbents.

Figure S12. SEM images of silica gel (A) and glass bead (B) showing uneven surface and sharp edges.

Figure S13. Height and adhesion force AFM images of glass beads before and after sorption.

Figure S14. Height and adhesion force AFM images of silica gel before and after sorption.

Table S1: Characteristic parameters of Sorbents. Surface roughness is measured using AFM for 2500 nm² area. Interaction parameters are taken from literatures. Surface charge for octadecane, phenyl and cyano functionalized surfaces are not available because of the difficulty to get this sorbents in to aqueous phase because of their hydrophobic nature.

Sorbents	Particle size (μm)	BET Surface area (m^2/g)	Surface roughness (nm)	Surface charge	Interaction parameters			
					e	S	a	b
OH func. Surface	5	258.8	10.30 ± 2	-0.27	- 0.64 ± 0.04^{30}	- 0.18 ± 0.05^{30}	- 0.22 ± 0.03^{30}	- 0.76 ± 0.06^{30}
Glass bead	80-120	0.0530	0.69 ± 0.04	-0.22	6.8^{48}	NA	0.89^{48}	1.06^{48}
Sand	80-130	0.7735	14.90 ± 5	-0.08	6.8^{48}	NA	0.89^{48}	1.06^{48}
Silica gel	60-130	551.6	9.47 ± 5	-0.16	6.8^{48}	NA	0.89^{48}	1.06^{48}
CN func. Surface	3	245.1	4.16 ± 0.3	NA	0.22 ± 0.04^{30}	- 0.14 ± 0.05^{30}	0.01 ± 0.04^{30}	- 1.40 ± 0.07^{30}
Ph func. Surface	3	248.8	4.70 ± 0.08	NA	0.16 ± 0.02^{30}	- 0.25 ± 0.03^{30}	- 0.38 ± 0.02^{30}	- 0.76 ± 0.03^{30}
C18 func. Surface	3	180.4	10.4 ± 6	NA	0.23 ± 0.04^{30}	- 0.64 ± 0.05^{30}	- 0.43 ± 0.04^{30}	- 1.59 ± 0.06^{30}

e = Van der Waals interactions, s = polar interactions, a = H- bond acceptor interactions,

b = H- bond donor interactions. NA= Not available

Table S2: Langmuir and Freundlich parameters for the sorption of silver nanoparticles to the sorbents and statistical parameters for fitting

Langmuir coefficient (K_L) L/g	Adsorption maximum (Q_{max}) $\mu\text{g/g}$	Freundlich coefficient (K_F) ($\mu\text{g}^{(1-n)}\text{L}^n$)/g	Freundlich exponent (n)	Chi2	R2	Chi2	R2	
OH func. surface	0.64 ± 0.1	54.8 ± 4.0	19.5 ± 1.0	0.53 ± 0.04	3.22	0.9886	4.41	0.9843
Glass bead	0.41 ± 0.09	62.6 ± 6.5	18.0 ± 1.3	0.55 ± 0.06	4.31	0.9844	6.54	0.9765
Sand	0.28 ± 0.03	58.7 ± 4.3	12.6 ± 0.5	0.70 ± 0.04	0.35	0.9974	0.95	0.9929
Silica gel	0.27 ± 0.1	79.2 ± 19.7	16.8 ± 0.9	0.70 ± 0.06	3.72	0.9811	2.90	0.9853
CN func. surface	0.18 ± 0.04	106.3 ± 14.2	16.2 ± 0.5	0.75 ± 0.03	1.24	0.9958	1.0	0.9966
Ph func. surface	0.05 ± 0.05	212.4 ± 211.9	9.9 ± 1.5	0.90 ± 0.1	7.90	0.9706	7.22	0.9731
C18 func. surface	0.02 ± 0.06	526.4 ± 1757.5	8.4 ± 1.8	0.96 ± 0.1	12.18	0.9552	12.24	0.9550

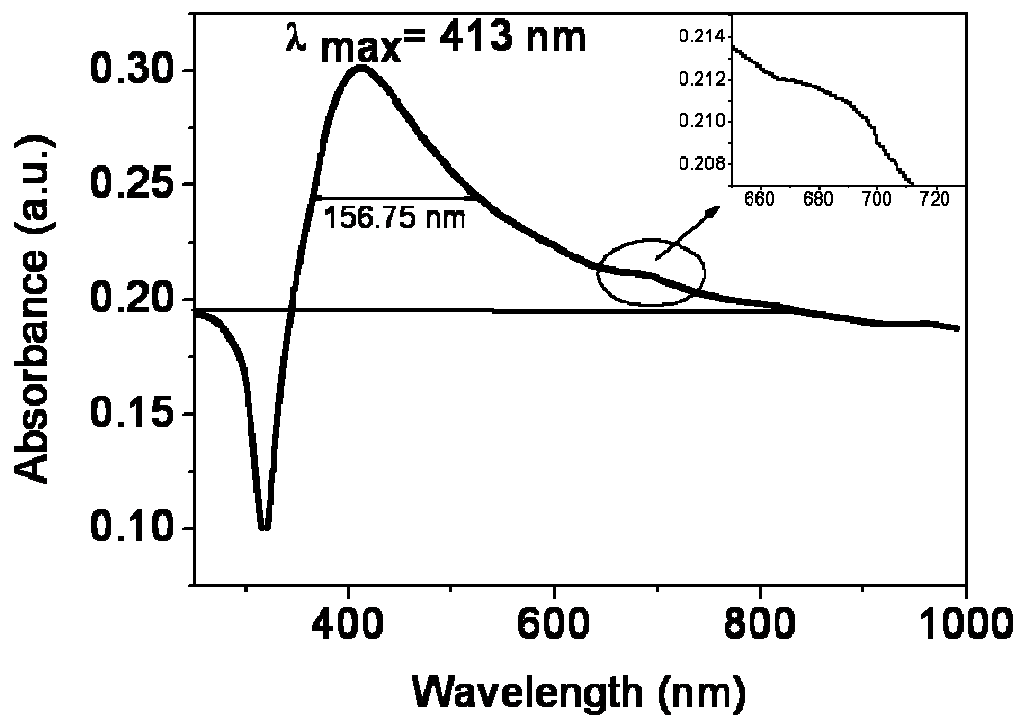


Figure S1. UV/VIS absorption spectra of silver nanoparticle suspension with a λ_{max} at around 413 nm.

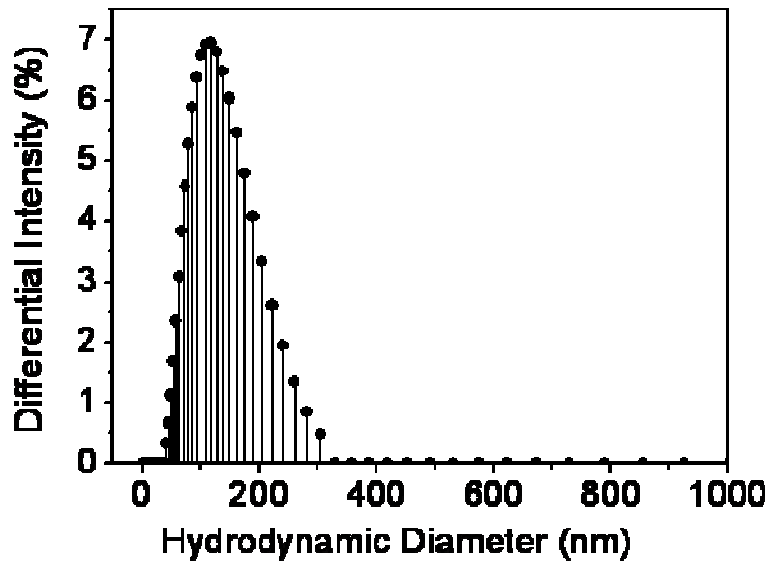


Figure S2. Intensity-weighted hydrodynamic size distribution of the *n*Ag suspension obtained by dynamic light scattering.

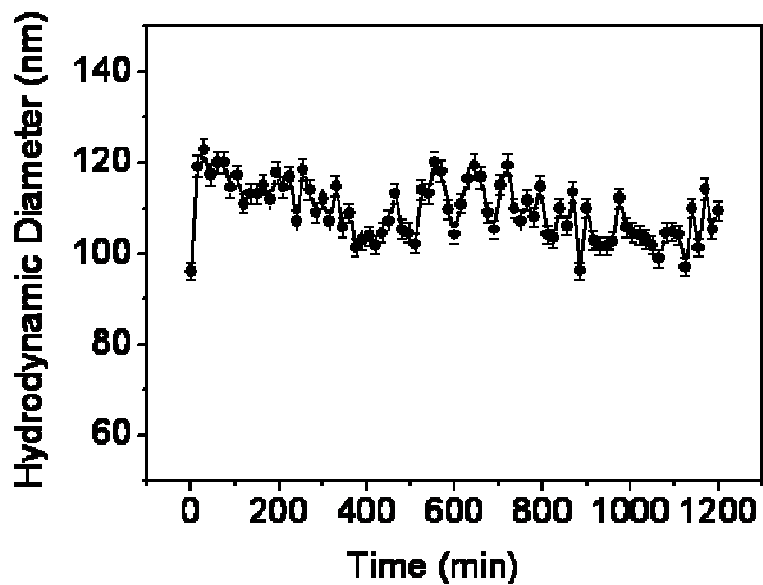


Figure S3. Time dependent particle size of silver nanoparticle suspension.

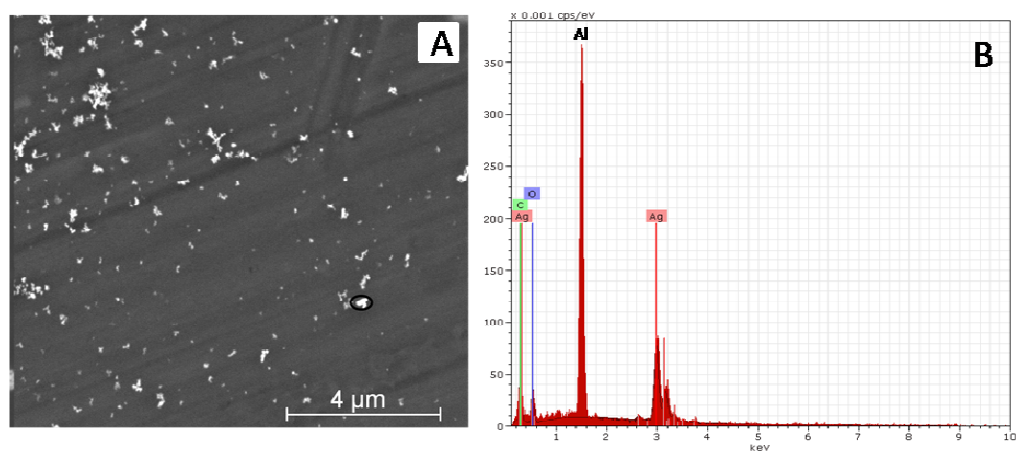


Figure S4. SEM images of silver nanoparticles prepared Aluminium disc (A) substrate, showing the point where EDX measurements has been done (marked with black ring) and EDX spectra (B).

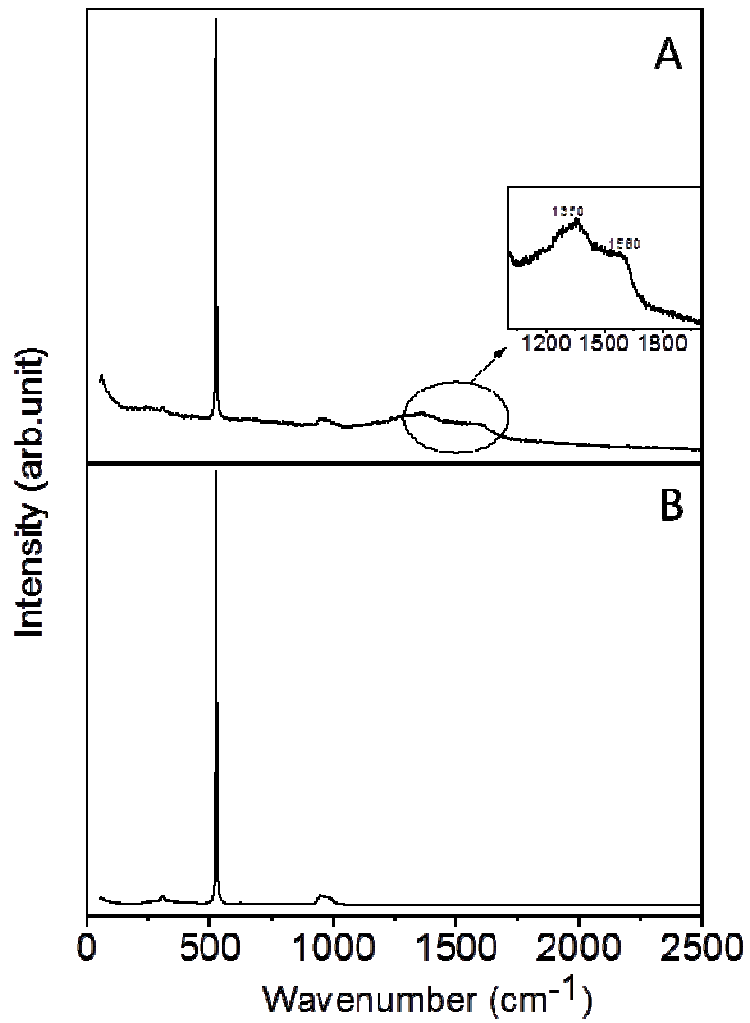


Figure S5. Raman spectra on silver nanoparticles drop casted on silicon wafer substrate (A) and on a blank silicon wafer substrate (B).

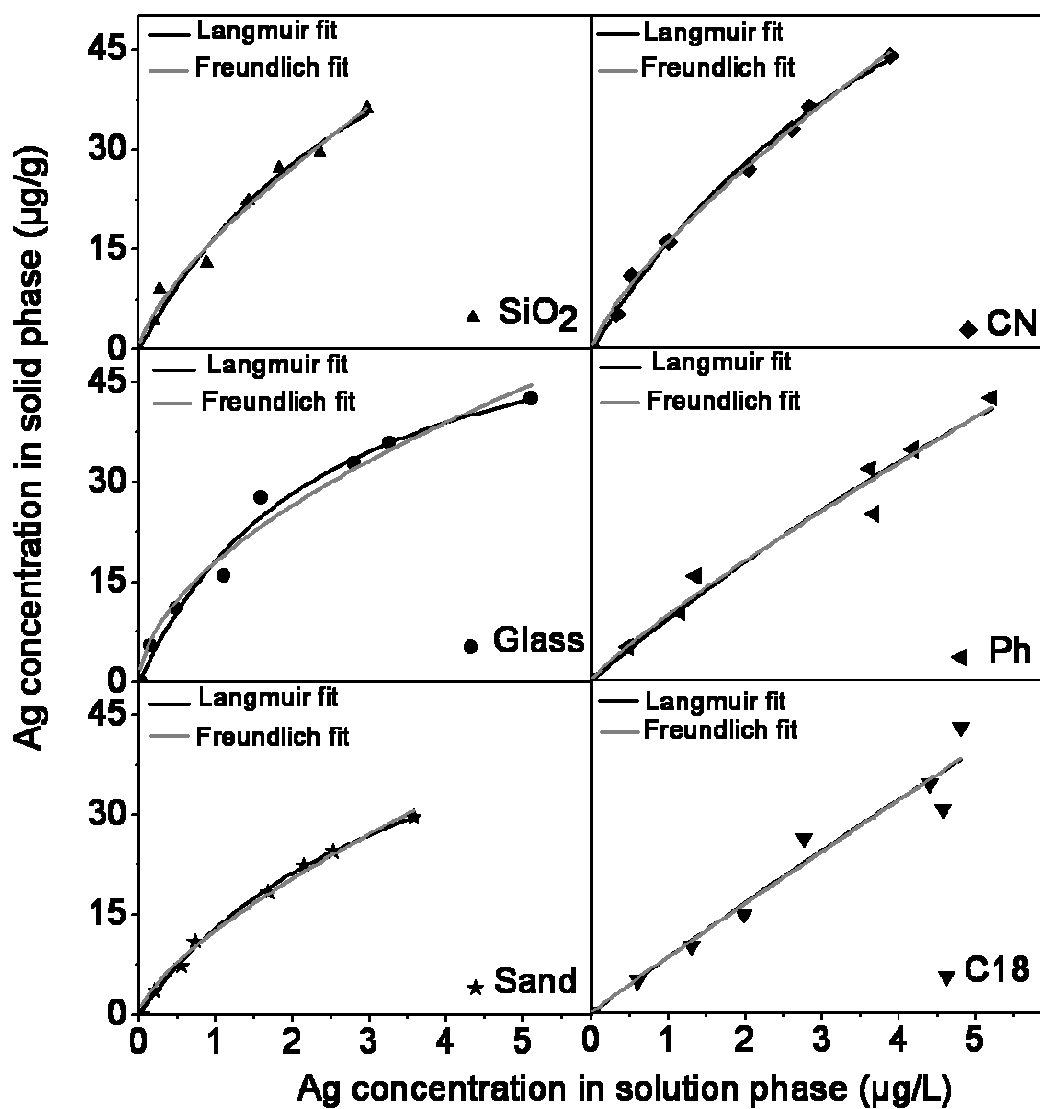


Figure S6. Sorption isotherms for the sorption of silver nanoparticles to different sorbent surfaces.

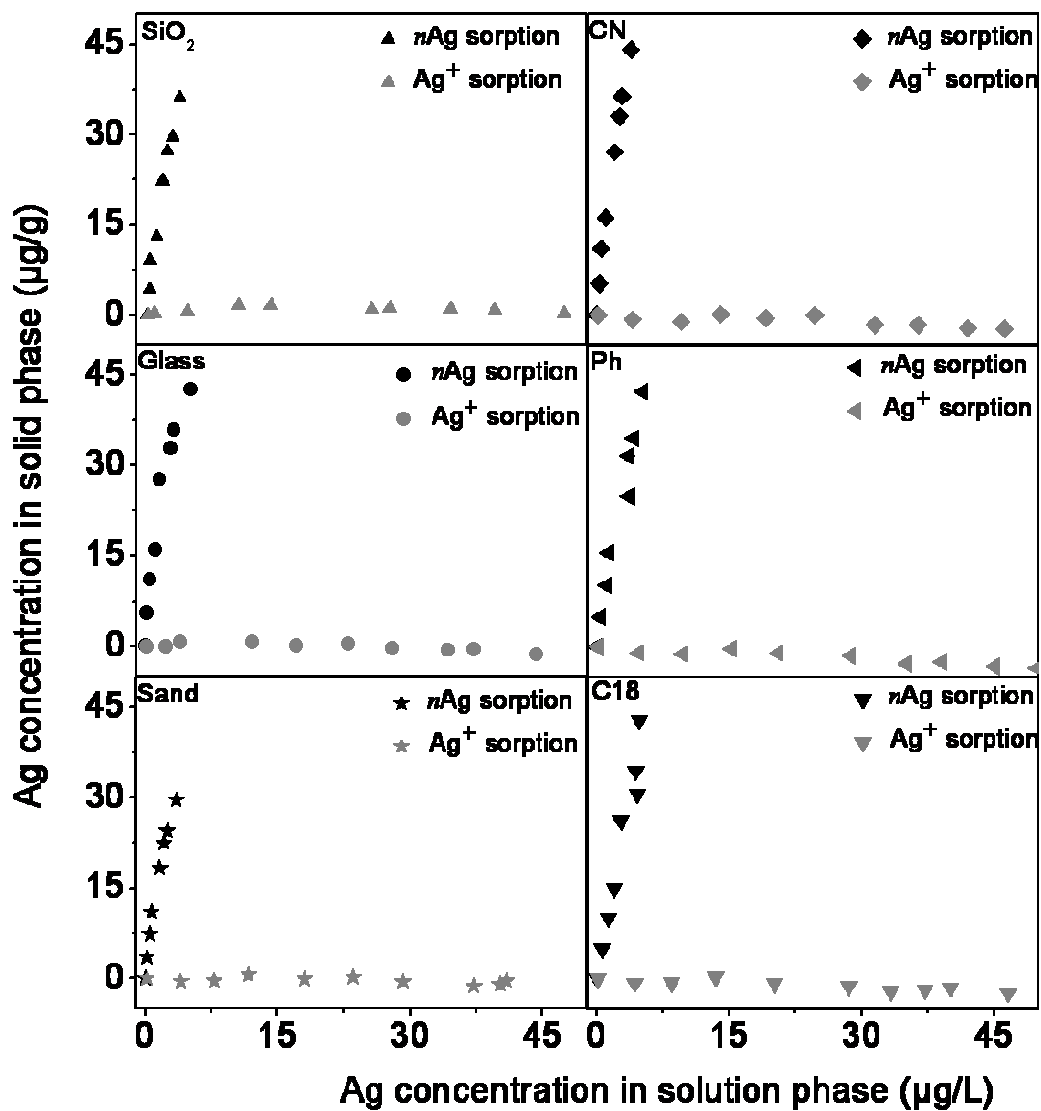


Figure S7. Comparison showing the sorption isotherms for the sorption of silver nanosuspension and ionic silver solution onto different sorbent surfaces

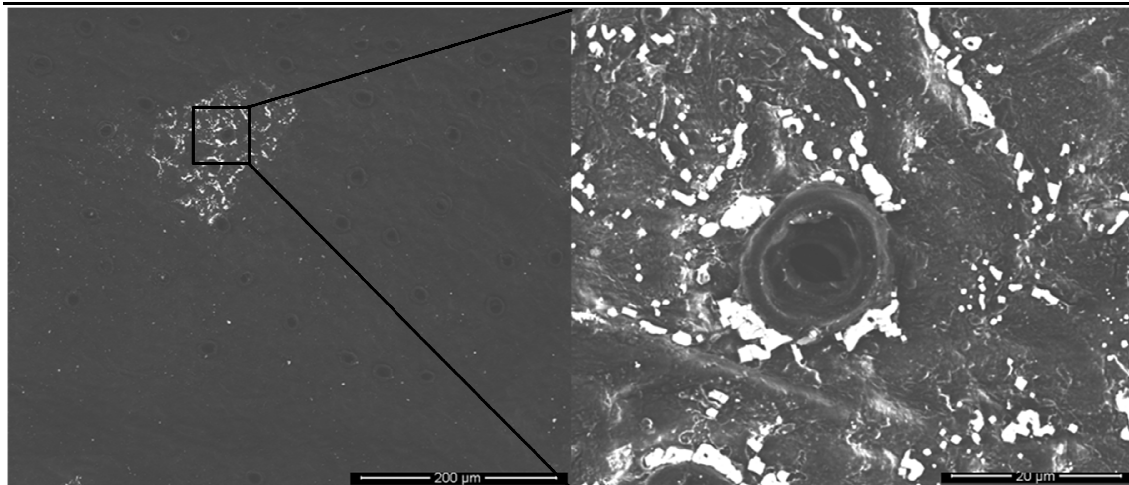


Figure S8. ESEM image of leaf disc after sorption showing silver nanoparticle (white region) aggregation

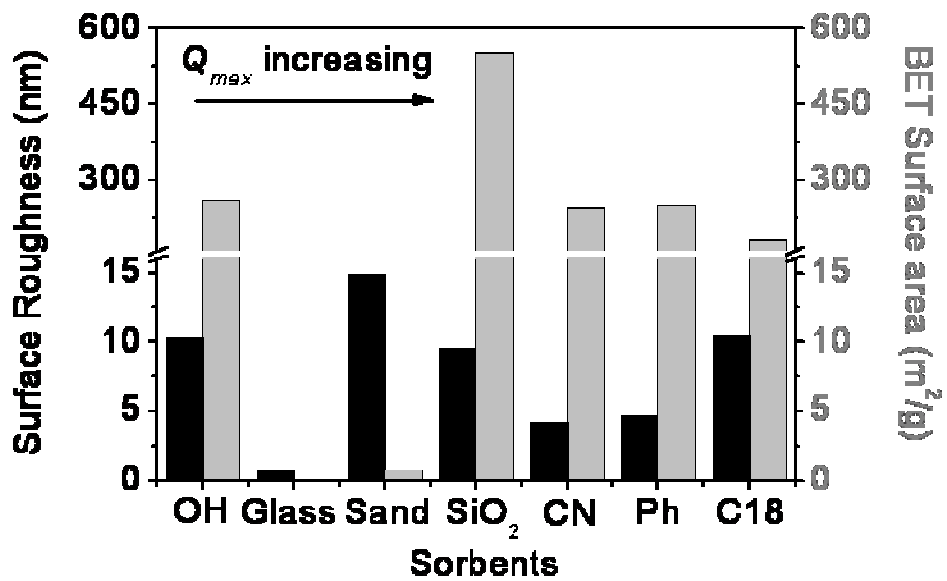


Figure S9. Variation of Q_{max} with surface roughness and BET surface area of the sorbents

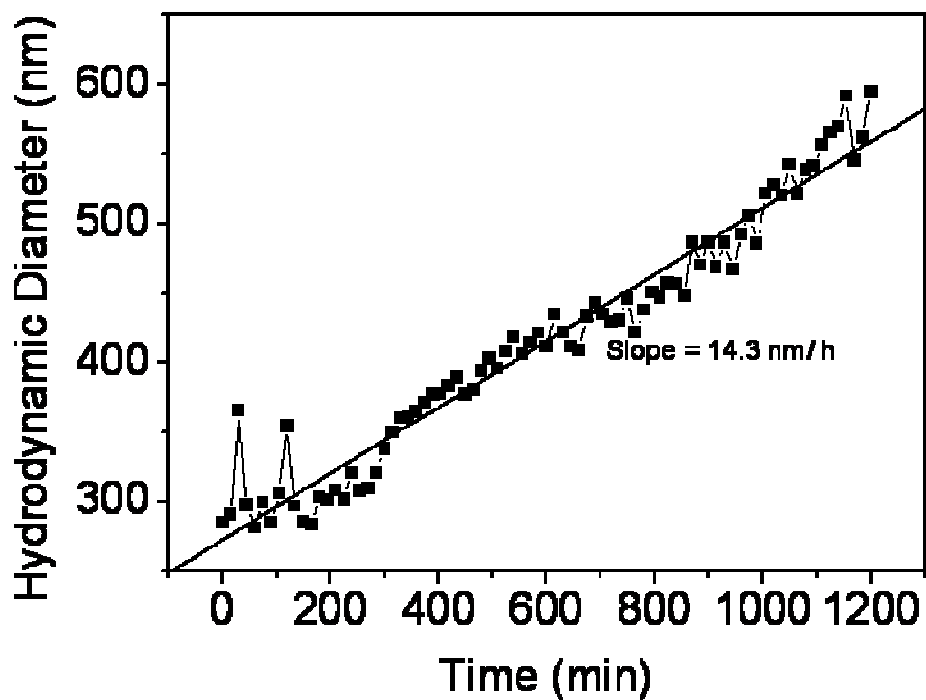


Figure S10. Time dependant size measurement of silver nanoparticle suspension, which is prepared by bath sonication of nano silver powder and without further filtration. This shows that the particle size is increasing with time.

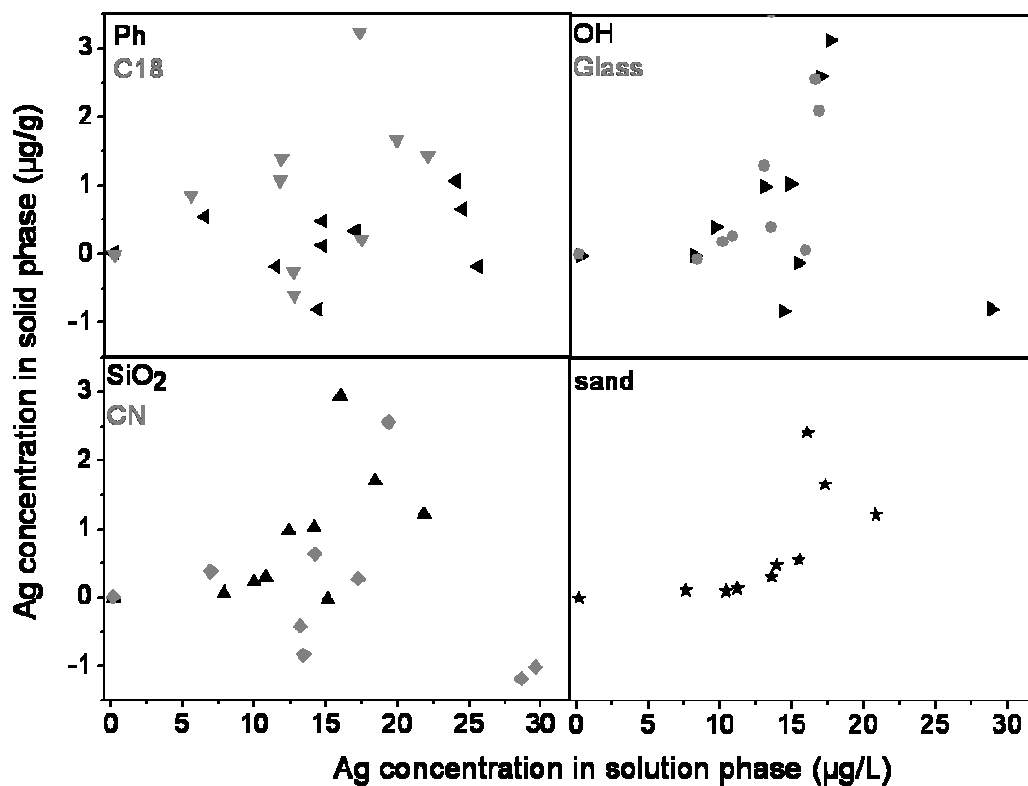


Figure S11. Sorption isotherms for the sorption of unstable silver nanoparticles to different sorbents.

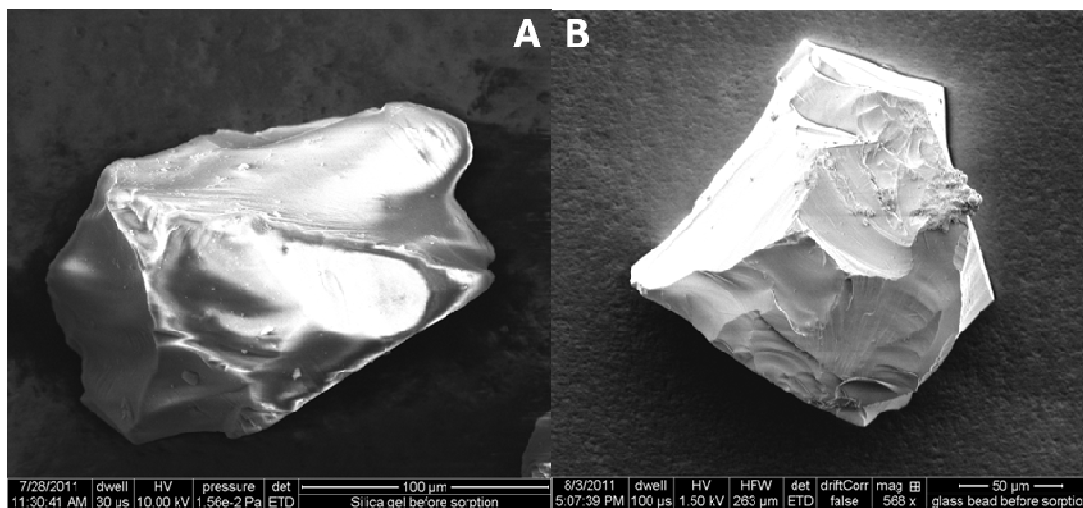


Figure S12. SEM images of silica gel (A) and glass bead (B) showing uneven surface and sharp edges.

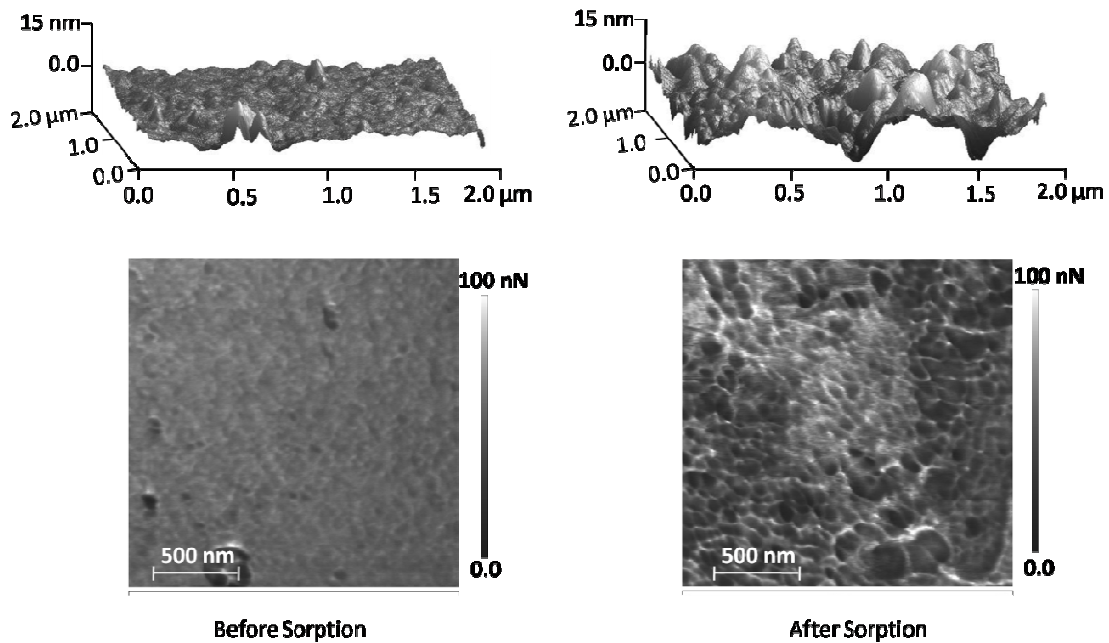


Figure S13. Height (upper images) and adhesion force (lower images) AFM images of glass beads before and after sorption.

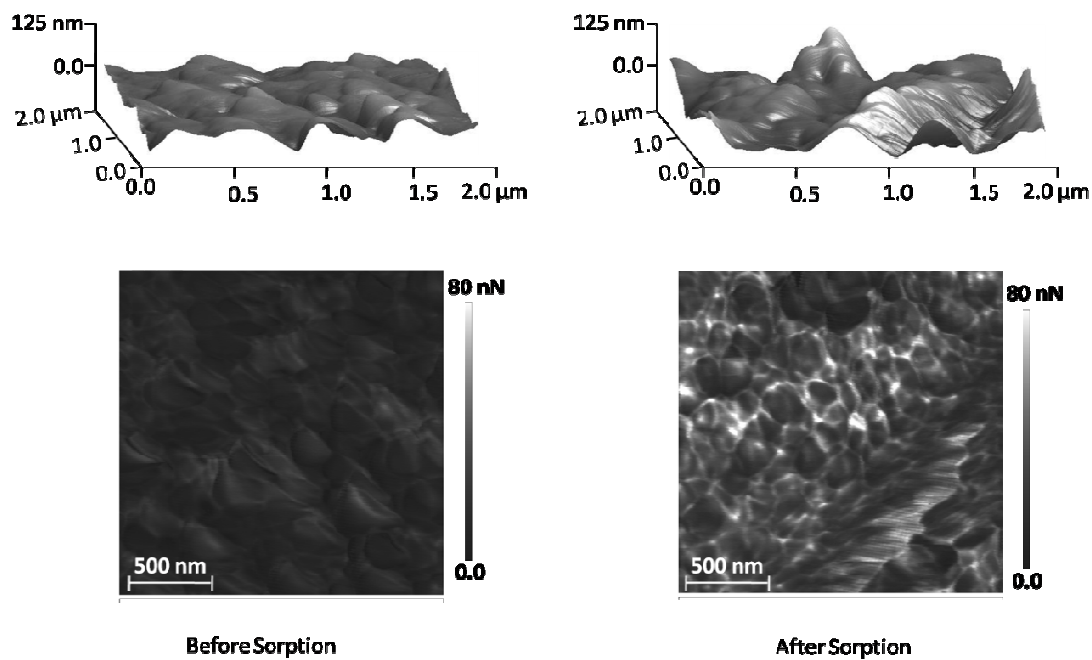


Figure S14. Height (upper images) and adhesion force (lower images) AFM images of silica gel before and after sorption.

Chapter-3

**Effect of humic acid on the sorption of bare and citrate coated silver
nanoparticles to environmental and model surfaces**

Priya Mary Abraham, Doerte Diehl, Sandra Barnikol and Gabriele E Schaumann

3.1 Abstract

In environmental systems, one of the major factors that alter the fate and transport of engineered nanoparticles are their interactions with different natural surfaces and the natural organic matter present in the environment. In this study, the interaction of *n*Ag from stable suspensions to different model surfaces (sorbents with specific chemical functional groups) and environmental surfaces (plant leaves, sand and silica gel) in the presence and absence of humic acid (HA) was investigated by means of batch sorption experiments. Four different types of interactions namely *n*Ag-HA, *n*Ag-surface, HA-surface and HA-HA are expected to play a role in this case and these interactions were studied to explain the sorption behavior.

Atomic force microscopy and fluorescence spectroscopy studies showed that in the presence of HA, *n*Ag was coated heterogeneously with HA molecules and the coating seemed to be physical in nature. In the presence of HA, *n*Ag-surface sorption was described by linear sorption isotherms for all the sorbents and the sorption was strongly suppressed compared to *n*Ag-surface sorption in the absence of HA. Moreover unlike *n*Ag-surface sorption in the absence of HA, the sorption was independent on the sorbent surface chemistry in the presence of humic acid. HA-surface interactions were also studied using batch sorption studies. The results show that the sorbent surfaces were coated with HA molecules. The sorption isotherms for all the sorbents showed linear behavior. The sorption quantity for HA-surface sorption was found to vary with the sorbent surface chemistry and its electrostatic nature in aqueous solutions. To understand the influence of particle size and coating, sorption experiments were repeated using citrate coated silver nanoparticles in the presence and absence of HA. The results showed the same pattern, but with suppressed sorption. The slopes for the sorption isotherms for both citrate coated and non coated nanoparticles showed a linear correlation in the presence and absence of HA. The sorption results suggest that the

sorption of humic acids on the sorbent surface prevents *n*Ag sorption by steric hindrance and masks the chemical specificities on the sorbent surface. A competition between *n*Ag and HA for the sorption sites available on the sorbents was observed.

3.2 Introduction

The demand and increasing application of silver nanoparticles (*n*Ag) in numerous commercial and consumer products (Benn et al. 2010; Quadros et al. 2013) makes their release into aquatic, soil and sedimentary environments increasingly inevitable. This may cause potential health risks to humans and aquatic organisms (Asharani Wu et al. 2008; Marambio-Jones et al. 2010), although it is still not clear whether the nanoparticles themselves are responsible for toxic effects (Fabrega et al. 2009; Levard et al. 2012).

The fate of engineered nanoparticles (ENP) in aquatic environments is mainly controlled by their ability to get deposited onto collector surfaces, to sediment following homo- or heteroaggregation, and to get transported (Hahn et al. 2003; Petosa et al. 2010). Hence, in order to assess the fate of nanoparticles, their interactions with natural organic matter and collector surfaces in environmental systems should be considered. These interactions are determined by the size, aggregation state and coating of the nanoparticles (Lin et al. 2012; Lin et al. 2012). E.g., *n*Ag toxicity towards lower organisms decreases upon introducing an organic matter coating (Fabrega et al. 2009; Gao et al. 2009; Gao et al. 2012). Natural organic matter (NOM) including humic acid (HA) and fulvic acid (FA) (Wu et al. 2009; Akaighe et al. 2012) which is ubiquitous in soil and aquatic environments (Buffle et al. 1998; Wilkinson et al. 1999) plays a critical role in the mobility and fate of colloidal particles (Aiken et al. 2011). Silver nanoparticles released into NOM rich environments show increased stability and thus higher mobility as compared to environments poor in NOM (Li et al. 2012; Bae et al. 2013; Furman et al. 2013). Liu and co-workers demonstrated that humic and fulvic acids

inhibit *nAg* dissolution. The proposed inhibition mechanisms are surface adsorption of NOM, which block oxidation of *nAg* and reduction of Ag^+ to Ag^0 by humic/fulvic acids (Liu et al. 2010). Gao et al. experimentally described the sorption of Suwannee River humic acid on *nAg* by Langmuir adsorption isotherm at pH 7 (Gao et al. 2012). Based on fluorescence spectroscopy and scanning electron microscopy, Manoharan et al. proposed the *nAg*- HA interaction as a continuous process in which both *nAg* and silver ions present in the suspension will be bound with HA. The *nAg*-HA species formed will continue releasing silver ions which will again bind with HA and thus repeating the process (Manoharan et al. 2013).

However, the implications of nanoparticle – NOM interactions are largely unknown (Furman et al. 2013). In environmental systems containing humic and fulvic acids *nAg* is susceptible to transformations including changes in surface characteristics and stability which will alter the physical, chemical and biological properties of *nAg*. Moreover in environmental systems the collector surfaces like clay, leaves, silica etc. are often covered by NOM and this will influence the *nAg* attachment or sorption on it (Song et al. 2011; Furman et al. 2013). Deposition behaviors of biological colloids and carbon based nanoparticles have shown to be significantly affected by NOM pre-coating on collector surface (Chen et al. 2008; Yuan et al. 2008). But the deposition of *nAg* has not been investigated in environmental context yet.

The most appropriate method to study the adsorption process of nanoparticles on collector surfaces is the determination of sorption isotherms. The type of sorption model and its underlying thermodynamic assumptions as well as the respective sorption parameters may give information about the adsorption mechanism and sorbate affinity (Kinniburgh 1986; Parimal et al. 2010).

In our previous study we investigated *n*Ag-surface interactions on the basis of sorption isotherms (Abraham et al. 2013). The study demonstrated that for non-coated silver nanoparticle in their stable suspensions, nanoparticle-surface interactions are controlled mainly by their ability to interact via each intermolecular interaction type (Abraham et al. 2013). However the influence of humic acids, a major component of aquatic and sediment environments on such sorption isotherms are unknown.

The objective of this study was to assess the influence of the presence of humic acid on *n*Ag-surface interactions. Therefore, sorption to model surfaces undergoing specific interactions (Tuelp et al. 2008) and to simple representants of environmental surfaces including sand, silica gel, glass bead and leaf discs were studied. The effect of HA on *n*Ag was investigated using fluorescence spectroscopy, UV/vis absorbance and adhesion force mapping of AFM to get an insight about how humic acid molecules interact with *n*Ag surface and coat them.

3.3 Materials and Methods

3.3.1 Preparation and characterization of *n*Ag-HA suspension.

The *n*Ag powder produced using plasma-chemical vapor deposition was purchased from io-li-tec (Ionic Liquid Technologies, Germany). Water soluble sodium humate powder (HUMINS 775) extracted from natural oxidized lignite was purchased from Humintech GmbH (Germany). Aqueous *n*Ag-HA suspension was prepared by a standard protocol using ultrasonic processor (Taurozzi et al. 2010; Abraham et al. 2013) in the presence of 5 mg/L sodium humate. Citrate reduced silver nanoparticles were synthesized by reducing silver nitrate (AgNO₃, Aldrich) with trisodium citrate solution (5 mM, Aldrich) at a pH of 11 by following a standard synthesis procedure (Dong et al. 2009).

UV/vis spectrum of *n*Ag-HA suspension was recorded using a SPECORD 50 device (Analytic Jena, Germany), to confirm the existence of surface plasmon resonance. Particle size was determined via dynamic light scattering (DLS, Beckman Coulter-Delsa Nano C) and atomic force microscopy (AFM, Veeco Nanoscope V, Bruker Corporation). The interaction of *n*Ag with HA was studied using fluorescence spectroscopy (Perkin-Elmer LS55) and AFM. Fluorescence spectra were obtained with excitation wavelength of $\lambda = 350$ nm (Klavins et al. 2010; Manoharan et al. 2013) and slit width of 10 nm, at a speed of 500 nm/min. For AFM measurements, samples were prepared on a freshly cleaved mica substrate treated with poly-lysine (Sigma-Aldrich) following the standard protocol for AFM sample preparation (McNeil et al. 2011). AFM images were captured in peak force quantitative nanomechanical mapping (PFQNM) mode (Pletikapić et al. 2011), to obtain adhesive force mapping between the tip and the nanoparticle surface. Chemically modified probes were used for adhesive force mapping in order to image the morphological features with chemical sensitivity (Okabe et al. 2000). Two chemically modified, -C18 (ST-PNP-CH3) functionalized and -COOH (ST-PNP-CO2H) functionalized AFM probes purchased from NanoAndMore GmbH (Germany) were used for PFQNM measurements. According to the manufacturer the probes were modified with specific functional groups using self assembled monolayers of thiols on gold. The thiol molecules used for the fictionalization were 1-Octadecanethiol and 1-Mercaptoundecanoic acid respectively for -C18 and -COOH modified probes. The probes were calibrated prior to measurement. The tip radius and spring constant were 6.1 nm and 5.6 N/m for -CH₃ modified probe and 2.6 nm and 6.7 N/m for -COOH modified probe. The probes were standardized for their chemical specificity using chemically modified standard samples (NanoAndMore GmbH, Germany), which undergo defined intermolecular interactions. The standard samples used were 5 chemically modified surfaces such as -C18 (ST-Si-CH3) functionalized, -C₆H₅ (ST-Si-C6H5) functionalized, -NH₂ (ST-Si-NH2)

functionalized, -OH (ST-Si-OH) functionalized and -COOH (ST-Si-CO₂H) functionalized.

The standard samples were purchased and according to the manufacturer they are produced by self assembled monolayer of thiol on gold and the thiol molecules used were 1-Octadecanethiol, 2-Phenylethanethiol, 11-Amino-1-undecanethiol, 11-Mercapto-1-undecanol, and 1-Mercaptoundecanoic acid respectively for each functional group modification. Adhesion force between sample and surface is known to be influenced by the atmospheric humidity (Jang et al. 2007; Farshchi-Tabrizi et al. 2008) and hence all AFM measurements were carried out in air at constant humidity of 28-29% by adjusting the humidity inside the sample chamber using silica gel and anhydrous CaCl₂ (Sigma-Aldrich). In order to correct the tip size influences on the force measurement, the adhesion force was normalized by dividing by the radius of the cantilever tip (Lin et al. 2008). This is a common approach to scale and compare adhesive force measurements. From each sample 10-15 nanoparticles were captured and analyzed using NanoScope analysis software. Spatial surface roughness was measured using power spectral analysis (PSD) (Fang et al. 1997; De Oliveria et al. 2012) function in the NanoScope software. The Adhesion force histogram was acquired by considering 4000 – 6000 adhesion force values (400 force curves from each particle surface) from the nanoparticles analyzed. To eliminate the adhesive force values at the edges of nanoparticle and therefore to exclude the contribution from surface morphology artifacts, we considered the force values only at the middle surface of nanoparticles (20x20 pixel dimension; pixel size- 40-50 nm).

The maximum possible fraction of dissolved silver ions in *n*Ag-HA suspension was estimated using centrifugal ultrafiltration with a 10 nm filter cutoff (3000 Da) (Abraham et al. 2013). The silver concentration in all suspensions was determined using inductively coupled plasma-quadrupole mass spectroscopy (ICP-MS, Thermo Fisher Scientific, Germany) after digesting the *n*Ag with 5 % HNO₃ for 24 h (Taurozzi et al. 2010; Abraham et al. 2013).

3.3.2 Model Surfaces for Sorption Experiment.

As model surfaces we used HPLC column packing materials having defined surface chemistry (Tuelp et al. 2008; Abraham et al. 2013) purchased from YMC Europe GmbH, such as YMC*Gel Pro C18 RS with octadecane (-C18) functional group, YMC*Gel Phenyl with phenyl (Ph) functional group, YMC*Gel Cyano with cyano (-CN) functional group, and YMC*Gel Diol with diol (-OH) functional group. In addition to these materials we used silica gel (Carl Roth GmbH) and glass beads as model surfaces and as simple representants of environmental surfaces, sand and leaf discs (*Ficus benjamina*, family: Moraceae) were used. Specific surface areas of all surfaces except leaf surface were measured using BET (Autosorb 1-MP Quantachrom) by nitrogen physisorption.

3.3.3 Sorption Experiments.

In order to obtain results comparable with former sorption experiments of *nAg* in the absence of HA, we followed the same procedure as in the previous study (Abraham et al. 2013). Specific amounts of sorbents (4 mg of chemically functionalized sorbents, 5 mg each of silica gel and glass beads, and 6 mg of sand) were added to *nAg*-HA suspension and agitated at a speed of 15 rpm for 14 h in an overhead shaker at 19°C. We used ten different initial concentrations of *nAg* ranging from 0 to 40 µg/L. The concentration of sodium humate was 2 mg/L TOC (Total Organic Carbon) in an environmentally relevant range (Mueller et al. 2008; Rodrigues et al. 2009). The sorbents were then separated by centrifugation using a speed of 3500 rpm for 20 min. Concentrations of silver before and after sorption were measured using ICP-MS. As described above we also performed a sorption experiment with sodium humate solution to determine the sorption of HA to the sorbents. The concentration of HA in the solution before and after sorption were determined using UV/vis absorbance at a wavelength $\lambda = 260$ nm and TOC analysis (multi N/C 2100s, Analytic Jena, Germany).

3.4 Results and Discussion

3.4.1 Characterization of *nAg*-HA.

The UV/vis adsorption spectra of *nAg* suspensions in the presence and absence of HA show a surface plasmon peak (λ_{max}) at 413 nm, which is characteristic for silver nanoparticles with a size range of around 35 – 50 nm (Abraham et al. 2013; Mulfinger et al. 2007) (Figure 8). The same λ_{max} in the presence and absence of HA indicate same average particle size for both the suspensions. However, intensity of absorbance increased in the presence of HA. This may indicate that a fraction of dissolved silver ions present in the *nAg* suspension is reduced to form secondary silver nanoparticles in the presence of HA as suggested in some recent studies (Akaighe et al. 2011; Adegboyega et al. 2012). This assumption is further supported by our observation that the silver fraction which passed through 10 nm cutoff filter decreased from 8% (Abraham et al. 2013) to 1% in the presence of humic acid. Considering the width of the spectrum, *nAg* spectra show a rather broad peak (full width at half maximum, $f_{\text{whm}} = 156$ nm) compared to *nAg*-HA ($f_{\text{whm}} = 86$ nm, for the spectra at 0 h and $f_{\text{whm}} = 110$ nm, for the spectra at 24 h). Broadness of the absorption peak indicates polydispersity and presence of homoaggregates in the suspension (Pillai et al. 2003). Thus the lower f_{whm} value of *nAg* in the presence of HA compared to bare *nAg* can be explained by the stabilizing functions of HA, which reduces the polydispersity of the suspension.

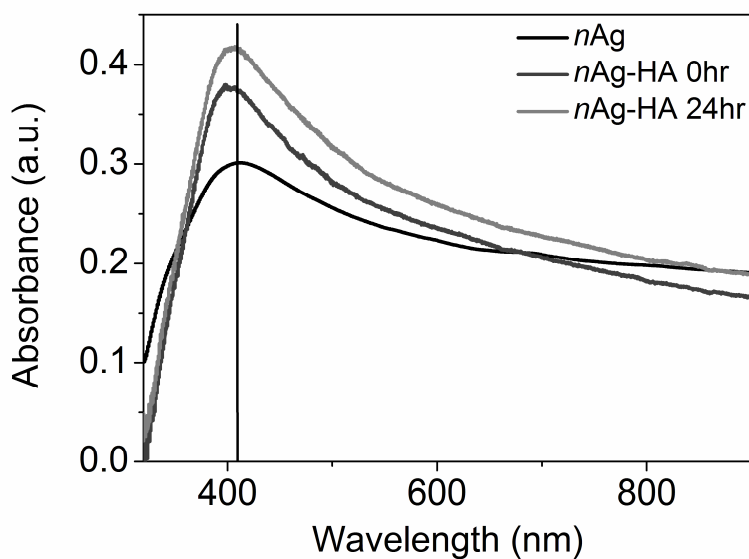


Figure 8. UV/vis absorption spectra of silver nanoparticle suspension before and after humic acid interaction.

DLS studies indicated an average hydrodynamic diameter of 107 ± 2 nm (Annex II, SI Figure S15) for nAg-HA suspension. Suspension of bare nAg show a comparable hydrodynamic diameter (105 ± 5 nm) (Abraham et al. 2013), which suggests the same average hydrodynamic diameter for the nAg suspensions in the presence and absence of HA. To test the suspension stability for the sorption experiment duration, we conducted a time dependent DLS measurement for 24 h. The hydrodynamic diameter of nanoparticles fluctuated between 105 and 140 nm during this time period (SI Figure S16). Thus, the suspension was regarded as stable containing homo aggregates for the sorption experiment duration (14 h). The zeta potential of the suspension was -44.7 ± 1.4 mV and pH was 7.5.

3.4.2 nAg-HA interactions.

To understand how humic acid coated silver nanoparticles interact with collector surfaces, it is important to investigate the nature of humic acid coating on the nanoparticles. Chemical force microscopy and fluorescence spectroscopy have been used here as tools to investigate nAg-HA interactions. CFM images with chemically modified probes showed the presence of

both isolated single nanoparticles and their homoaggregated forms (Figure 9 and SI Figure S17). Figure 9 demonstrates height and adhesive force mapping AFM images of silver nanoparticle, before (Figure 9A, 9C) and after (Figure 9B, 9D) humic acid treatment, captured using -COOH modified probe. The images captured with -CH₃ modified probe are shown in SI Figure S17.

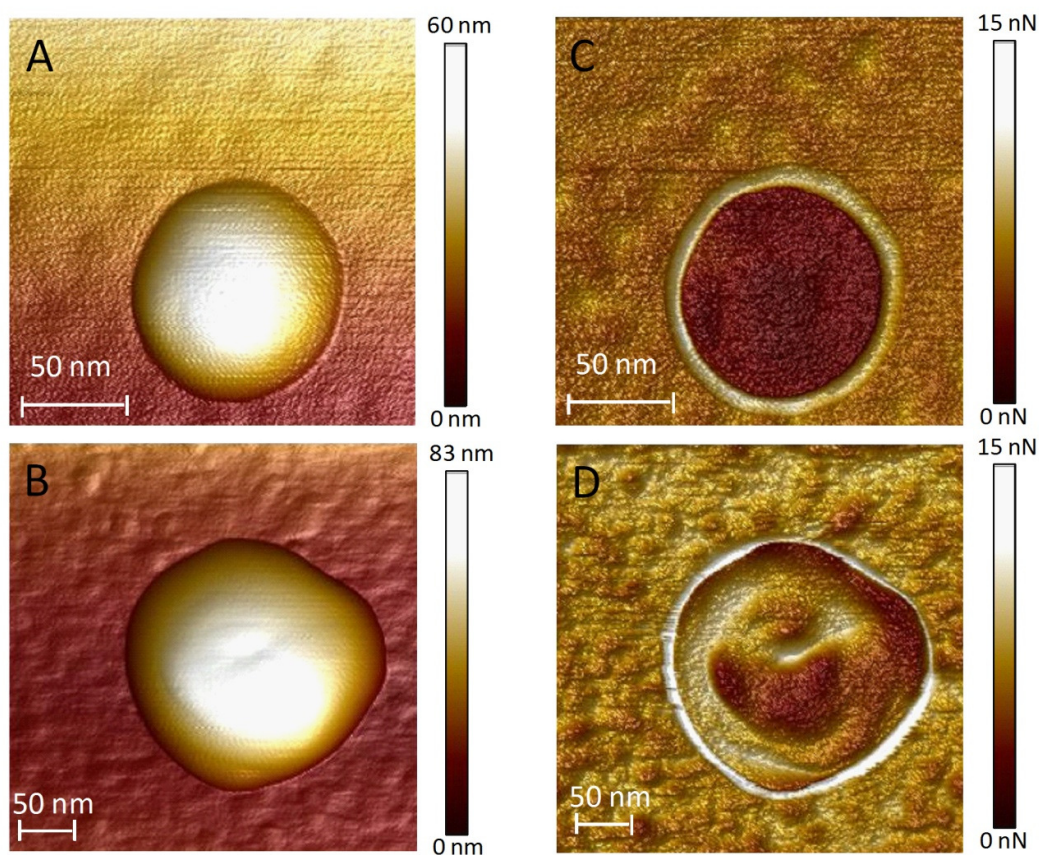


Figure 9. AFM height (A, B) and adhesion (C, D) images of silver nanoparticle before (A, C) and after (B, D) humic acid treatment, captured by -COOH modified probe in PFQNM mode.

For isolated particles AFM height measurement (in z coordinate) is accepted as nanoparticle size since sample features in x-y plane underlie broadening artifacts during scanning due to tip size and geometry influences (Klapetek et al. 2011; McNeil et al. 2011; Ukraintsev et al. 2012). The size of nanoparticles shown in Figure 9 is 60 nm (9A) and 83 nm (9B)

respectively. The size difference between these two individual particles is, however, not representative for the complete *n*Ag. DLS and UV/vis results showed that the average particle size of the suspension remains same even in the presence of HA. However, the spatial surface roughness of *n*Ag surface was larger in the presence of HA (6.2 ± 2.8 nm with -COOH modified probe and 4.9 ± 1.5 nm with -C18 modified probe) than in the absence of HA (1.9 ± 0.3 nm with -COOH modified probe and 0.9 ± 0.1 nm with -CH₃ modified probe). This increase in spatial surface roughness for *n*Ag-HA can be due to heterogeneously sorbed humic acid on the silver nanoparticle surface.

3.4.2.1 Adhesion force analysis: Standardization of probe.

Prior to the CFM measurements on the nanoparticles, the chemical sensitivity of both the -COOH functionalized and -C18 functionalized probes were checked for a set of functional groups. PFQNM measurement was done on all the 5, differently functionalized standard sample surfaces using both AFM probes.

The histograms of the normalized adhesion force between the chemically functionalized probes and chemically modified standard samples show a monomodal distribution (Figure S18 and S19 in SI). The average adhesion value, obtained from the Gaussian fit of the monomodal curves, for each interaction type accessed from Gaussian peak fit increased in the same order for both -CH₃ modified and -COOH modified AFM tip (Figure 10).

The -C18 modified probe demonstrated low force values with each surfaces compared to -COOH modified probe interaction, with the respective surfaces. This can be explained by the polar nature of -COOH functional group and its ability to act as a hydrogen bond donor/acceptor.

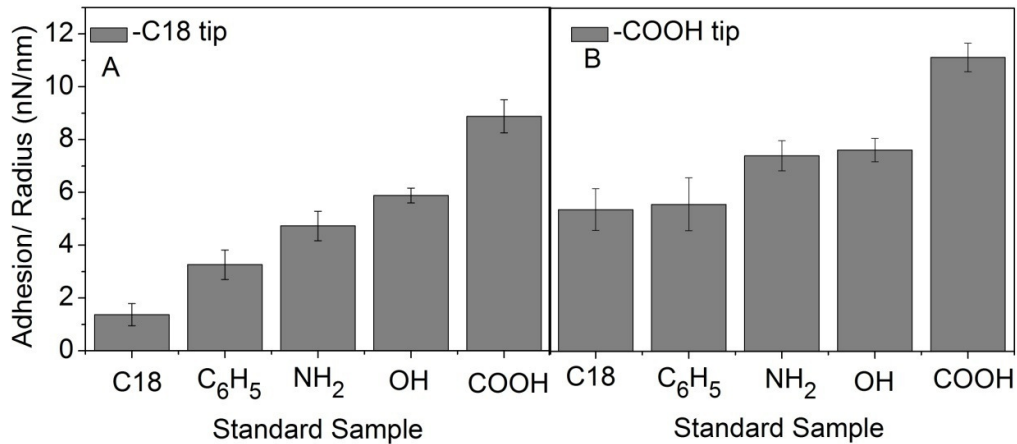


Figure 10. Average scaled adhesion forces (F/R) of chemically functionalized standard sample surfaces, measured by AFM using -C18 modified probe (A) and -COOH modified probe (B).

The surfaces having polar and hydrophilic functional groups (-COOH, -OH, and -NH₂) showed higher interaction forces with the probes, compared to the surfaces with nonpolar and hydrophobic functional groups (-C18 and -C₆H₅). These results are in accordance with the expectations based on chemical intermolecular interaction forces acting between probes and surfaces. However, all AFM measurements are done at a relative humidity of 29%, which may result in some capillary force effects as well. In addition, there will be a chance that some water molecules get absorbed on to both the sample surface and probe tip. In that case, polar functional groups can get dissociate thereby changing the surface charge. This change will also affect the adhesion force value (Vezenov et al. 1997).

The adhesion force for -C18 (tip) /-COOH (surface) interaction and -COOH (tip) /-C18 (surface) interaction are not the same in magnitude even though the chemical natures of both inter molecular interactions are the same. The reason for this observation is not directly understandable. Capillary condensation of water molecules on the -COOH functionalized surface can be a reason, which will result in dissociation of -COOH group and increase in

surface charge, thereby increasing the adhesion force for -C18(tip)/-COOH (surface) interactions. Another difference between the two surfaces is the chain length for the functionalizations (C10 spacer for the -COOH functionalization and C 17 spacer for the -C18 functionalization). Hence the discrepancy in adhesion forces may be due to the change in surface properties caused by the difference in chain length. It is known that surface properties like deformation and surface roughness have an effect on adhesion force values (Tabor 1977; Jacobs et al. 2013). Deformation is the depth of indentation by the AFM probe on the sample surface (Pletikapić et al. 2011). To check this contribution towards adhesion force, the deformation and surface roughness was measured using AFM. For -COOH modified surface, no deformation could be detected when scanned by -C18 modified probe, whereas for -C18 modified surface, when scanned with -COOH modified probe the average deformation was 1.2 ± 0.3 nm. The average surface roughness of the -C18 modified surface was large (10.3 ± 1 nm) compared to the -COOH modified surface (2.2 ± 0.1 nm). Hence the lower value (5.3 ± 0.9 nN/nm) of adhesion force for -COOH(tip)/-C18(surface) interaction compared to -C18(tip)/-COOH (surface) interaction (8.8 ± 0.6 nN/nm) may be due to the higher surface roughness and elastic deformation of -C18 modified surface when scanned with -COOH modified probe (Jacobs et al. 2013). The standardization results thus show the chemical specificity of the probes, for a range of chemical functional groups.

3.4.2.2 Adhesion force measurement on nanoparticle surface

CFM measurements were done on the nanoparticle surface using the same AFM probes. Adhesion force mapping shows more areas with higher adhesion force on the nanoparticle surface after humic acid treatment than before (Figure 9C and 9D). The humic acid treatment significantly increased the fraction of points with higher adhesion force in *n*Ag-HA surface (Figure 11). This suggests the presence of more polar functional groups on the nanoparticle surface when coated with HA. The polar groups will show higher intermolecular interaction

strength compared to non polar functional group, and there are chances for them to dissociate and increase the charge on the surface.

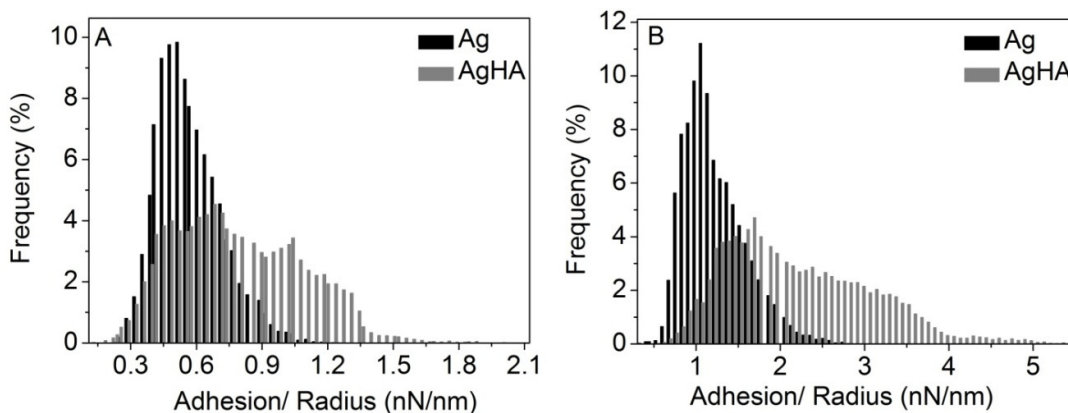


Figure 11. Adhesion force histograms for silver nanoparticles before and after humic acid treatment , captured with $-C18$ functionalized probe (A) and $-COOH$ functionalized probe (B).

The reason for this can be explained as due to the sorbed humic acid molecules present on the nanoparticle surface which usually contains polar phenolic, carbonyl and carboxylic functional groups (Struyk et al.2001; Litvin et al. 2012). Additionally the adhesion force values are higher with $-COOH$ functionalized probe, which is more polar in nature as compared to that with $-C18$ functionalized probe. This can be explained by the order of intermolecular interaction strengths. Polar functional group shows stronger specific interactions than nonpolar methyl group. $-COOH$ group may undergo hydrogen bond donor/acceptor interactions with the polar groups of humic acid there by increasing the adhesion force value. $-CH_3$ functional group can only probe vander Waals forces, while $-COOH$ group can probe dipole-dipole interactions, dipole-induced dipole interactions and hydrogen bond donor-acceptor interactions. Thus higher adhesion force values with $-COOH$ functionalized tip indicates the presence of polar groups on the nanoparticle surface after HA

coating. But the comparison of the adhesion force values with the standardization experiment, to study the chemical group responsible for each forces is not possible, here due to the carbon chain length difference in each case.

After humic acid interaction, the adhesive force histogram shows a peak broadening from 0.23 - 1.2 nN/nm for -C18 and 0.34 - 2.9 nN/nm for -COOH functionalized probe on bare *n*Ag surfaces to 0.23 - 2.1 nN/nm and 0.53 - 5.5 nN/nm for -C18 and -COOH functionalized probe on *n*Ag-HA surfaces, respectively (Figure 11). This peak broadening can be due to, either chemical heterogeneities or morphological heterogeneities or due to both. The increase in chemical heterogeneities on the nanoparticle surface after humic acid coating can be explained as due to the presence of a variety of functional groups on the humic acid. morphological heterogeneities can arise due to topographic effects of sample surface, like change in grain size and the change in multiplicity of contacts between the tip and convexities of the grain (Sato et al. 2003), which also relates to the higher spatial surface roughness for *n*Ag-HA surface. Currently it is difficult to distinguish between the chemical and morphological heterogeneities since both has a role here. Using AFM probes with other functionalizations may help to investigate chemical heterogeneities in detail.

Thus AFM study helps to detect the presence of humic acid on *n*Ag surface after humic acid treatment and the adhesion mapping shows that the *n*Ag surface is not homogeneously coated with humic acids, as regions with same force values existed along with an increased force value region after humic acid treatment.

3.4.5 Fluorescence spectroscopy analysis

Fluorescence spectroscopy helps to reveal the nature of interface between HA and *n*Ag (Kruszewski et al. 2008; Manoharan et al. 2013). Figure 12 shows the fluorescence spectra of HA in the presence and absence of *n*Ag. The fluorescence of HA (excitation wavelength

$\lambda = 350$ nm) seems to be enhanced in the presence of *nAg*. When an organic molecule interacts with metallic nanoparticles possessing a strong plasmon field, either enhancement or quenching of fluorescence intensity can be observed (Kang et al. 2011). Quenching usually arises due to molecular interactions including ligand exchange between the nanoparticles and organic molecules, fluorescence energy transfer, molecular rearrangements, ground state complex formation and excited state reactions (Manoharan et al. 2013; Umadevi et al. 2013) whereas enhancement happens when the plasmon field generated around the particle by the incident light increases the excitation decay rate of the organic molecule and thus enhances the fluorescence intensity (Kang et al. 2011; Manoharan et al. 2013).

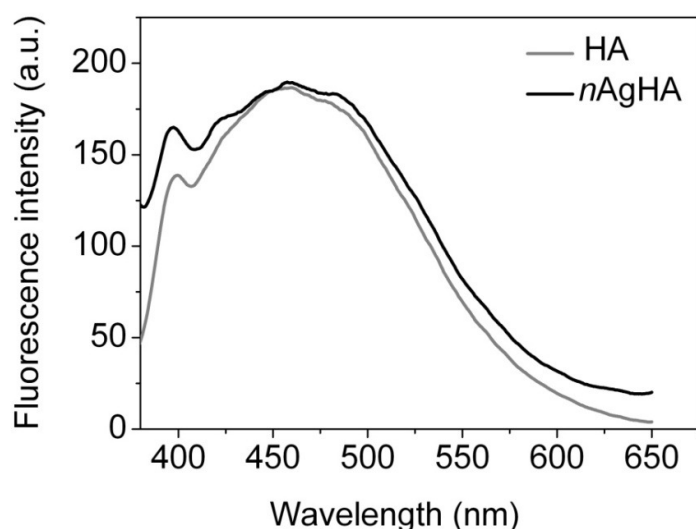


Figure 12. Fluorescence emission spectra of sodium humate solution showing an intensity enhancement after *nAg* interaction.

The observed enhancement in fluorescence intensity of humic acid molecules in the presence of *nAg* indicates that the interface distance between the HA molecules and *nAg* is greater than the fluorescence energy transfer distance (Manoharan et al. 2013) and also the interface distance is optimal enough for the plasmon field of nanoparticles to influence the humic acid molecules. But it also indicates that there is no bond formation between *nAg* surface and

fluorescence active centers of humic acid molecules and the attachment of HA may be due to physical sorption or via functional groups not linked with the fluorophore.

3.4.6 Batch Sorption Study.

***n*Ag and *n*Ag HA sorption:** Sorption isotherms for the sorption of *n*Ag-HA to all the sorbents were linear (SI Figure S20). This is in contrast to the findings of our previous study of *n*Ag sorption in the absence of NOM, which resulted in Langmuir like sorption isotherms (Abraham et al. 2013). The difference in type of isotherms suggests a different sorption mechanism for the studied HA concentration range. For quantitative comparison of both sorption data, we determined the initial slope obtained from linear sorption (by considering the initial four concentrations from the Langmuir sorption isotherms) of *n*Ag and the slope obtained from the sorption isotherms of *n*Ag-HA sorption (Figure 13A).

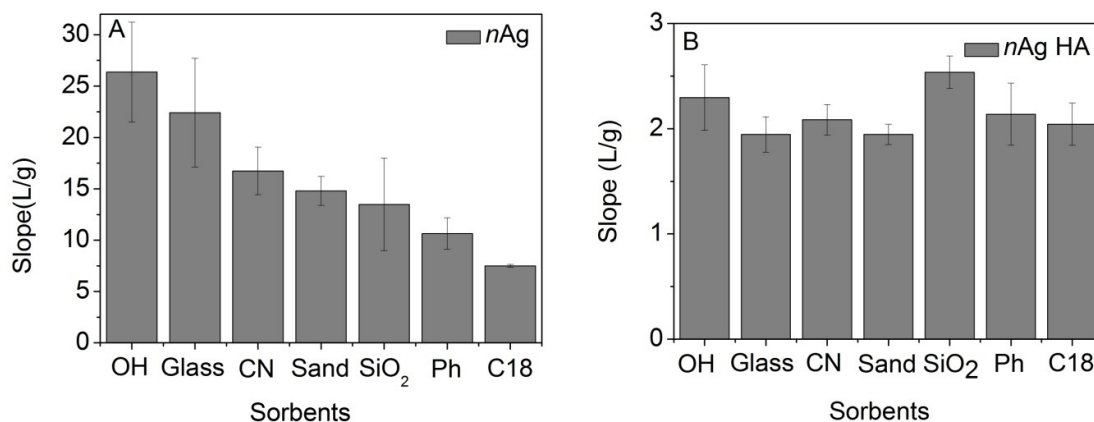


Figure 13. Slopes obtained from the linear sorption isotherms for the sorption of bare silver nanoparticles and silver nanoparticles treated with humic acid on to different model and environmental surfaces.

After humic acid treatment there is a decrease in the sorption coefficient of silver nanoparticles as seen by the ten times lower magnitude of slopes in the case of *n*Ag-HA compared to *n*Ag (Figure 13B). This can be due to the prevention of silver nanoparticle sorption by the steric layer of humic acid molecules which are already sorbed on to the

sorbents, Similar results are described by Furman et al. for a deposition study using quartz crystal microgravimetry showing a decrease in silver nanoparticle deposition in the presence of humic acid (Furman et al. 2013).

For *n*Ag sorption, the sorption isotherm slopes varied depending on the chemical nature of sorbents used: for instance nonpolar alkyl and phenyl coated surfaces having least specific interactions showed lower sorption than surfaces having polar groups like -OH. On the contrary, for *n*Ag-HA sorption such chemical specificity was not observed. This result indicate that presence of HA masks the direct *n*Ag-surface interaction. This masking effect can be due to HA coating on sorbent surface and nanoparticle surface. From CFM and florescence studies, it was clear that nanoparticle surface is coated with humic acid. But coating on nanoparticle only will not mask the effect of surface chemistry. When sorbent surfaces get coated with HA, it masks the chemical specificity of the sorbents which can mask the effect of surface chemistry in the sorption experiments. Hence it is important to investigate HA-surface interactions, which can be found further below.

In the case of *n*Ag-HA sorption, the slopes for all the isotherms were nearly the same except for silicagel surface, considering the error limits. Only silicagel surface showed a slightly higher sorption. This suggests the influence of some factor, other than chemical specificity, in the sorption experiments. Additionally for leaf discs, linear sorption of *n*Ag-HA gives the slope as 3.6 L/g which is not comparable to the linear slope obtained for octadecane surface, even though the chemical constituents of both the surfaces are comparable. But for *n*Ag sorption the slopes obtained for leaves and octadecane surface were comparable (Abraham et al. 2014). This again suggests the masking effect of HA.

HA sorption: To detect the sorption of humic acid to the sorbent surface, we conducted a batch sorption experiment with humic acid solution. Figure S21 (supporting Information)

show the calibration of UV/vis absorbance of sodium humate solution with TOC concentration. UV/vis absorbance values of sodium humate solution before and after the sorption were converted into TOC concentrations using the calibration slope. The amount of humic acid sorbed was comparably small. The sorption isotherms for humic acid sorption were linear for all sorbents (Figure S22 in SI).

The slopes decrease in the order: glass > diol > phenyl > sand > cyano > octadecane > silica gel (Figure 14).

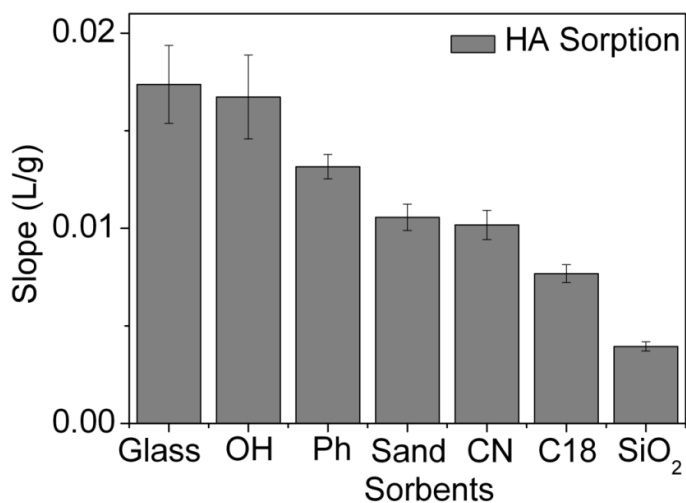


Figure 14. Slopes obtained from the linear sorption isotherms for the sorption of humic acid on to different model and environmental surfaces.

From the order of the slopes, it can be seen that the concept of intermolecular interaction fails in some cases. Phenyl group is expected to show lower binding strengths similar to alkyl group because of its nonpolar nature. However aromatic compounds exhibit noncovalent interactions (π - π interactions) with dissolved humic acid (Nanny et al. 2001; Simpson et al. 2004). Thus higher binding strength of phenyl functionalized sorbent toward humic acid, compared to that of octadecane and cyano functionalized sorbents may be due to the π - π interactions between the aromatic ring of phenyl group and aromatic components of humic

acid. The silica gel sorbent showed the lowest sorption of humic acid, which may be due to the electrostatic repulsion (Yang et al. 2013). Glass bead and sand, which are silica based materials, however showed higher sorption than silica. For the sand the higher sorption may be due to metal impurities like iron impurities or the presence of some calcium salts (since it is ocean sand) along with the basic component silica. In the case of glass, even higher sorption was observed, which may be due to the presence of metal oxides like CaO, Al₂O₃, MgO, K₂O etc.

From the HA sorption results it is clear that HA sorption to the SiO₂ surface is the weakest, average sorption is observed for Ph, Sand, CN and C18 surfaces, and strong sorption is observed for glass and OH surfaces. Thus for SiO₂ surface, uncoated *n*Ag may sorb stronger than coated *n*Ag. This can explain the stronger sorption of *n*AgHA to SiO₂ surface compared to other sorbents.

***n*Ag citrate and *n*Ag citrate-HA sorption:**

To investigate the effect of surface charge and size of nanoparticles on their sorption behavior, the same sorption experiment was done using citrate reduced silver nanoparticle (*n*Ag-citrate) suspension, in the presence and absence of HA. The average hydrodynamic diameter of the particles was around 45 nm and it was stable for the sorption experiment time duration (Figure S23 in SI). Zeta potentials of the nanoparticles obtained by DLS measurements were -66.7 ± 0.2 mV and -67.3 ± 0.5 mV for *n*Ag-citrate, *n*Ag-citrate HA respectively. Similar to the results obtained for the sorption experiment with bare silver nanoparticles, sorption isotherms for the sorption of *n*Ag-citrate to all the sorbent surfaces were nonlinear in the absence of HA (Figure S24 in SI) and linear in the presence of HA (Figure S25 in SI). Both Freundlich and Langmuir model were tried to describe the experimental sorption data for the nonlinear sorption of *n*Ag-citrate to sorbents (Figure S24).

Based on statistical parameters for fitting, Langmuir model appeared more suitable at least for few sorbents (Table S2 in SI). Thus a monolayer sorption is favored for *n*Ag-citrate, which suggests that particle-surface interactions are more prominent than particle-particle interactions in this case. This can be due to electrostatic repulsion between each nanoparticle which results in blocking effect. The linear sorption in the presence of HA suggests that both particle-particle interactions and particle-surface interactions are contributing to this sorption behavior. This can also be due to very low coverage of nanoparticles on the surface which may cause the sorption to remain in a quasi linear range of the langmuir isotherm.

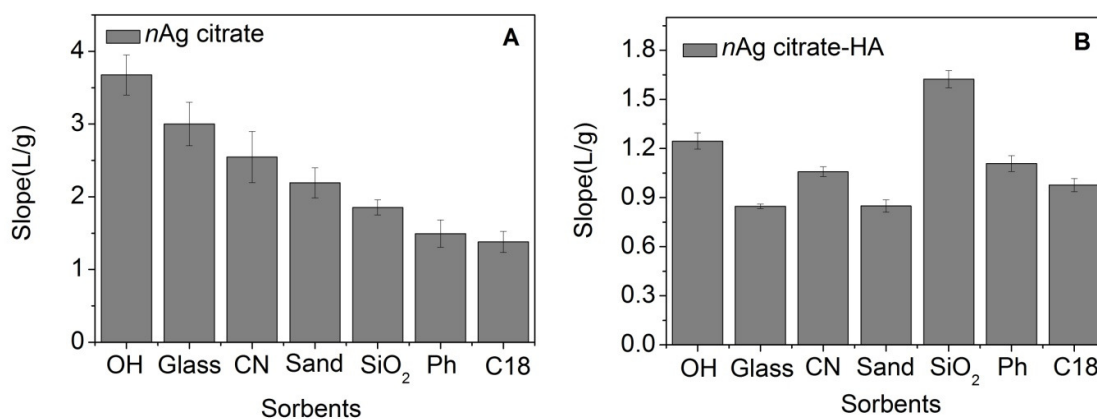


Figure 15. Slopes obtained from the linear sorption isotherms for the sorption of citrate reduced silver nanoparticles (A) in the presence and (B) in the absence of humic acid on to different model and environmental surfaces.

Slopes of the linear part of isotherms (first 4 data points) for *n*Ag-citrate sorption show dependence on the chemical functional group present on the sorbent surface and decreased in the order: Diol > Glass > Cyano > Sand > Silica gel > Phenyl > Octadecane (Figure 15A).

This trend is similar to that observed for bare silver nanoparticles (*n*Ag) and can be explained on the basis of intermolecular interactions between the sorbent surface and nanoparticles. This also indicates that the type and quality of interactions are the same when comparing *n*Ag and *n*Ag citrate.

Comparing the sorption quantities of *nAg* (Figure 13A) and *nAg*-citrate (Figure 15A), citrate reduced nanoparticles show less affinity towards the sorbents than bare *nAg*. This can be explained by the more negative zeta potential of *nAg*-citrate (-66.7 ± 0.2 mV) compared to that of *nAg* (-44.3 ± 0.7 mV). Since all the considered sorbents are negatively charged in aqueous phase, more repulsion between *nAg*-citrate and sorbents results in a lower affinity. Furthermore, the more negative zeta potential results in better stabilization of *nAg* citrate compared to *nAg*, thereby increasing the tendency of *nAg* citrate to remain in the aqueous phase.

There was no relation between the BET surface area of the sorbents and the slopes for the sorption of *nAg*-citrate suspension just as *nAg* suspension (Figure S26 in SI). Thus nanoparticle charge is also a factor that controls the sorption process.

For the sorption of *nAg*-citrate HA, the slopes show no dependence on the sorbent surface chemistry (Figure 15, right). Also the sorption quantity is significantly decreased, compared to the sorption without HA. Similar to *nAg* HA sorption, silica gel sorption isotherm had the highest slope of all studied sorbents. These observations again confirms that in the presence of HA, both the nanoparticles and sorbent surfaces get coated with HA, which masks the chemical specificity of nanoparticle-surface interaction.

The sorption isotherm of *nAg*-citrate nanoparticles on to leaf discs shows a linear slope of 1.4 ± 0.03 L/g which is comparable to the slope of sorption on to octadecane functionalized sorbent (1.4 ± 0.04 L/g). This can be due to the similar chemical nature of both the surfaces as the leaf surface contains cuticular layers consisting of wax layers which contain aliphatic carbon chains. But for the sorption of *nAg*-citrate on to leaf discs in the presence of HA the linear slope was 0.64 ± 0.04 L/g, which is lower than that for the sorption on to octadecane

surface (0.98 ± 0.04 L/g). This again shows that in the presence of HA, sorption of nanoparticles is not varying with respect to the chemical nature of the sorbent.

3.4.6 Comparing the sorption

Considering electrostatic forces, the zeta potential of nanoparticles in the presence and absence of HA was comparable for both types of nanoparticles (-44.3 ± 0.7 mV for *nAg*, -44.7 ± 1.4 mV for *nAg* HA, -66.7 ± 0.2 mV for *nAg* citrate, and -67.3 ± 0.5 mV for *nAg*-citrate HA), this suggests that the sorption does not depend solely on electrostatic forces. The slopes for the sorption in the presence of humic acid showed dependence on the BET specific surface areas of the sorbents, for both type of nanoparticles. The slopes obtained from isotherms of *nAg*-citrate and *nAg*-citrate HA sorption to the sorbent surfaces seem to increase with increase in specific surface areas of the sorbents (Figure S27 in SI).

Moreover there was a linear correlation, between the slopes obtained for *nAg*-citrate and bare *nAg* both in the absence (Figure 16A) and presence (Figure 16B) of humic acid. In the absence of HA the sorbents are arranged in the increasing order of polarity (from -C18 to -OH, Figure 16A) and in the absence of HA the sorbents are arranged in the increasing order of their specific surface area (from glass beads to silica gel, Figure 16B). These results confirm that in the presence of HA, the sorption of nanoparticles to sorbents depends mainly on sorbent surface area and, in the absence of HA, the sorption depends mainly on the surface chemistry of the sorbents irrespective of nanoparticle size, and preparation method.

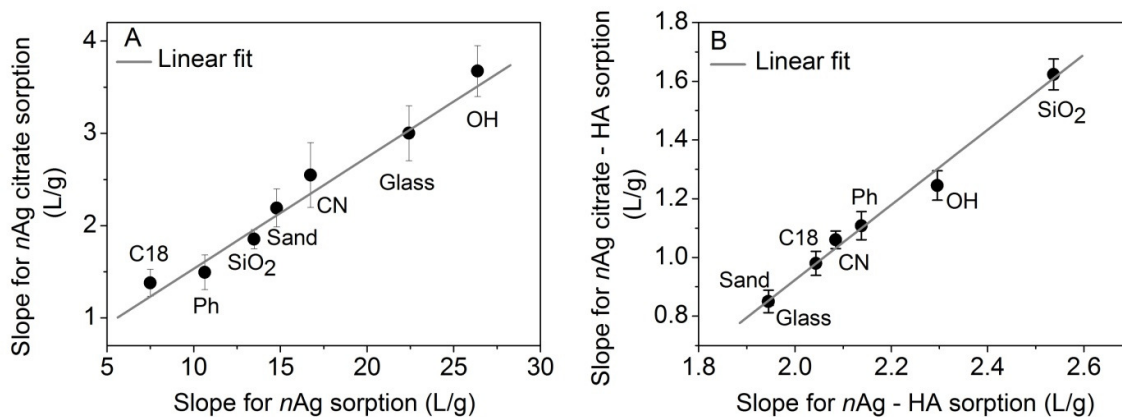


Figure 16. Correlation between the slopes obtained from the linear sorption isotherms for the sorption of citrate reduced silver nanoparticles and bare silver nanoparticles in the absence of HA (A) and in the presence of HA (B) to different sorbent surfaces

This study thus helps to understand the influence of humic acid in particle-surface interactions on the basis of sorption isotherms, thereby helping to assess the fate of nanoparticles in the environment. In natural environments containing unbound humic acid, a surface coating of nanoparticles and collector surfaces decrease nanoparticle sorption on to collector surfaces, irrespective of the collector surface chemistry thereby increasing the transport of nanoparticles.

3.5 Conclusion

In summary, the factors determining sorption behavior of nanoparticles are found to be different in the presence and absence of humic acid. In the absence of humic acid, the results show that the sorption is controlled mainly by the chemical groups present on the sorbent surface than the surface area available. In contrast, the presence of humic acid results in covering both the nanoparticle and sorbent surface with humic acid and thus the chemical specificity of the sorbents are getting masked. Thus in the presence of HA, the sorption of silver nanoparticles seems to be controlled mainly by the surface area of the sorbent, for the concentrations used in this study.

Comparing the sorption quantity for the sorption of silver nanoparticles in the presence and absence of humic acid, the results show that the amount of nanoparticle getting sorbed is higher in magnitude in the absence of humic acid for both type of silver nanoparticle suspensions studied. In the presence of humic acid, the sorbents surfaces are getting coated with humic acid as shown by AFM studies and thus there are less available sorption sites for nanoparticle sorption. Sorbent surfaces like SiO₂ having weak humic acid interactions (Figure14), show comparatively high sorption quantity for the sorption of both type of silver nanoparticles in the presence of humic acid. On the contrary, sorbent surfaces like Glass, having strong humic acid interactions (Figure 14) show low sorption quantity as shown in the schematic diagram (Figure 17).

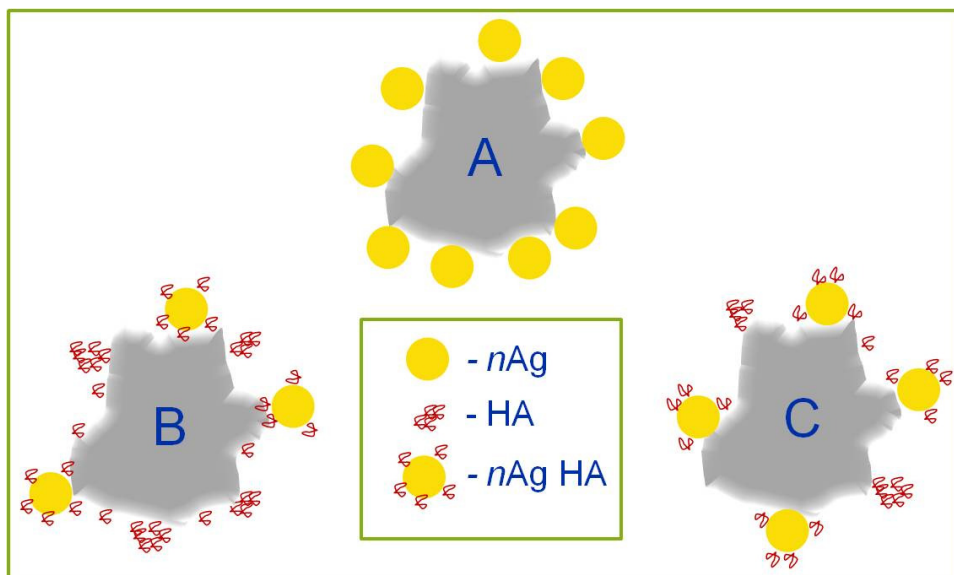


Figure 1. Thematic diagram showing the difference in sorption behavior of silver nanoparticles to different sorbent surfaces in the presence and absence of humic acid. Where, A : Sorption in the absence of humic acid, showing surface-nAg interaction, B: Sorption in the presence of humic acid and for the surfaces having strong HA-surface interactions, showing surface-HA-nAg and surface-HA interactions, and C: Sorption in the presence of humic acid and for the surfaces having weak HA-surface interactions, showing surface-nAg and surface-HA interactions.

However the nanoparticles undergo a wide variety of transformations in the environmental systems depending on the nature and coating of nanoparticle and also on the factors causing the transformation. Hence to gain a more general understanding about nanoparticle fate in environment we must investigate a larger set of suspensions in a similar way.

3.6 Supporting Information

Table S3: Langmuir and Freundlich parameters for the sorption of citrate reduced silver nanoparticles to the sorbents and statistical parameters for fitting.

Figure S15. Intensity-weighted hydrodynamic size distribution of the *n*Ag-HA suspension obtained by dynamic light scattering.

Figure S16. Time dependent particle size of *n*Ag-HA suspension.

Figure S17. AFM height (A, B) and adhesion (C, D) images of silver nanoparticle before (A, C) and after (B, D) humic acid treatment captured by $-\text{CH}_3$ modified probe in PFQNM mode.

Figure S18. Scaled adhesion force histogram for the adhesion between $-\text{CH}_3$ modified probe and chemically modified standard samples.

Figure S19. Scaled adhesion force histogram for the adhesion between $-\text{COOH}$ modified probe and chemically modified standard samples.

Figure S20. Sorption isotherms for the sorption of silver nanoparticle treated with humic acid (*n*Ag-HA) to model and environmental sorbents.

Figure S21. Calibration graph for the UV/vis absorbance of sodium humate solutions with respect to the determined TOC concentration.

Figure S22. Sorption isotherms for the sorption of humic acid to different model and environmental surface.

Figure S23. Time dependent particle size for n Ag citrate suspension in the presence (right) and absence (left) of humic acid.

Figure S24. Sorption isotherms for the sorption of citrate reduced silver nanoparticles to different model and environmental surfaces.

Figure S25. Sorption isotherms for the sorption of citrate reduced silver nanoparticles in the presence of HA to different model and environmental surfaces.

Figure S26. Variation of the slopes for the sorption of bare silver nanoparticles and citrate reduced silver nanoparticles in the absence of HA to the sorbent surfaces, with the specific surface area of the respective sorbents.

Figure S27. Variation of the slopes for the sorption of bare silver nanoparticles and citrate reduced silver nanoparticles in the presence of HA to the sorbent surfaces, with the specific surface area of the respective sorbents.

Table S3: Langmuir and Freundlich parameters for the sorption of citrate reduced silver nanoparticles to the sorbents and statistical parameters for fitting.

Sorbents	Langmuir parameters		Freundlich parameters		Langmuir fitting		Freundlich fitting	
	Langmuir coefficient (K_L) L/g	Adsorption maximum (Q_{max}) $\mu\text{g/g}$	Freundlich coefficient (K_F) ($\mu\text{g}^{(1-n)}\text{L}^n$)/g	Freundlich exponent (n)	Chi ²	R ²	Chi ²	R ²
OH func. surface	0.11±0.01	45.3±2.1	7.1±1.2	0.49±0.06	6.85	0.97	14.11	0.94
Glass bead	0.13 ± 0.01	34.0±1.8	5.9±0.9	0.45±0.05	1.03	0.99	3.90	0.96
Sand	0.06±0.02	63.3±9.1	5.9±1.5	0.60±0.09	0.50	0.99	0.83	0.99
Silica gel	0.03±0.01	81.7±12.4	3.3±0.6	0.73±0.07	0.80	0.99	0.99	0.98
CN func. surface	0.11±0.01	33.9±1.6	5.1±0.6	0.5±0.04	1.36	0.99	6.86	0.96
Ph func. surface	0.02±0.005	74.0±12.3	1.9±0.3	0.81±0.05	0.94	0.99	1.06	0.99
C18 func. surface	0.01±0.003	163.4±44.6	2.1±0.3	0.86±0.04	2.12	0.98	4.43	0.98

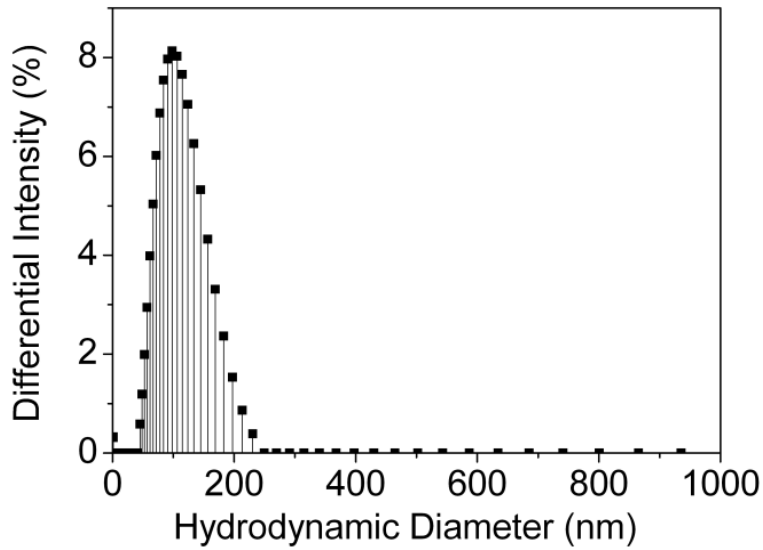


Figure S15. Intensity-weighted hydrodynamic size distribution of the *n*Ag-HA suspension obtained by dynamic light scattering

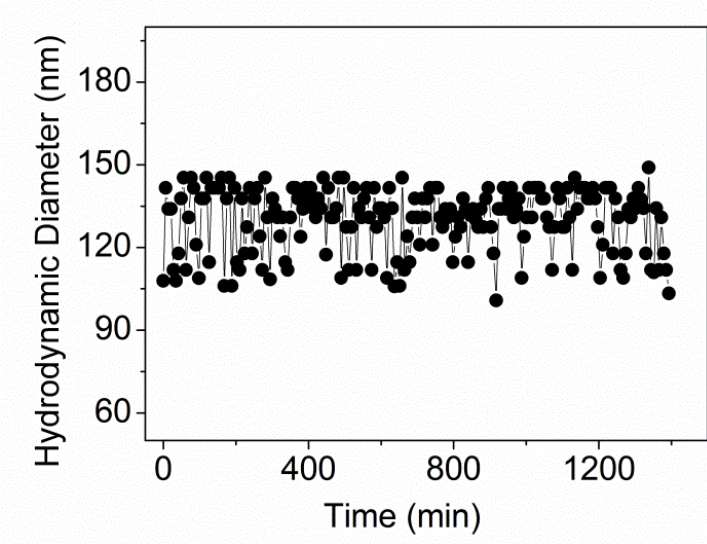


Figure S16. Time dependent particle size of *n*Ag-HA suspension.

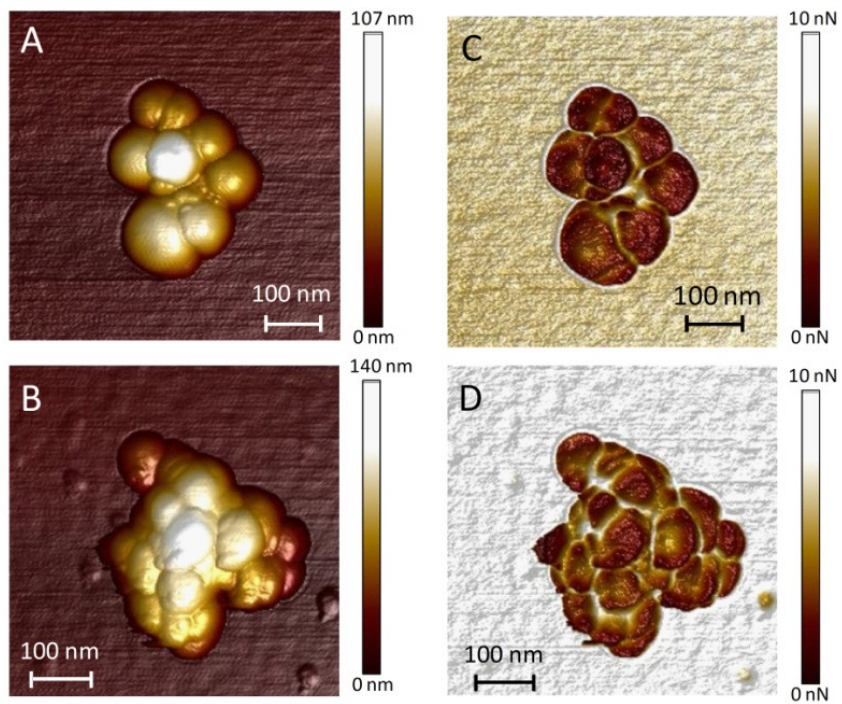


Figure S17. AFM height (A, B) and adhesion (C, D) images of silver nanoparticle before (A, C) and after (B, D) humic acid treatment captured by $-\text{CH}_3$ modified probe in PFQNM mode.

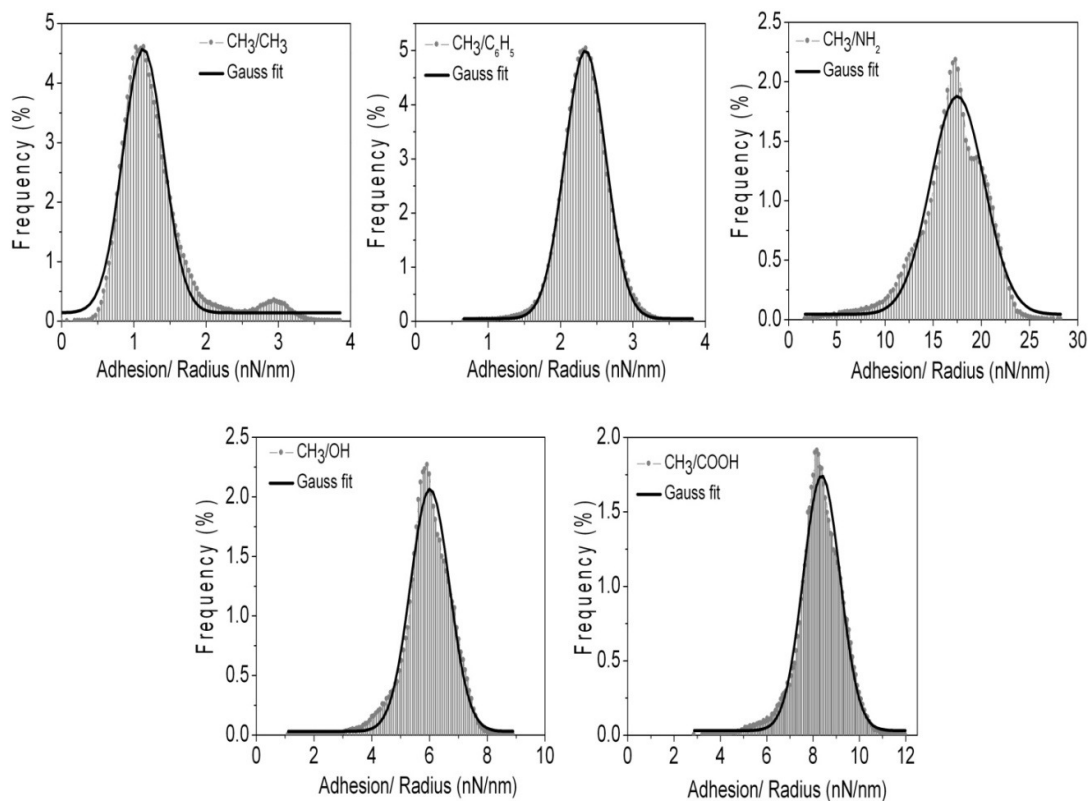


Figure S18. Scaled adhesion force histogram for the adhesion between $-\text{CH}_3$ modified probe and chemically modified standard samples. The solid black line represents the Gaussian fit.

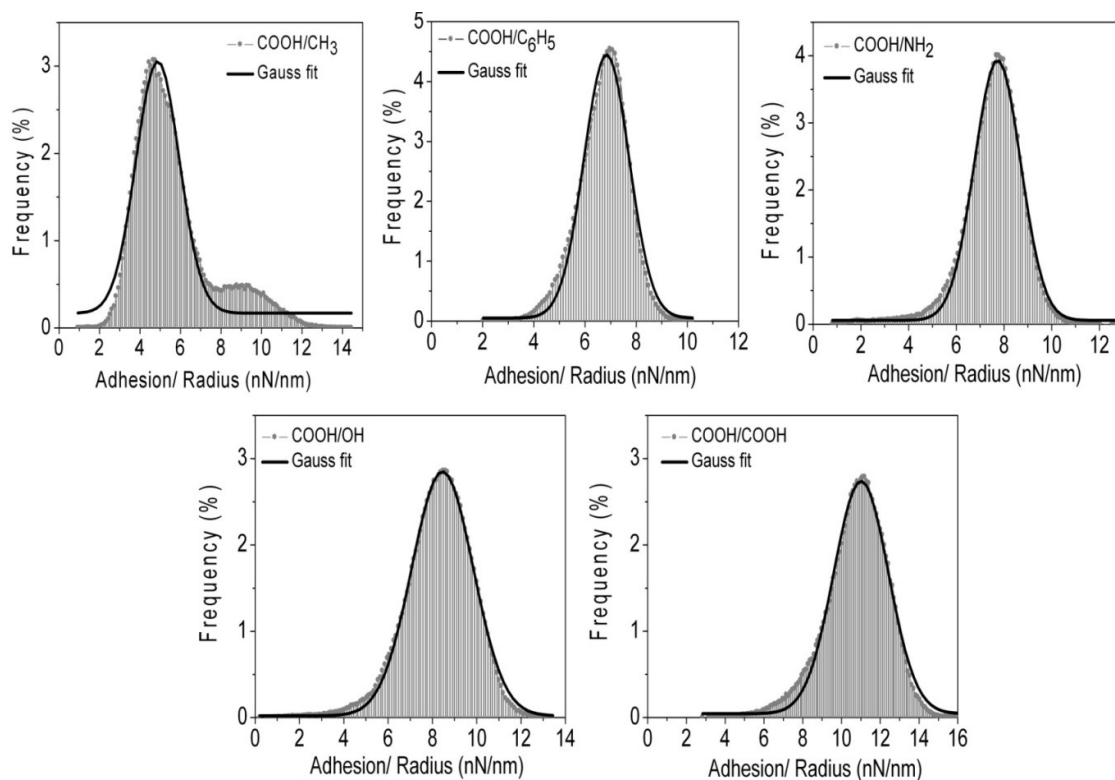


Figure S19. Scaled adhesion force histogram for the adhesion between -COOH modified probe and chemically modified standard samples. The solid black line represents the Gaussian fit.

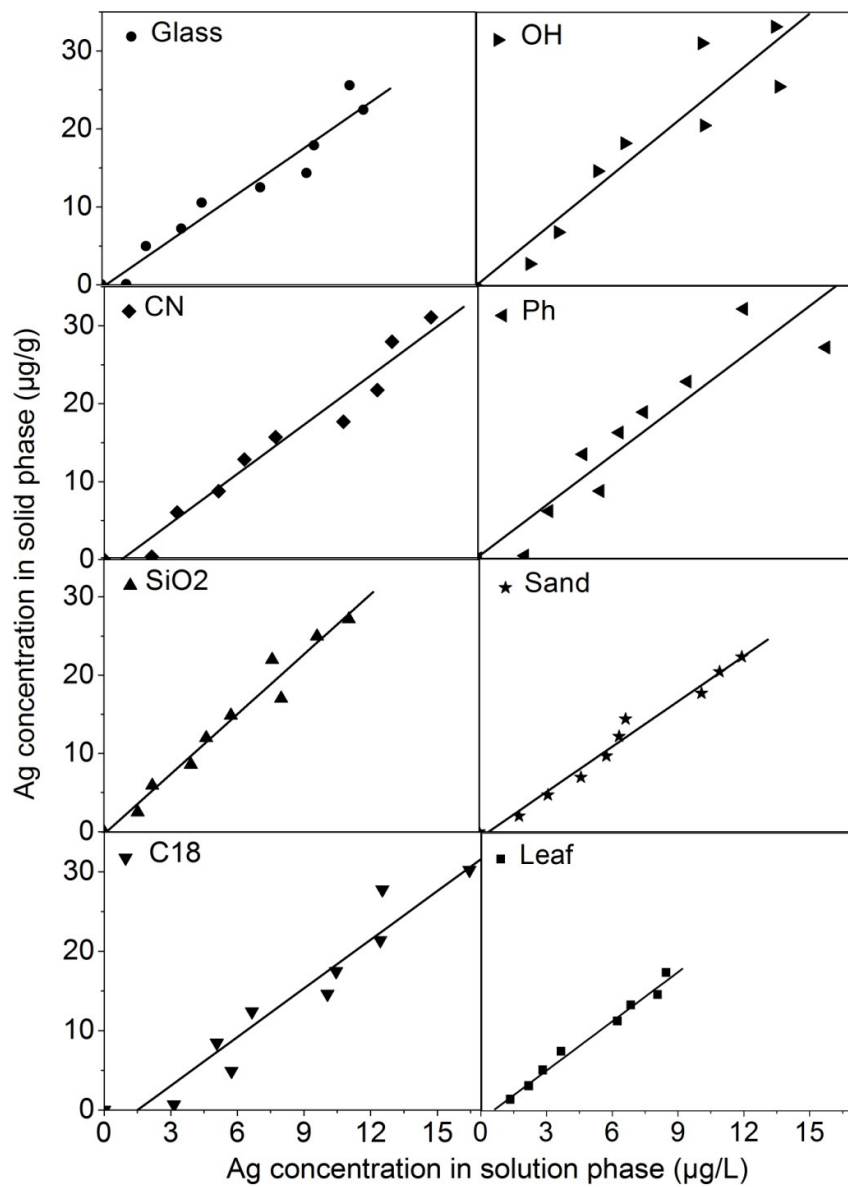


Figure S20. Sorption isotherms for the sorption of silver nanoparticle treated with humic acid ($nAg-HA$) to model and environmental sorbents.

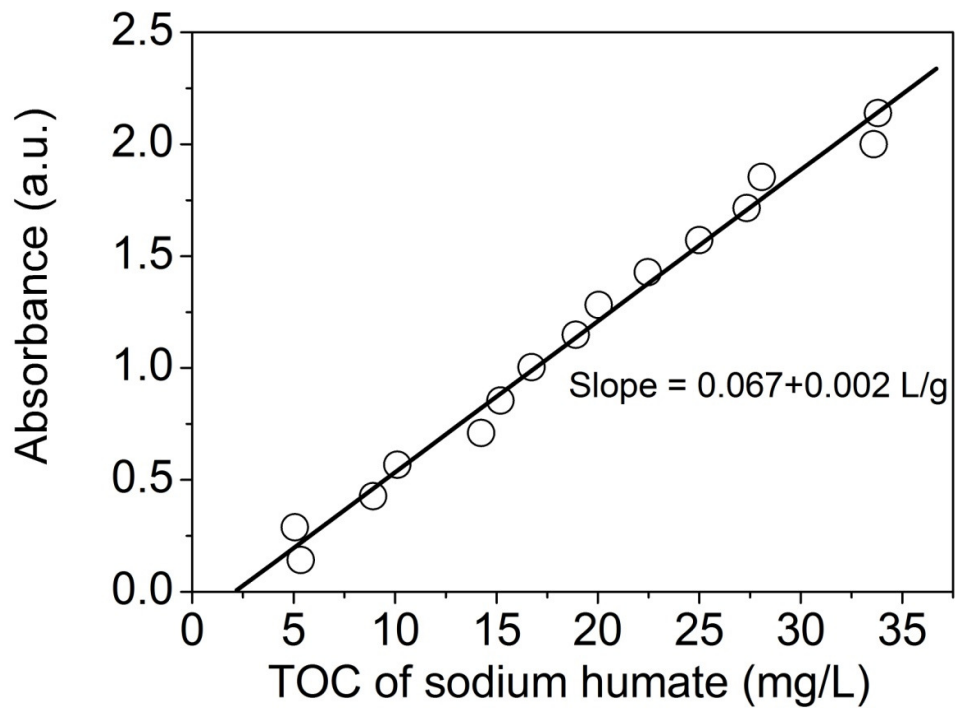


Figure S21. Calibration graph for the UV/vis absorbance of sodium humate solutions with respect to the determined TOC concentration.

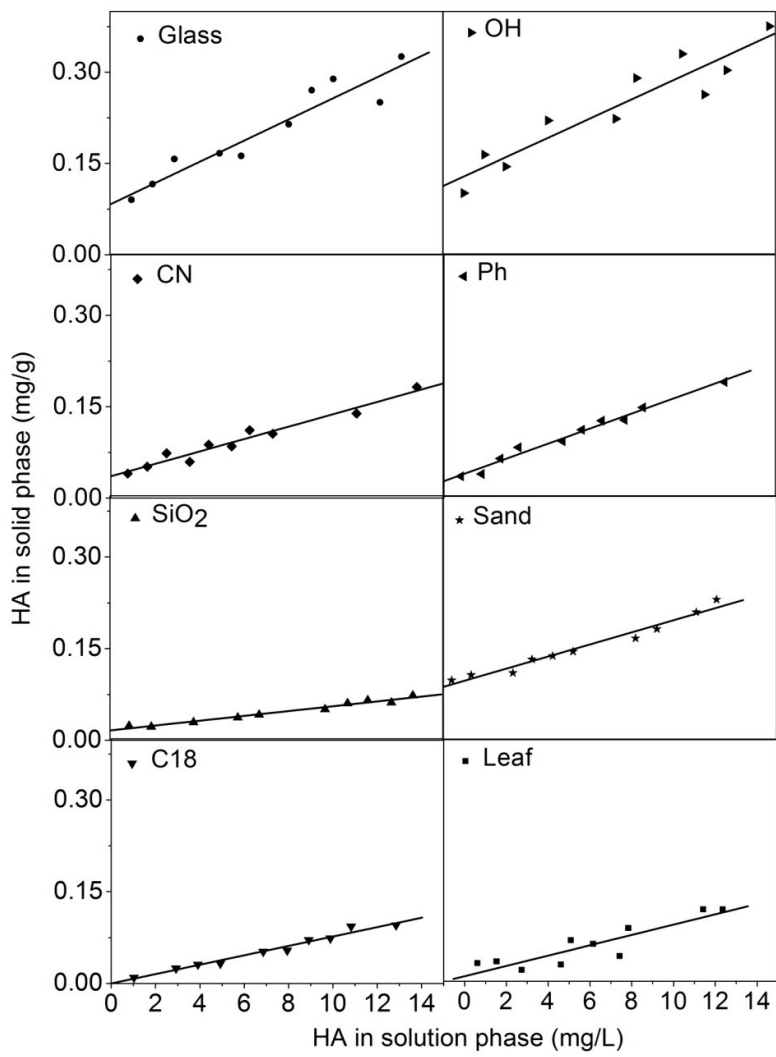


Figure S22. Sorption isotherms for the sorption of humic acid to different model and environmental surfaces.

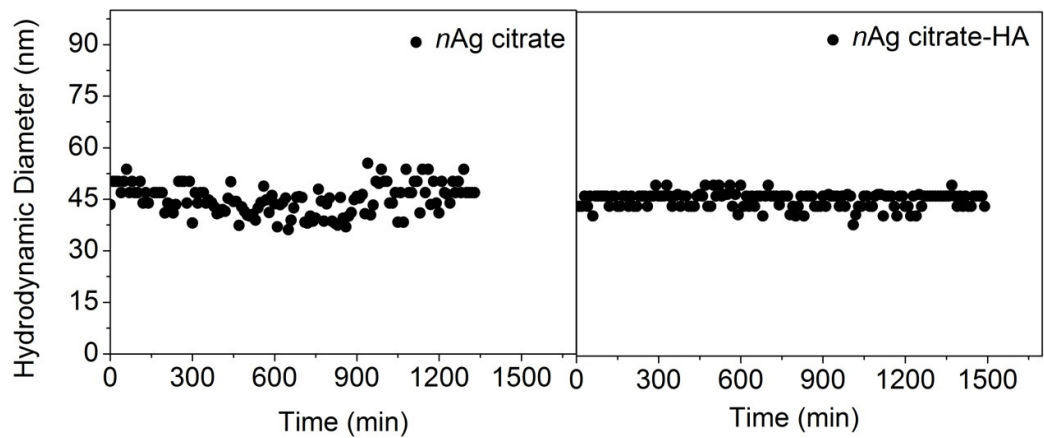


Figure S23. Time dependent particle size for *n*Ag citrate suspension in the presence (right) and absence (left) of humic acid.

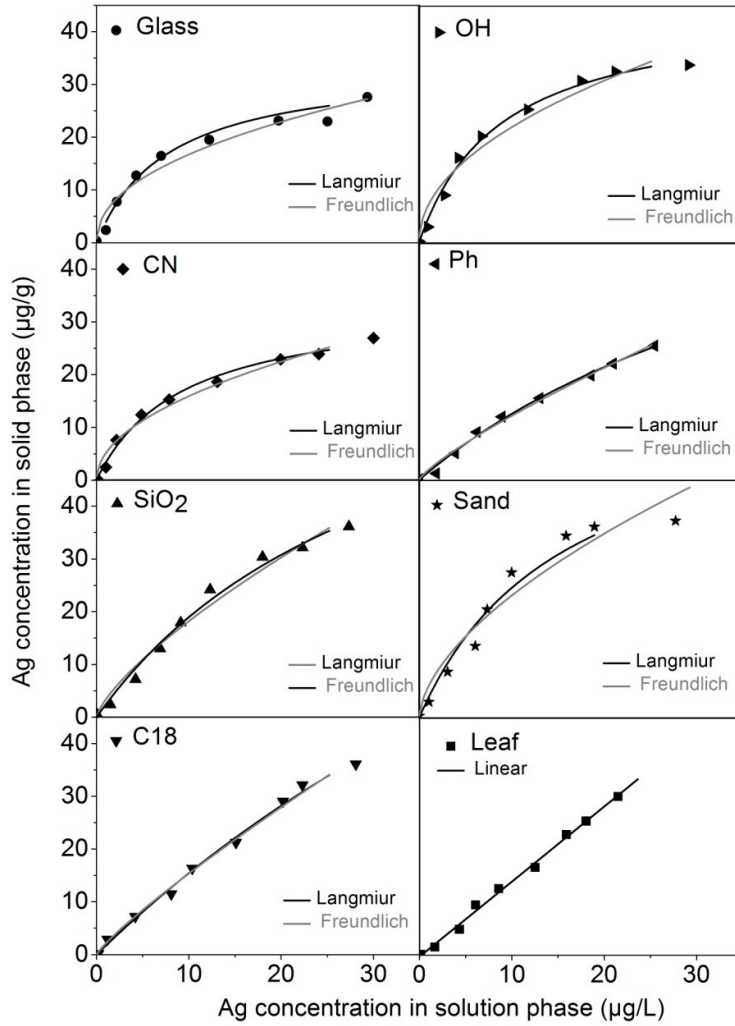


Figure S24. Sorption isotherms for the sorption of citrate reduced silver nanoparticles to different model and environmental surfaces.

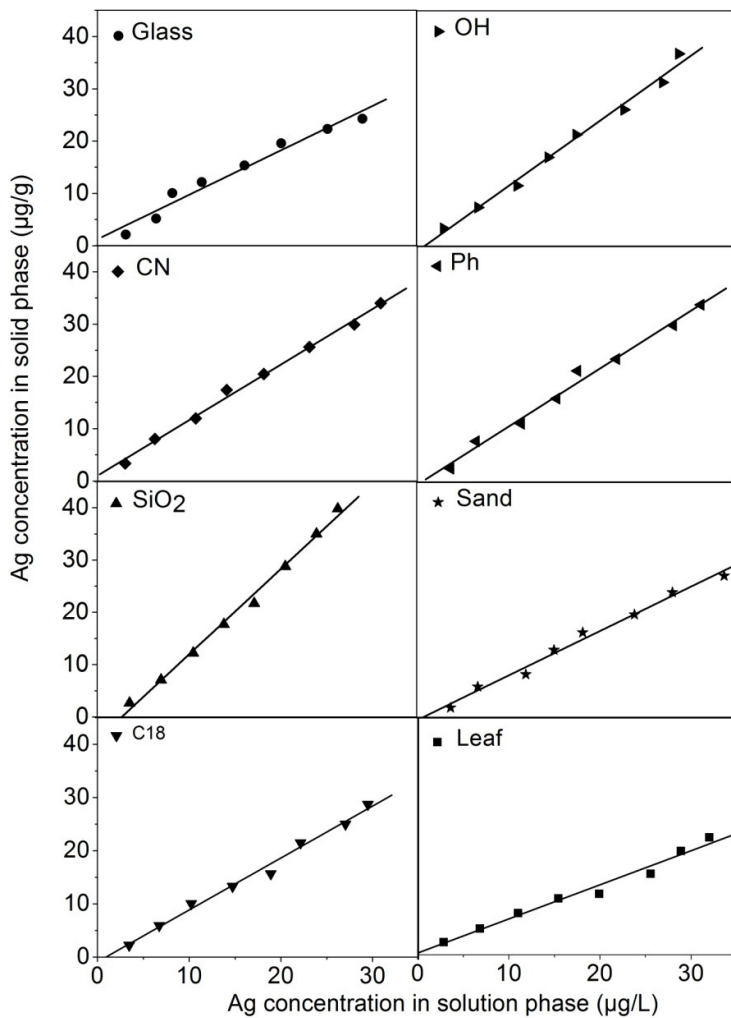


Figure S25. Sorption isotherms for the sorption of citrate reduced silver nanoparticles in the presence of HA to different model and environmental surfaces.

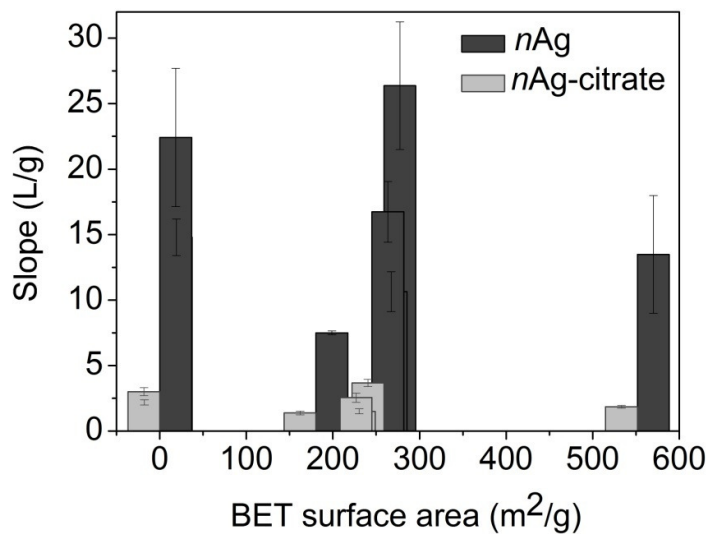


Figure S26. Variation of the slopes for the sorption of bare silver nanoparticles and citrate reduced silver nanoparticles in the absence of HA to the sorbent surfaces, with the specific surface area of the respective sorbents

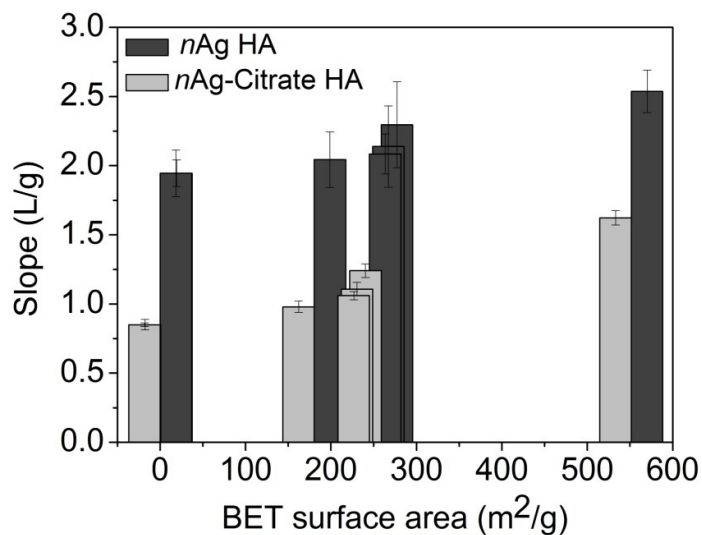


Figure S27. Variation of the slopes for the sorption of bare silver nanoparticles and citrate reduced silver nanoparticles in the presence of HA to the sorbent surfaces, with the specific surface area of the respective sorbents.

Chapter-4

Chemical Force Microscopy – A promising tool to analyze nanoparticle surface modifications

Priya Mary Abraham and Gabriele E Schaumann

4.1 Abstract

Characterization of nanoparticles for their surface properties is necessary to ensure reliable and reproducible results regarding the study of nanoparticle fate, transport, transformations and toxicity. Without such proper and accurate characterizations, there will be an unknown variability in different experimental conditions of nanoparticles. In this study the potential of chemical force microscopy (CFM), an AFM based technique, for the intricate characterization of nanoparticle surfaces has been evaluated. AFM probes with five different chemical modifications, undergoing different intermolecular interactions were used for CFM analysis and they were standardized with chemically functionalized standard surfaces to check the chemical sensitivity of each probe type. The nanoparticles used for CFM analysis were, bare silver nanoparticles (*nAg*), citrate coated silver nanoparticles (*nAg-citrate*), and humic acid coated silver nanoparticles (*nAg-HA*). The results demonstrate the capability of CFM to differentiate between different surface coatings. The results also showed the potential of differently modified probes to differentiate between polar or nonpolar interactions, and hydrophobic or hydrophilic interactions.

4.2 Introduction

The fate of ENPs in the environmental compartments depends on the transformations the nanoparticles undergo due to influences from the environmental conditions like pH, presence of organic matter, flow conditions and presence of other elements which can react with ENPs (Levard et al. 2012; Lowry et al. 2012; Lowry et al. 2012). There is an increased awareness of the need to understand the health, safety, and environmental impacts of ENPs in both their synthesized and environmentally transformed form (Baer et al. 2010). One of the main challenge in ENPs risk assessment in environmental systems are analysis and characterisation issues of nanoparticles (Tiede et al. 2008). There is a growing consensus on the importance of systematic and accurate characterization of nanoparticles on environmental media and

biological systems (Cong et al. 2011). Some of the current conflicting results from nanotoxicological tests could also be better explained if the adequate nanoparticle characterization results are available (Cong et al. 2011).

4.2.1 Need for nanoparticle surface analysis techniques.

There are many issues and challenges associated with characterization of nanoparticles. Subtle differences in synthesis, storage and processing can produce nanoparticles with different surface properties even if the material is same. With time nanoparticle properties may change in many ways including aggregation, growth, phase separation, oxidation, and absorbing contaminants (Baer 2011). The unique physical and chemical properties of nanoparticles differing from the respective bulk form, is due to its small size, which makes a large portion of the atoms in the nanoparticles to present at or near the surface of the particles. Hence it is important to put efforts in characterizing the nanoparticle surfaces and interfaces. The small size also makes it challenging to characterise the nanoparticles in the environmental compartments. The composition, structure, and physical/chemical nature of the nanoparticle surface plays an important role in determining the properties and performances of nanoparticles and its fate. The importance of nanoparticle surface chemistry in determining its fate and toxicity has been underemphasized in literatures (Karakoti et al. 2006). There is an increasing need for improved analysis methods, to characterize nanoparticle surface, including surface chemical analysis which can give important information to determine the fate of nanoparticles in the environment.

The main surface chemistry characterization techniques available for nanoparticle analysis are Auger electron spectroscopy (AES), X-ray photoelectron spectroscopy (XPS), Secondary Ion-Mass spectroscopy (SIMS), Atomic force microscopy, Vibrational spectroscopy, energy dispersive x-ray methods, low energy ion scattering techniques etc (Baer et al. 2010). All methods have their own advantages and disadvantages. Among these methods atomic force

microscopy is superior in terms of spatial resolution it can achieve. However characterization by a number of complementary analysis methods is important for adequate characterization of nanoparticles.

4.2.2 AFM for nanoparticle surface characterisation

Atomic force microscopy (AFM) is a powerful imaging technique, which enabled many major advances in nanotechnology. The heart of an AFM is a sharp tip mounted on a cantilever (together called probe), that interacts with a sample surface at a distance of atomic dimensions (Eastman et al. 1996). AFM cantilevers and tips are critical elements for obtaining reliable, high-resolution data (Muller et al. 2007) and they are generally made of silicon or silicon nitride using micro fabrication techniques. This technique can provide both qualitative and quantitative information including nanoparticle size, surface morphology, surface texture and surface roughness. These parameters are obtained from the interaction force with the sample, sensed by the tip as it scans across the surface. Depending up on the made of AFM either the probe or the sample will be mounted on a piezoelectric scanner which ensures 3D positioning with high accuracy. The interaction forces are measured by the deflection of cantilever as the tip scans the surface, which is detected by a laser beam focused on the free end of the cantilever and reflected into a photo diode. Additionally evaluation of force-distance curves between the surfaces and AFM probe provides nano-mechanical properties of the respective surfaces, in nano meter resolution. To obtain force-distance curves, the cantilever deflection is recorded as a function of vertical displacement of the scanner as the tip is pushed towards the sample and retracted (Dufrene 2008). This cantilever deflection versus scanner displacement curve can be transformed into a force-distance curve using appropriate corrections (Dufrene 2008). Different AFM imaging modes are available, which differ mainly the way the tip is scanning across the sample. The pulsed-force mode of AFM, in which AFM cantilever is oscillated and taps the surface periodically, enabled

adhesion and stiffness properties to be calculated at each point on a surface rapidly (Marti 1997). An extension of pulsed-force mode with improved force resolution and noise reduction is PeakForce Quantitative Nanomechanical Mapping mode, developed by Bruker AXS, CA, USA (Young et al. 2011). With this mode real time calculation of mechanical properties like, Adhesion, Young's modulus, deformation etc. at each surface contact can be done. can be done (Young et al. 2011).

4.2.3 Chemical force measurements for nanoparticle surface characterisation

However, the utility of the standard AFM setup for measuring specific forces is severely limited by the unknown chemical composition of the AFM tip. The normally used, silicon and silicon nitride probes has a poorly defined chemical interface, also the chances of contamination is high for them (Noy 2006). Lieber and coworkers introduced chemical force microscopy (CFM), which replaces poorly characterised tip-sample interface with a defined interface produced by deliberate functionalisation of AFM tip and sample surface (Frisbie et al. 1994). Thus CFM can measure specific well defined chemical interactions (Okabe et al. 2000). By detecting interaction forces between chemically modified tip and sample surface, it becomes possible to discriminate chemical inhomogeneities on the sample.

Researchers have used CFM for a number of applications including adhesion and friction measurements, as well as high resolution imaging (vezenov et al. 2005; Noy et al.1997). Fundamental CFm experiments with functionalized tips and samples in ethanol medium showed the capacity of CFM to discriminate interactions between polar and apolar groups (Frisbie 1994; Noy 1995). Also, hydrogen bonding $-\text{COOH}$ groups show stronger adhesion compared to $-\text{CH}_3$ groups which can only interact through van der Waals interactions. All these fundamental experiments were conducted in different solvents (Noy et al.1997). CFM is also used in investigation the double layer interactions in aqueous solutions. By monitoring the adhesion force with an ionizable AFM probe, researchers

detected changes in surface charge induced by the dissociation of acidic (COOH) or basic (NH₂) groups on the surface (Vezenov et al. 1997).

CFM has found its application throughout physical and life sciences. In life science it has been used to map the hydrophobicity of live cells to understand their role in mediating different cellular events (Dague et al. 2007). In polymer systems, CFM is used widely to characterise chemical heterogeneities of the polymer coatings. Chemical force microscopy has been already used in literatures to characterize nanoparticle surface, by attaching the particles to the tip and then scanning the tip to chemically modified surfaces (Yang et al. 2002). However there was no study till date done to analyse nanoparticle surface using chemically functionalized probe. Force measurements carried out on ambient air are more difficult to interpret since capillary forces are usually 1-2 orders of magnitude higher than specific chemical interactions (Noy et al. 1997). Moreover capillary condensation will emphasize relative degree of wettability and can be a basis for discrimination between hydrophilic and hydrophobic groups when imaging under ambient conditions (Wilbur et al. 1995).

In this study the potential of chemical force microscopy in characterising differently coated and stabilized silver nanoparticles is illustrated using a set of AFM probes with different chemical functionalizations.

4.3 Materials and methods:

4.3.1 Nanoparticle suspensions and AFM sample preparation:

Three different kinds of nanoparticle suspensions were used for the CFM analysis: (1) non coated silver nanoparticles (*nAg*), (2) silver nanoparticles coated with humic acid (*nAg*-HA), and (3) citrate ion coated silver nanoparticles (*nAg* citrate). Bare silver nanoparticles were purchased as powder form from io-li-tec (Ionic Liquid Technologies, Germany). According to the manufacturer, they were produced using plasma chemical vapour deposition (CVD)

and the primary particle size of the nanoparticles was 35 nm. Aqueous nanoparticle suspension was prepared from the powder by following a standard protocol using ultrasonic processor without stabilizing agent (Taurozzi et al. 2010). The suspension was prepared using Milli Q water and the pH of the suspension was 6.4. Humic acid coated silver nanoparticles were also prepared from the same bare silver nanoparticle powder but while making the aqueous suspension, ultrasonic processor was used with sodium humate solution (5 mg/L) as a stabilizing agent. Water soluble sodium humate powder (HUMINS 775) extracted from natural oxidized lignite was purchased from Humintech GmbH, Germany. The pH of the suspension after preparation was 7.5. Citrate reduced silver nanoparticles were synthesized by reducing silver nitrate (AgNO_3 , Aldrich) with trisodium citrate solution (5mM, Aldrich) at a pH of 11 by following a standard synthesis procedure (Dong et al. 2009).

For AFM measurements, samples were prepared on freshly cleaved mica substrate. To facilitate the binding of nanoparticles on to mica surface, the mica is modified using poly-lysine by following a standard protocol (McNeil et al. 2011). This treatment leads to the formation of positively charged clusters on the mica surface (Niemeyer et al. 2006) and make it possible for negatively charged nanoparticles (zeta potential for $n\text{Ag} = -44.3 \pm 0.7$ mV, for $n\text{Ag HA} = -44.7 \pm 1.4$ mV, and for $n\text{Ag-citrate} = -66.7 \pm 0.2$ mV) to bind to the mica surface.

4.3.2 AFM measurements:

Atomic force microscopy (AFM, Veeco Nanoscope V, Bruker Corporation) images were captured using Peak Force Quantitative nanomechanical mapping (PFQNM) mode. PFQNM is a patent pending AFM mode developed by Veeco in which high resolution mapping of mechanical properties is possible (Pittenger et al.). In this mode the probe and the sample are intermittently brought together to contact the surface for a short period of time, which helps to eliminate lateral forces. The peak force during the probe-sample interaction period is kept constant by the system feedback and it is termed as feedback set point.

During PFQNM scanning, the piezoelectric scanner pushes the probe tip towards the sample and as the tip approaches the surface, the cantilever is pulled down toward the surface by attractive forces like van der Waals, capillary and electrostatic forces. The piezoelectric scanner pushes the probe further until peak force set point is reached and then the probe starts to withdraw from the sample surface. Probe tip breaks free off the sample at maximum adhesion point and the force corresponding to this point is adhesion force (Pittenger et al.). This measurement takes place at each tip-sample contact point and a force-distance curve (figure 18) is generated at each pixel point in an image.

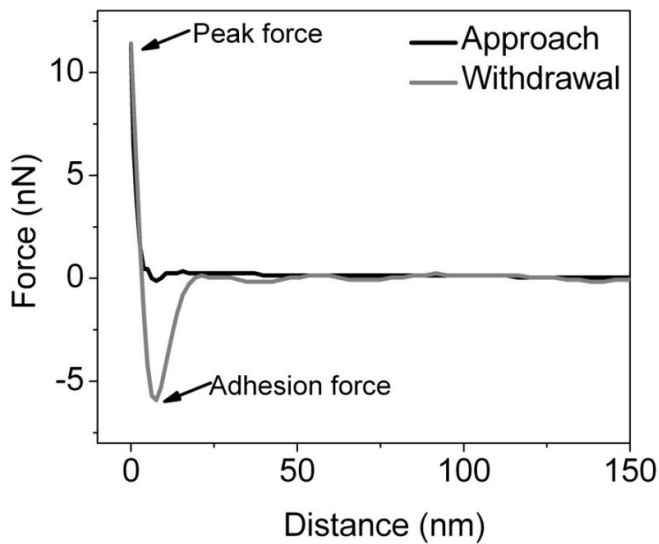


Figure 18. Force distance curve.

The peak force setpoint is a user input value which represents the imaging force and which determines the magnitude of tip-sample interactions (BrukerCorporation 2011). As the applied peak force setpoint increases, the AFM tip will be forced to remain in contact with the sample surface till it experience the peak force. This will in turn increase the contact time between the tip and the sample and thus the adhesion force will shift to higher values (Drelich 2005). Peak force setpoint was kept constant (5 nN) for all the measurements, since adhesion force showed dependence on the setpoint value (figure 19). Adhesion force histogram showed a shift in adhesion force values with increased peak force setpoint (figure 19).

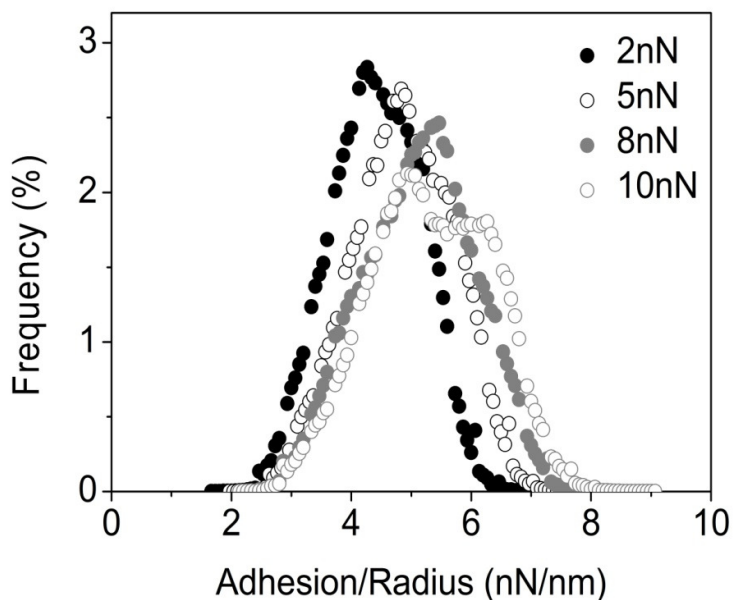


Figure 19. Dependence of Adhesion force values on peak force setpoint: Scaled Adhesion force histogram of $-NH_2$ functionalized surface scanned by $-OH$ functionalized probe, with 5 different peak force setpoints (2nN, 5nN, 8nN, and 10nN). The sample position scanned was exactly the same ($2\ \mu\text{m} \times 2\ \mu\text{m}$ area) with all the setpoints and 2,62,144 force values, with each peak force setpoint measurements were analyzed for adhesion force histogram.

The atmospheric humidity is known to have influence on Adhesion force measurements (Jang et al. 2007; Farshchi-Tabrizia et al. 2008). Hence All AFM measurements were carried out in the air at constant humidity of 28-29 %. This humidity is acquired in the AFM sample chamber by using silica gel and anhydrous CaCl_2 (Sigma-Aldrich). Adhesion force is known to have a dependence on the radius of the tip used for scanning and hence dividing the adhesion force by tip radius to get the scaled adhesion forces (F/R) is a common approach (Sugawara et al. 1993; Seog et al. 2002; Poggi et al. 2005). This approach is followed in this chapter to represent adhesion force.

10-15 nanoparticles were captured and analyzed from each nanoparticle suspension using NanoScope software. To avoid the surface morphology artifacts at the edge of the nanoparticles, the adhesion force values at the middle of the nanoparticle surface (20x20 pixels) were considered to plot adhesion force histograms (Paredes et al. 2000). Thus 400

force-distance curves were analyzed from each nanoparticle surface and each adhesion force histogram contains 4000-6000 adhesion force values.

4.3.3 Chemical force microscopy

Chemically modified AFM probes, purchased from NanoAndMore GmbH, Germany were used for nanoparticle analysis in PFQNM mode. The chemical modifications used were -C18 (ST-PNP-CH3) modification, -C₆H₅ (ST-PNP-C6H5) modification, -NH₂ (ST-PNP-NH2) modification, -OH (ST-PNP-OH) modification, and -COOH (ST-PNP-CO2H) modification. According to the manufacturer the probes were modified with specific functional groups using self assembled monolayers of thiols on gold (NanoAndMoreGMBH). The thiol molecules used for each modification were 1-Octadecanethiol for -C18 probe, 2-Phenylethanethiol for -C₆H₅ probe, 11-Amino-1-undecanethiol for -NH₂ probe, 11-Mercapto-1-undecanol for -OH probe, and 1-Mercaptoundecanoic acid for -COOH probe respectively (figure 20).

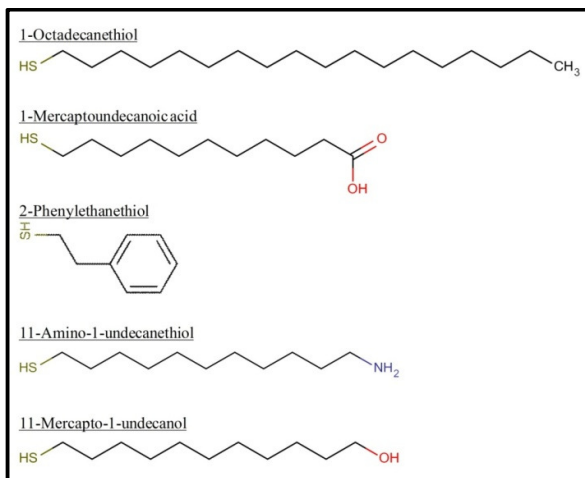


Figure 20. Thiol molecules used for the modification of AFM probes and standard surfaces.

The probes were calibrated prior to the measurement to find out tip radius and spring constant and the results are shown in table 1.

Probe	Tip radius (nm)	Spring constant (N/m)
-C18	6.1	5.6
-C ₆ H ₅	4.0	4.8
-NH ₂	3.02	1.3
-OH	4.5	5.2
-COOH	2.6	6.7

Table 1. Calibrated tip radius and spring constant of the surface functionalized probes used to image nanoparticle surfaces.

AFM probes were standardized for their chemical specificity using chemically modified standard surfaces (NanoAndMore GmbH, Germany) which can undergo defined intermolecular interactions. The chemical modifications were same as that with the probes: -C18 (ST-Si-CH₃) modification, -C₆H₅ (ST-Si-C₆H₅) modification, -NH₂ (ST-Si-NH₂) modification, -OH (ST-Si-OH) modification, and -COOH (ST-Si-CO₂H) modification. These standard surfaces are gold coated silicon wafers on with the thiol groups are chemically attached via gold-thiol linkage. From each sample surface 5 different positions with 2 μm x 2 μm size were scanned and analyzed. Adhesion force histograms for each surfaces were plotted with the force values (13,10,720 numbers) obtained from the whole scanned area. Only one tip per type has been used for the measurements, since slight change in tip properties will have effect on adhesion force measurements and its difficult to get two tips with exact same properties.

4.4 Results and discussion.

4.4.1 Standardisation of AFM probes:The AFM probes were checked for their chemical specificity using chemically modified standard surfaces. Average surface roughness obtained

for surfaces with each probe are given in table 2. For -C18 modified surface, the surface roughness was between 5-10 nm, but for all the other surfaces, the roughness value was between 1-3 nm.

Tip Sample	-C18	-C ₆ H ₅	-NH ₂	-OH	-COOH
-C18	5.7±0.8 nm	5.3±0.6 nm	6.0±0.8 nm	5.0±0.5 nm	10.3±1.2 nm
-C ₆ H ₅	1.6±0.1 nm	1.9±0.1 nm	2.0±0.1 nm	1.6±0.04 nm	1.7±0.1 nm
-NH ₂	2.0±0.2 nm	2.1±0.1 nm	1.8±0.1 nm	1.8±0.1 nm	1.6±0.1 nm
-OH	2.1±0.1 nm	2.8±0.3 nm	2.1±0.1 nm	2.3±0.1 nm	1.8±0.1 nm
-COOH	2.1±0.1 nm	2.5±0.2 nm	2.5±0.1 nm	2.5±0.1 nm	2.2±0.1 nm

Table 2. Average surface roughness of chemically modified, standard surfaces imaged with chemically modified probes. The error represents the standard deviation from five images.

The higher surface roughness in the case of -C18 modified sample, compared to others may be due to some defects (pits) or aggregates of molecules present on the surface (Kim et al. 1992). Moreover -C18 modified surface has the thiol molecule (1-Octadecanethiol, C 17 spacer) with larger molecular length used for chemical modification among all samples. Chemical modifications on the probes do not seem to have any effect on the surface roughness values on the sample surface except for -C18 modified surface.

Figure 21 shows representative height and Adhesion images of the chemically modified, standard sample surfaces when imaged with -C18 modified probe. Height images of all the samples appear similar but there is a clear change in adhesion images due to different chemical interactions. All other probes show similar results where height images were identical and adhesion images show clear differences. To study these interactions in detail, scaled adhesion force histograms were plotted for each standard sample/probe interactions.

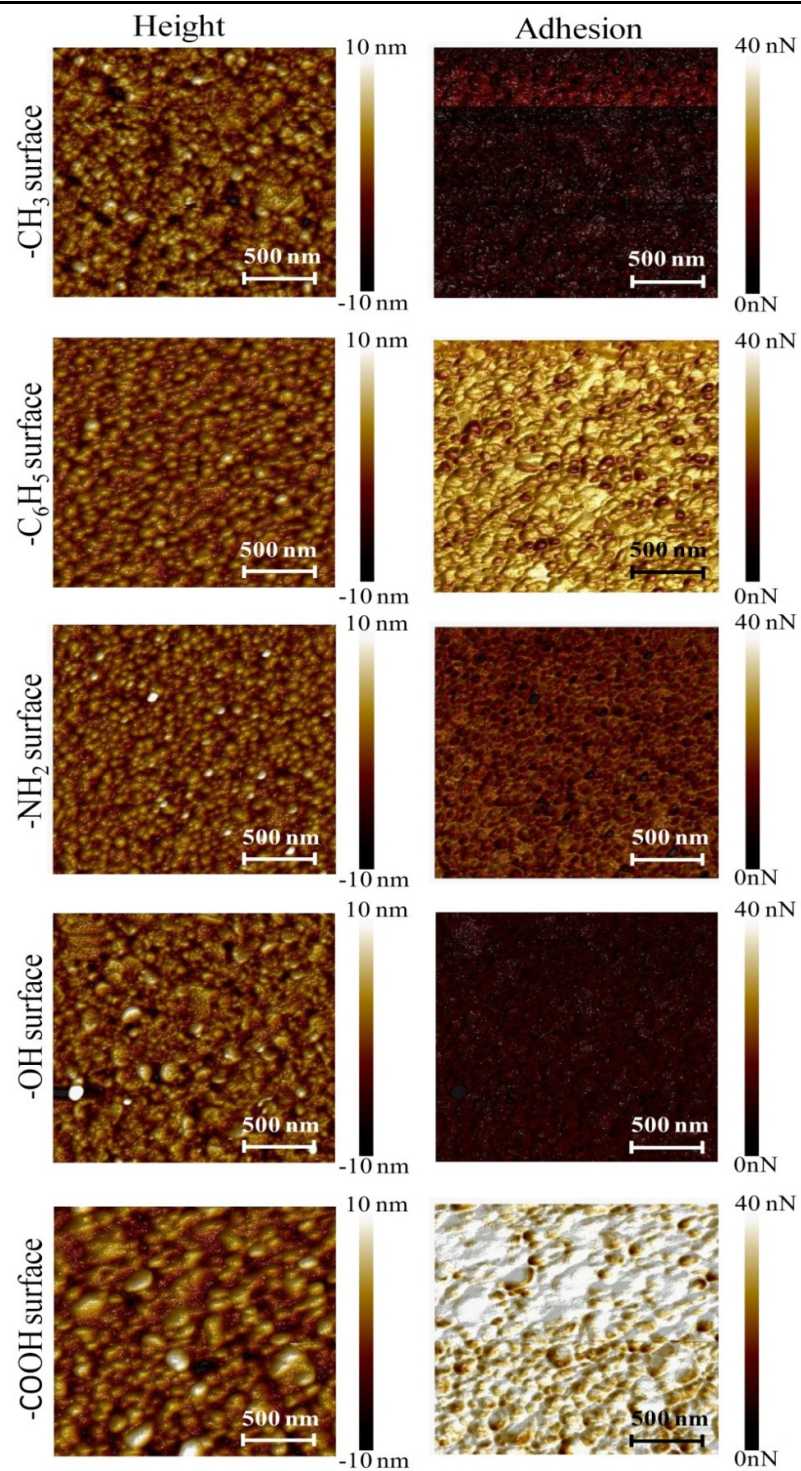


Figure 21. Height and adhesion images of all chemically modified surfaces scanned with $-\text{C18}$ modified probe.

Figure 4, 5, and 6 shows the histogram for the adhesion between the standard surfaces and -C₆H₅ modified probe, -NH₂ modified probe, and -OH modified probe, respectively. For -COOH and -C18 modified probes the histograms are showed and explained in earlier chapter (Figure S18 and S19).

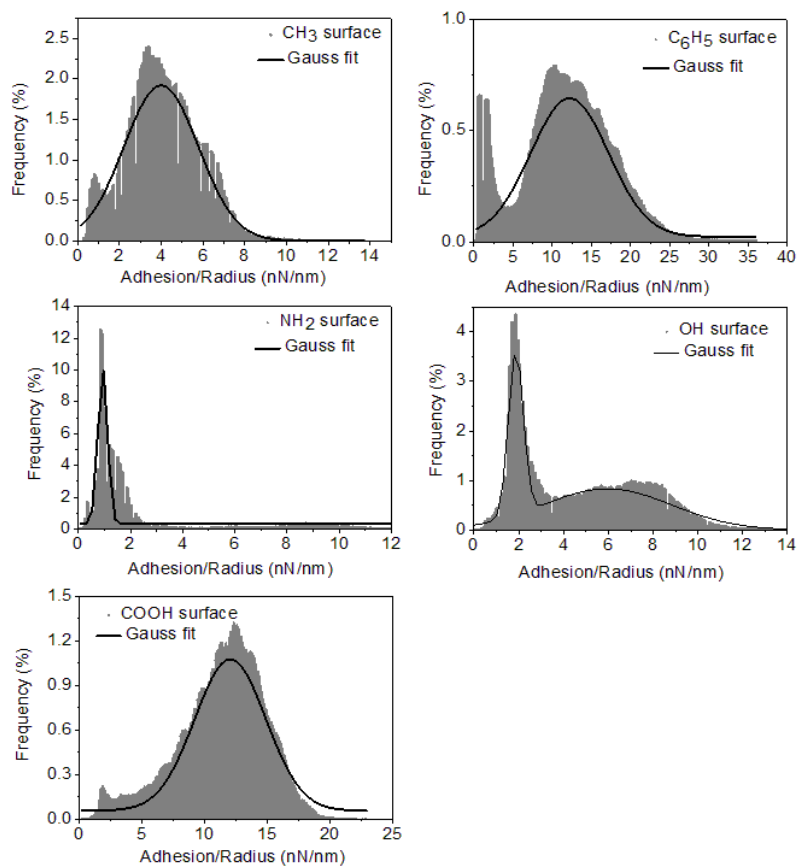


Figure 22. Scaled adhesion force histograms for the adhesion of -C₆H₅ modified probe with the standard surfaces.

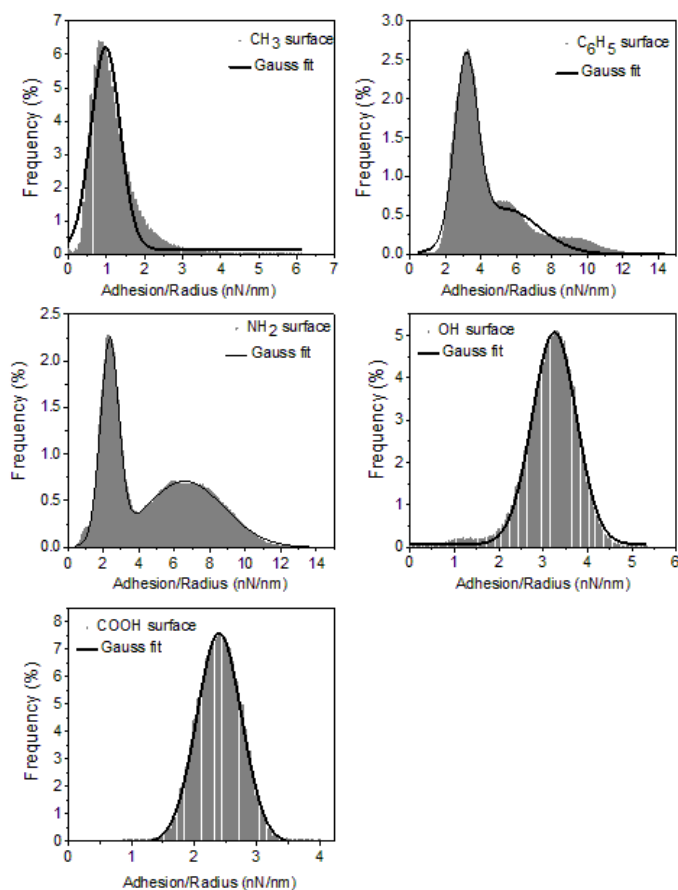


Figure 23. Scaled adhesion force histograms for the adhesion of $-NH_2$ modified probe with the standard surfaces.

Histograms for all probe - sample interactions were either monomodal or bimodal. The reason behind the bimodal distribution is not fully clear, however, this may be due to the heterogeneous sample surface which can arise due to some patches or pits resulted from molecular aggregates present on the surface (Kim et al. 1992). This may also depend on the molecular chain length of the molecules used for the surface functionalisation, showing more aggregates for high chain length molecule. In addition water molecules can also form patches on the surfaces causing increased adhesion force due to the contribution from capillary water bridges (Malotky et al. 2001). The AFM measurements were carried out in the presence of 28-29 % relative humidity and so the sample and tip was not in a fully dried condition. Hence

there is a possibility of forming water molecular layers on the sample as well as on the tip, especially for the surfaces having polar functional groups.

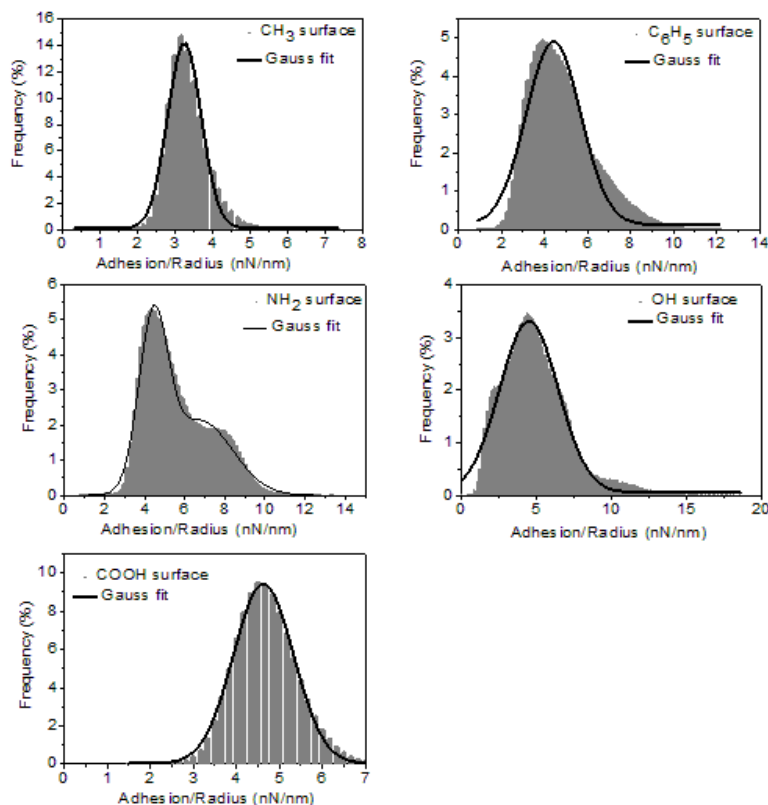


Figure 24. Scaled adhesion force histograms for the adhesion of $-OH$ modified probe with the standard surfaces and their Gaussian fit.

With phenyl functionalized probe also a bimodal distribution was observed (figure 22), although phenyl is not a polar group. One of the reasons for the two force values for all interactions involving phenyl group can be predicted as the different conformations possible for the molecule. Ten conformations are possible for 2-Phenylethanethiol (thiol molecule used for $-C_6H_5$ modification) and their energies are given in table 3. The conformer structures were drawn and the energies were calculated using MarvinSketch software (MarvinSketch 6.2.0).

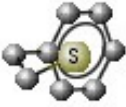
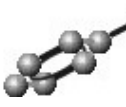
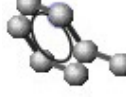
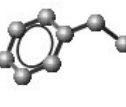
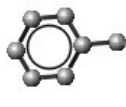
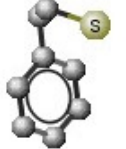
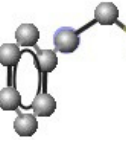
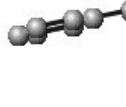
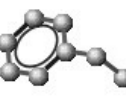
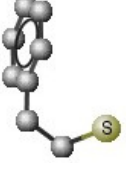
17.62 kcal/mol 	17.66 kcal/mol 	17.69 kcal/mol 	17.7 kcal/mol 	17.78 kcal/mol 
17.78 kcal/mol 	17.83 kcal/mol 	17.91 kcal/mol 	17.91 kcal/mol 	17.95 kcal/mol 

Table 3. Different conformations possible for 2-Phenylethanethiol molecule and the corresponding energies.

Considering all the conformations, it can be predicted that when the molecule gets attached to the AFM probe tip, it can orient exposing the phenyl ring sidewise (figure 25A), or exposing the phenyl ring endwise (figure 25B).

In the sidewise orientation, the whole phenyl ring interacts with the sample surface, while in endwise orientation only the end atom interacts with the sample surface. The interaction forces will be different in both cases. The bimodal histogram indicates the presence of both molecular orientations in one tip, one having lower interaction force than the other. The chemical group present on the sample surface seems to determine the preferable orientation of phenyl group.

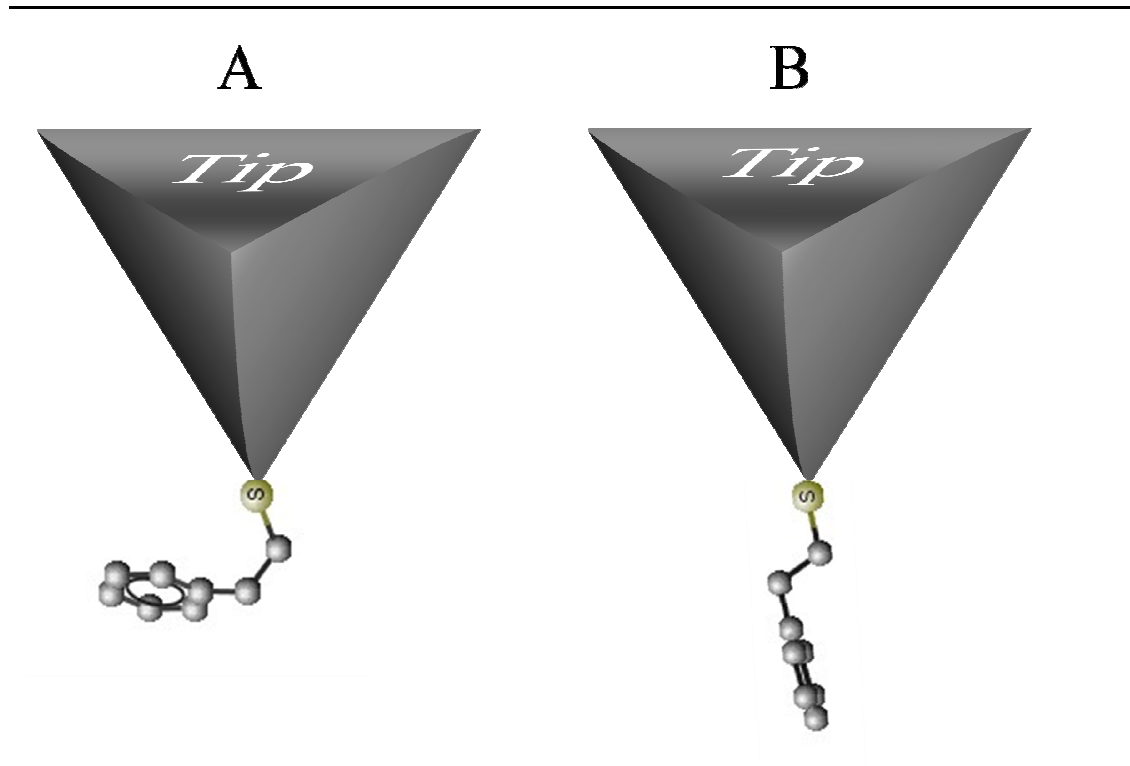


Figure 25. Graphical representation showing the possible orientations of phenyl ring on the AFM probe tip. There will be a number of such thiol molecules in one modified probe.

The adhesion force value obtained from the Gaussian fit was considered as the average adhesion force for each interaction (figure 26). The tip-sample interaction forces seem to vary in accordance with the intermolecular interaction strengths between the functional groups, except for phenyl functionalized surfaces and tips.

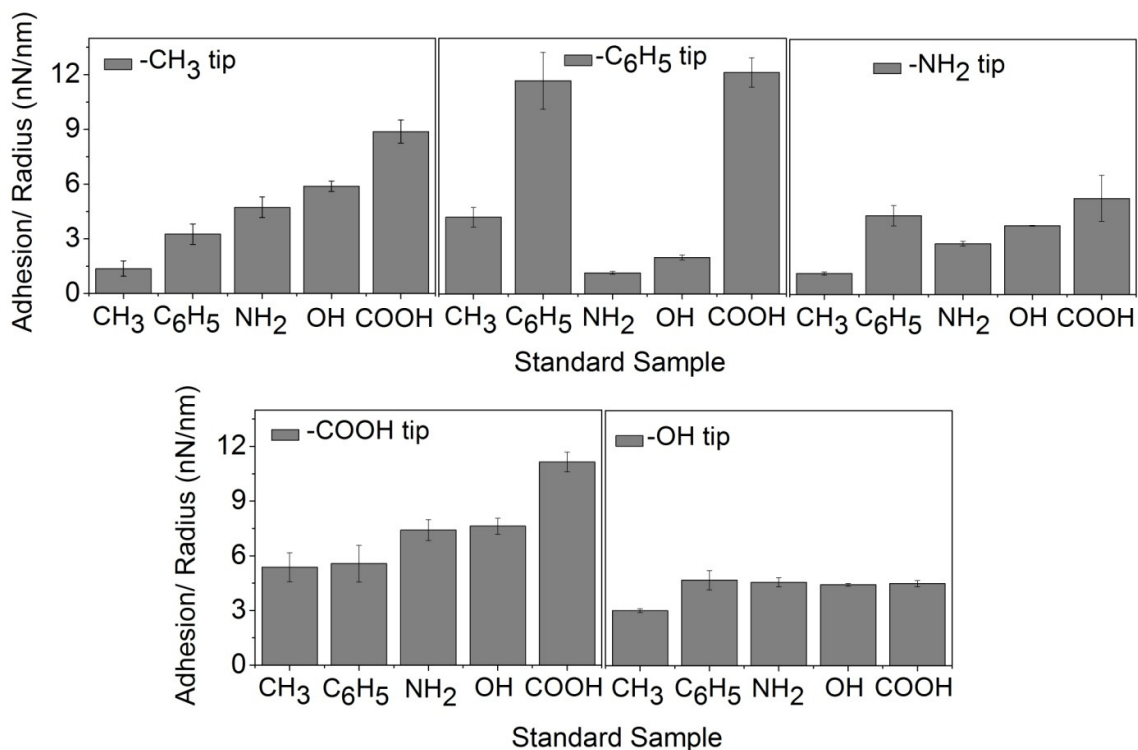


Figure 26. scaled adhesion force between the chemically modified surfaces and probes measured by AFM in PFQNM mode. The error bars corresponds to the standard deviation of adhesion values from five different histograms obtained from five different scans.

For the tips, the adhesion force value with the surfaces increased in the following order:

For -C₁₈ tip, -C₁₈ < -C₆H₅ < -NH₂ < -OH < -COOH

For -C₆H₅ tip, -NH₂ < -OH < -C₁₈ < -C₆H₅ < -COOH

For -NH₂ tip, -C₁₈ < -NH₂ < -OH < -C₆H₅ < -COOH

For -COOH tip, -C₁₈ < -C₆H₅ < -NH₂ < -OH < -COOH and

For -OH tip, -C₁₈ < -OH < NH₂ < -COOH < -C₆H₅

It is clear that the adhesion force values were smaller for surfaces with nonpolar functional group (-C₁₈) and were higher for polar functional group (-COOH, -OH, -NH₂). However, phenyl which is a nonpolar group showed higher adhesion force values. This may be due to the different orientation possible for phenyl group as discussed above and when the phenyl group orients in sidewise manner the resonant π electrons will be interacting with the surface

which may increase the interaction force. Among all tip-surface interactions, the one involving $-C_6H_5$ tip and $-C_6H_5$ surface showed the maximum adhesion force, indicating π - π interaction between them. In the case of $-OH$ functionalized tip all surfaces showed comparable adhesion force, considering the error limits. The reason behind this observation is not understood clearly. The chance for some defects during functionalization cannot be neglected; also since it is a polar group, water can be absorbed to the tip surface which may mask the interaction properties of $-OH$ group.

Thus there are a number of factors to consider while analyzing chemical force microscopy results including, the sample heterogeneity and roughness, the relative humidity, the conformations and orientations of the end molecule, and the molecular chain length of the spacer molecule used for functionalization. Each of these factors may contribute separately or at once, towards the adhesion force between the modified surface and the tip.

4.4.2 Chemical Force Microscopy analysis on nanoparticles:

Bare silver nanoparticles (nAg), silver nanoparticles coated with citrate (nAg -citrate) and silver nanoparticles coated with humic acid (nAg -HA) were analysed using chemical force microscopy. Representative AFM images of nAg -citrate are shown in figure 27. There were both spherical and rod shaped nanoparticles present in the suspension. Particles with sizes ranging from 20 nm to 60 nm were detected, but for adhesion force analysis particles in the larger size range were considered.

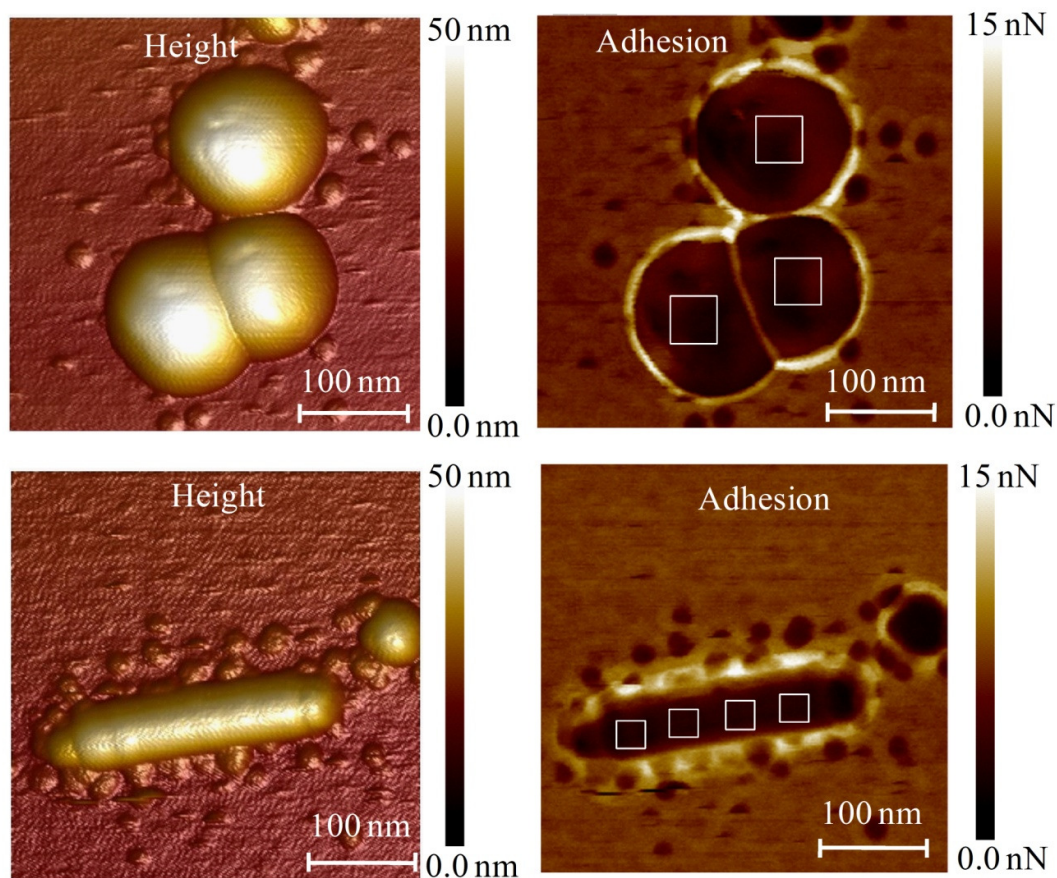


Figure 27. Height and adhesion images of nAg citrate nanoparticles scanned by $-\text{COOH}$ modified probe. White square in the adhesion image represents the area on the nanoparticles, selected to plot adhesion force histogram.

AFM images of nAg and nAg-HA are already shown in chapter 3 (figure 9 and SI figure S17). Adhesion force between the nanoparticles and the chemically modified probes were measured and scaled adhesion force histogram was plotted for each particle-tip interactions (figure 29) along with the Gaussian fit. Monomodal distribution was observed for all histograms, except for those corresponding to the interaction with phenyl modified probe. The bimodal histograms for phenyl modified tip interactions can again be explained on the basis of two types of orientations possible for phenyl group. To compare the adhesion forces, the peak value obtained from Gaussian curve was considered as the average adhesion force.

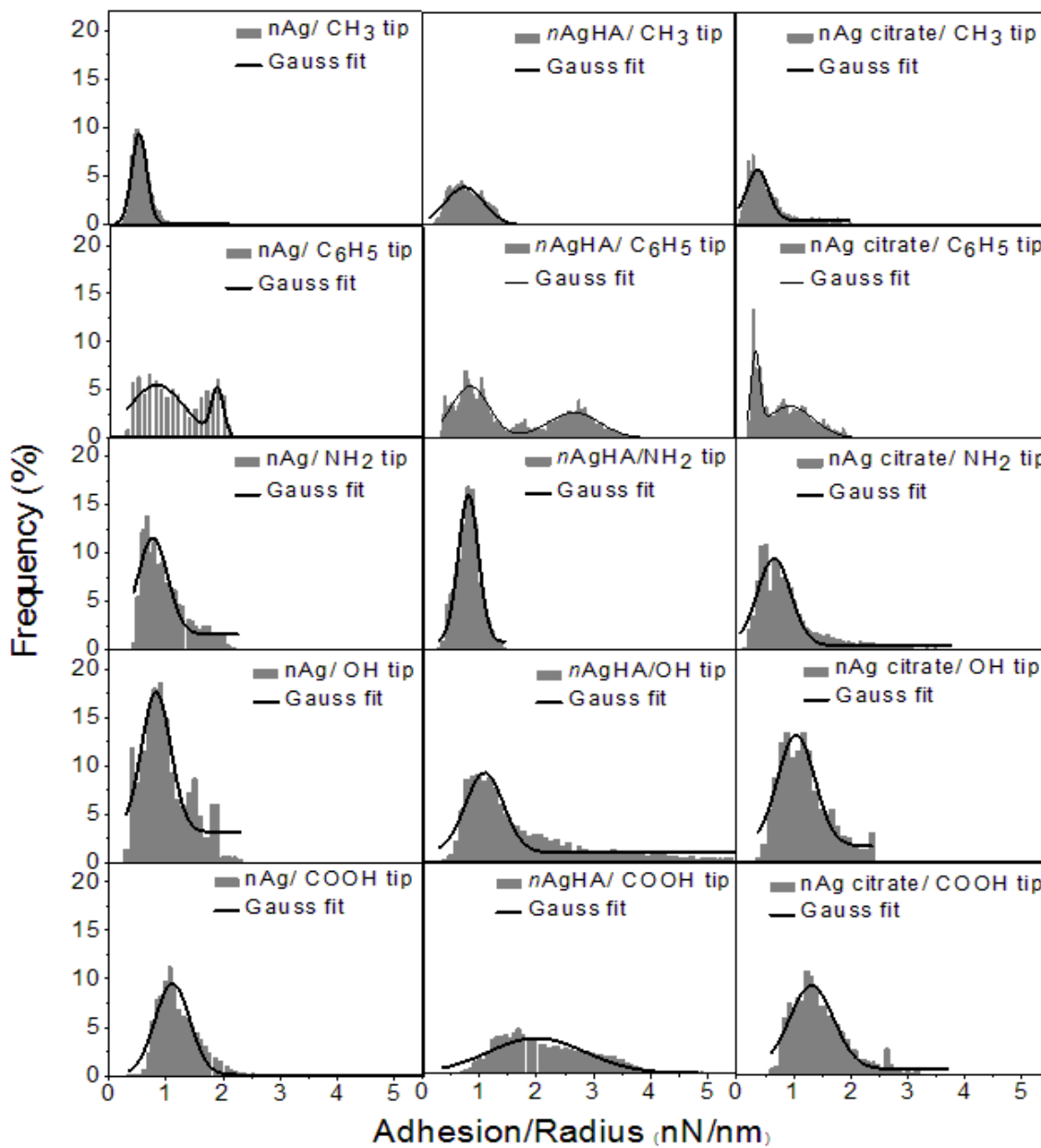


Figure 29. Scaled adhesion force histograms for the adhesion between nanoparticle surfaces and chemically modified probes and their Gaussian fit.

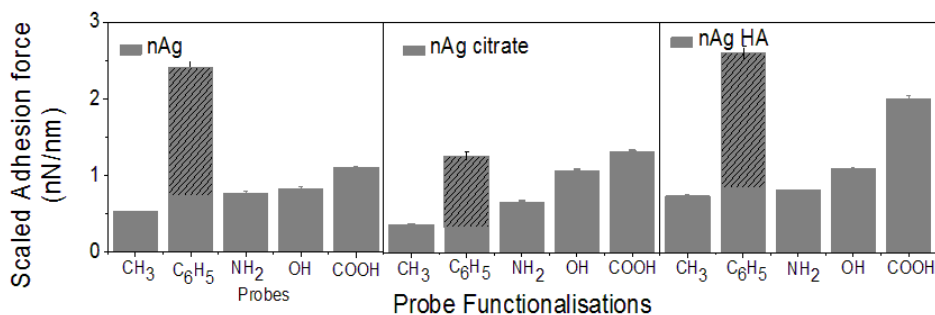


Figure 30. Average scaled adhesion force between the chemically functionalized AFM probes and the nanoparticle surfaces, measured using PFQNM mode of AFM.

The adhesion force values are compared for each nanoparticle surfaces (figure 30). Phenyl functionalized probe showed a bimodal distribution with all the nanoparticle surfaces (figure 29), and hence the adhesion forces corresponding to both the peaks are demonstrated in figure 30. This two different force values can be due to the different orientations possible for phenyl group as discussed earlier.

The particle surfaces show lower force values when scanned with nonpolar functional groups (-C18), where hydrogen bond donor/acceptor interactions were not present. While when imaged with polar groups (-NH₂, -OH, -COOH) which can undergo hydrogen bond donor/acceptor interactions, all nanoparticles show increased adhesion force.

For bare nanoparticles, some carbon materials were detected on the surface (chapter 2), which can be the reason for the hydrogen bond donor/acceptor properties exhibited here. Citrate coated nanoparticles show higher force values compared to bare nanoparticles when scanned with polar functional groups. This can be related to the presence of polar citrate ions on the nanoparticle surface which can increase the magnitude of intermolecular interactions compared to non coated nanoparticle surface. Humic acid coated nanoparticle shows the highest adhesion force value comparing to other two types of particles. Humic acid molecules

contain both aromatic/aliphatic parts and polar functional groups. Hence when scanned with alkyl and phenyl functionalized probes there will be hydrophobic interactions present and when scanned with polar groups, there will be polar interactions present.

However for polar functionalized groups like –OH and –NH₂, the adhesion forces are weak. Moreover the difference in adhesion force scanned by –CH₃ and –COOH groups are only in the range of 1-2 nN. In the case of hydrogen bond acceptor/donor interactions, much larger forces are expected. This suggests that no hydrogen bond donor/acceptor interactions are probed in these measurements and the difference in forces may be due to different orientations possible for different functional groups. If scan speed is controlled and measurement is done in much lower scan speed, there is a possibility of presence of hydrogen bond interactions due to increased contact time. Thus by varying the contact time between the AFM tip and surface, we can investigate the difference in adhesion forces due to hydrogen bond interactions and due to different molecular orientations.

This result demonstrates the importance of using a set of probes which can undergo different intermolecular interactions for CFM analysis. If the probe is functionalized with polar chemical group which can exhibit hydrogen bond donor/acceptor interactions, we can use this probe to differentiate between polar and nonpolar sample surface. On the other hand, probe with aromatic or aliphatic functionalization will help to differentiate between sample surfaces which are hydrophobic and hydrophilic. The results thus demonstrate that chemical force microscopy can be used as a potential tool for the nanoparticle surface analysis.

4.5 Conclusion

The results show the potential of chemical force microscopy to characterize nanoparticle surface. Silver nanoparticles with different surface coating showed differences in adhesion force values. Use of probes with a wide range of chemical functionalizations will give more reliable results, since the adhesion force seems to vary with intermolecular interaction types.

Thus this method finds its use in determining the surface modifications of nanoparticles as it reaches the environment, which will help in risk assessment of nanoparticles.

However there are a number of factors which have a direct effect on CFM results such as relative humidity, sample surface heterogeneities, possible orientations of the end group, scan speed of the measurement and the molecular chain length of the spacer molecule used for functionalization. These are the major limitations faced while analyzing CFM results. To overcome these limitations it is advisable to do CFM measurements in vacuum or in inert gas atmosphere, or in liquid to minimize capillary forces. Also using molecules having same spacer molecular chain length will help to improvise the CFM analysis.

Chapter-5

General conclusions and Outlook

5.1 Observations and conclusions

To elucidate the objectives and hypotheses in chapter 1, a systematic batch sorption study is conducted between silver nanoparticles with different coating, size and zeta potential and, sorbent surfaces exhibiting different intermolecular interactions. Results presented in chapter 2 and 3 demonstrate the possibility to describe nanoparticle-surface interactions by classical sorption models and to study the interaction on the basis of sorption quantities and parameters obtained.

5.1.1 Sorption of *n*Ag and *n*Ag-citrate in the absence of HA: The interaction studies of both *n*Ag and *n*Ag-citrate gives the conclusion that these nanoparticles form a monolayer on the sorbents following Langmuir sorption isotherms. Bare nanoparticle show higher sorption coefficient compared to citrate coated ones. This can be explained on the basis of electrostatic interactions as *n*Ag-citrate had more negative zeta potential compared to *n*Ag.

In both cases, sorption was influenced by collector surface chemistry. Sorption coefficient was larger for surfaces having stronger intermolecular interaction forces and was smaller for surfaces with weak intermolecular interactions. The slopes for the sorption of these two nanoparticles to collector surfaces show a linear dependence.

5.1.2 Sorption of *n*Ag and *n*Ag-citrate in the presence of HA: In the presence of HA, both the nanoparticles and collector surfaces are getting coated with HA and this masks the chemical specificity of sorption. The sorption is no longer influenced by the collector surface chemistry, but varies with specific surface area of collector surfaces. Even in this case, the slopes for the sorption of *n*Ag and *n*Ag citrate to the collector surfaces showed a linear dependence.

In these experiments, both the nanoparticles were having a negative zeta-potential and the entire model and environmental surfaces were also having negative charge. Under this unfavorable condition, the particle-surface attachment is expected to occur in secondary

minima, where the interaction is reversible. Hence these particle-surface interactions are considered to be happening in a quasi equilibrium condition.

Both the nanoparticle surface chemistry and collector surface chemistry have an impact on nanoparticle-surface interactions. These interactions will decide the fate and transport of nanoparticles in environmental compartments.

Thus surface characterization of nanoparticles with chemical sensitivity becomes more and more important. In Chapter 4, the potential of chemical force microscopy, an AFM based method, for the surface characterization of nanoparticles is discussed. CFM analysis using five AFM probe types with different chemical modifications undergoing different intermolecular interactions, it was possible to differentiate silver nanoparticles having different surface coatings. Possible artifacts during the measurements are also discussed in the chapter.

5.2 Open questions for future research

The particle-surface interaction study presented here considers only the attachment or sorption of nanoparticles on to the collector surfaces. Detachment or desorption of nanoparticles from the collector surfaces is also an important process here since the interaction is reversible. The ease of detachment of nanoparticle from the collector surface will also determine the fate of nanoparticle in the environment. The study of desorption processes will improve our understanding about the equilibrium state of the particle-surface interactions. The kinetic study of the same interactions will also be an add-on which will give us information about sorption and desorption rates. These topics can be considered for a future research.

In the case of the Langmuir sorption isotherms obtained for bare silver nanoparticles, the adsorption maximum Q_{\max} was not correlated with the BET specific surface area obtained.

Hence it is important to find the surface area of the sorbent which is available for the nanoparticle sorption. A method to find out such a quantity which describes the available surface area on the sorbents for $n\text{Ag}$ needs to be developed.

Particle-surface interaction study thus gives us information regarding the fate of nanoparticles in the environment by describing its tendency to get deposited or get transported. But different nanoparticles with different coatings need to be experimented in the similar way, to get a general understanding.

Chemical force microscopy is a promising technique for surface characterizations. However cautions should take to avoid the possible artifacts of this method. For example, it is important to remove the contribution of capillary forces by doing the experiment in vacuum or in inert gas atmosphere. Moreover, the same molecular chain length for the thiol molecules used for probe modification will make the result interpretations easier. In addition, the measurement in liquid phase may help more to probe hydrophobic interactions, and hence may improvise our knowledge regarding the interactions.

References

- Abraham, P. M., S. Barnikol, et al. (2013). "Interaction of silver nanoparticles with environmental and model surfaces." Environmental Science & Technology **47**(10): 5083–5091.
- Abraham, M. H., R. A. McGill, et al. (1987). Determination of olive oil-gas and hexadecane-gas partition coefficients, and calculation of the corresponding olive oil-water and hexadecane-water partition coefficients. *J. Chem. Soc., Perkin Trans. 2*: 797–803.
- Adamson, A. W., Petry, A. (1997). *Physical Chemistry of Surfaces*; JohnWiley and Sons: New York.
- Adamczyk, Z., J. Bławdziewicz, et al.(2009). Streaming potential studies of colloid, polyelectrolyte and protein deposition. *Adv. Colloid Interface Sci.* **153** (1–2): 1–29.
- Adegboye, N. F., V. K. Sharma, et al. (2012). "Interactions of Aqueous Ag⁺ with Fulvic Acids: Mechanisms of Silver Nanoparticle Formation and Investigation of Stability." Environmental Science & Technology **47**(2): 757-764.
- Aiken, G. R., H. Hsu-Kim, et al. (2011). "Influence of Dissolved Organic Matter on the Environmental Fate of Metals, Nanoparticles, and Colloids." Environmental Science & Technology **45**(8): 3196-3201.
- Akaighe, N., S. W. Depner, et al. (2012). "The effects of monovalent and divalent cations on the stability of silver nanoparticles formed from direct reduction of silver ions by Suwannee River humic acid/natural organic matter." Science of The Total Environment **441**: 277-289.
- Akaighe, N., R. I. MacCusprie, et al. (2011). "Humic Acid-Induced Silver Nanoparticle Formation Under Environmentally Relevant Conditions." Environmental Science & Technology **45**(9): 3895-3901.
- Asharani, P. V., Y. L. Wu, et al. (2008). "Toxicity of silver nanoparticles in zebrafish models." Nanotechnology **19**(25): 8.
- Amendola, V., F. Stellacci, et al.(2010). A study of the surface plasmon resonance of silver nanoparticles by the discrete dipole approximation method: Effect of shape, size, structure, and assembly. *Plasmonics* **5** (1): 85–97.
- Auffan, M., J. Rose, et al. (2009). "Towards a definition of inorganic nanoparticles from an environmental, health and safety perspective." Nat Nano **4**(10): 634-641.
- Badawy, A. M. E., T. M. Tolaymat, et al. (2010) Impact of environmental conditions (pH, ionic strength, and electrolyte type) on the surface charge and aggregation of silver nanoparticles suspensions. *Environ. Sci. Technol.* **44** (4): 1260–1266.
- Bae, S., Y. S. Hwang, et al. (2013). "Effects of Water Chemistry on Aggregation and Soil Adsorption of Silver Nanoparticles." Environ Health Toxicol **28**.
- Baer, D. R. (2011). Surface Characterization of Nanoparticles: critical needs and significant challenges JOURNAL OF SURFACE ANALYSIS, Surface Analysis Society of Japan.
- Baer, D. R., D. J. Gaspar, et al. (2010). "Application of surface chemical analysis tools for characterization of nanoparticles." Analytical and Bioanalytical Chemistry **396**(3): 983-1002.
- Baumann, T., Werth, C. J. (2005). Visualization of colloid transport through heterogeneous porous media using magnetic resonance imaging. *Colloids Surf., A* **265** (1–3): 2–10.
- Benn, T., B. Cavanagh, et al. (2010). The Release of Nanosilver from Consumer Products Used in the Home. **39**: 1875-1882.

-
- Benn, T. M. and P. Westerhoff (2008). "Nanoparticle Silver Released into Water from Commercially Available Sock Fabrics." Environmental Science & Technology **42**(11): 4133-4139.
- Bondarenko, O., K. Juganson, et al. (2013). "Toxicity of Ag, CuO and ZnO nanoparticles to selected environmentally relevant test organisms and mammalian cells in vitro: a critical review." Archives of Toxicology **87**(7): 1181-1200.
- Bönnemann, H. and Ryan M. Richards (2001). "Nanoscopic Metal Particles – Synthetic Methods and Potential Applications." European Journal of Inorganic Chemistry **2001**(10): 2455-2480.
- Braydich-Stolle, L., S. Hussain, et al. (2005). "In Vitro Cytotoxicity of Nanoparticles in Mammalian Germline Stem Cells." Toxicol. Sci. **88**(2): 412-419.
- Bruker Corporation. (2011). "Introduction to Bruker's ScanAsyst and PeakForce Tapping AFM Technology, Application Note #133, http://www.bruker.com/fileadmin/user_upload/8-PDF-Docs/SurfaceAnalysis/AFM/ApplicationNotes/Introduction_to_Brukers_ScanAsyst_and_PeakForce_Tapping_Atomic_Force_Microscopy_Technology_AFM_AN133.pdf."
- Buffle, J., K. J. Wilkinson, et al. (1998). "A Generalized Description of Aquatic Colloidal Interactions: The Three-colloidal Component-Approach." Environmental Science and Technology **32**(19): 2887-2899.
- Burton, Z., Bhushan, B. (2006). Surface characterization and adhesion and friction properties of hydrophobic leaf surfaces. Ultramicroscopy **106** (8–9): 709–719.
- Cappella, B., G. Dietler, (1999). Force-distance curves by atomic force microscopy. Surf. Sci. Rep. **34** (1): 5–104.
- Carlson, C., S. M. Hussain, et al. (2008). "Unique Cellular Interaction of Silver Nanoparticles: Size-Dependent Generation of Reactive Oxygen Species." The Journal of Physical Chemistry B **112**(43): 13608-13619.
- Chen, K. L. and M. Elimelech (2008). "Interaction of Fullerene (C60) Nanoparticles with Humic Acid and Alginate Coated Silica Surfaces: Measurements, Mechanisms, and Environmental Implications." Environmental Science & Technology **42**(20): 7607-7614.
- Chen, K. L., Elimelech, M. (2006). Aggregation and deposition kinetics of fullerene (C-60) nanoparticles. Langmuir **22** (26): 10994–11001.
- Chiou, C. T., Kile, D. E. (1998). Deviations from sorption linearity on soils of polar and non-polar organic compounds at low relative concentrations. Environ. Sci. Technol. **32**: 338–343.
- Cho, J. M.; et al. (2004). Surface Forces on Nanoparticles determined by direct measurement. In Dekker Encyclopedia of Nanoscience and Nanotechnology-Six Volume Set; Schwarz, J. A., Contescu, C. I., Eds.; CRC press: Boca Raton, FL.
- Collaborative Research: Near-Surface Repulsion and Mixing- Limitations: Upscaling of Colloid Transport in Non-Uniform Media under Unfavorable Conditions; National Science Foundation, 2012; http://www.nsf.gov/awardsearch/showAward?AWD_ID=1215726
- Cong, Y., C. Pang, et al. (2011). "Importance of characterizing nanoparticles before conducting toxicity tests." Integrated Environmental Assessment and Management **7**(3): 502-503.
- Dague, E., Dufrene, Y.F et al. (2007). "Chemical force microscopy of single live cells." Nano Letters **7**(10): 3026-3030.
- De Oliveria, R. R. L., D. A. C. Albuquerque, et al. (2012). Measurement of the Nanoscale Roughness by Atomic Force Microscopy: Basic Principles and Applications. Atomic

-
- Force Microscopy - Imaging, Measuring and Manipulating Surfaces at the Atomic Scale. V. Bellitto, InTech.
- Dong, X., X. Ji, et al. (2009). "Shape Control of Silver Nanoparticles by Stepwise Citrate Reduction." The Journal of Physical Chemistry C **113**(16): 6573-6576.
- Drelich, J. M. K. L. K. (2005). Atomic force microscopy in adhesion studies. Utrecht; Biggleswade, VSP ; Extenza Turpin [distributor].
- Dufrene, Y. F. (2008). "Atomic force microscopy and chemical force microscopy of microbial cells." Nat. Protocols **3**(7): 1132-1138.
- Eastman, T. and D.-M. Zhu (1996). "Adhesion Forces between Surface-Modified AFM Tips and a Mica Surface." Langmuir **12**(11): 2859-2862.
- Elimelech, M., J. Gregory, et al. (1995). Particle Deposition & Aggregation: Measurement, Modelling and Simulation (Colloid & surface engineering), Butterworth-Heinemann, Oxford.
- Evanoff, D. D. and G. Chumanov (2005). "Synthesis and Optical Properties of Silver Nanoparticles and Arrays." ChemPhysChem **6**(7): 1221-1231.
- Fabrega, J., S. R. Fawcett, et al. (2009). "Silver Nanoparticle Impact on Bacterial Growth: Effect of pH, Concentration, and Organic Matter." Environmental Science and Technology **43**(19): 7285-7290.
- Fang, S. J., S. Haplepete, et al. (1997). "Analyzing atomic force microscopy images using spectral methods." Journal of Applied Physics **82**(12): 5891-5898.
- Farshchi-Tabrizi, M., M. Kappl, et al. (2008). "Influence of humidity on adhesion: An atomic force microscope study." Journal of Adhesion Science and Technology **22**(2): 181-203.
- Frisbie, C. D., L. F. Rozsnyai, et al. (1994). Functional Group Imaging by Chemical Force Microscopy. **265**: 2071-2074.
- Furman, O., S. Usenko, et al. (2013). "Relative Importance of the Humic and Fulvic Fractions of Natural Organic Matter in the Aggregation and Deposition of Silver Nanoparticles." Environmental Science & Technology **47**(3): 1349-1356.
- Fatissou, J., N. Tufenkji, et al. (2009). Deposition of TiO₂ Nanoparticles onto silica measured using a quartz crystal microbalance with dissipation monitoring. Langmuir **25** (11): 6062-6069.
- Fuji, M., M. Chikazawa, et al. (1999). Effect of wettability on adhesion force between silica particles evaluated by atomic force microscopy measurement as a function of relative humidity. Langmuir **15** (13): 4584-4589.
- Furman, O., B. L. T. Lau, et al. (2013). Relative importance of the humic and fulvic fractions of natural organic matter in the aggregation and deposition of silver nanoparticles. Environ. Sci. Technol. **47** (3): 1349-1356.
- Gao, J., K. Powers, et al. (2012). "Influence of Suwannee River humic acid on particle properties and toxicity of silver nanoparticles." Chemosphere **89**(1): 96-101.
- Gao, J., S. Youn, et al. (2009). "Dispersion and Toxicity of Selected Manufactured Nanomaterials in Natural River Water Samples: Effects of Water Chemical Composition." Environmental Science & Technology **43**(9): 3322-3328.
- García-Alonso, J., E. Valsami-Jones, et al. (2011) Cellular internalization of silver nanoparticles in gut epithelia of the estuarine polychaete *Nereis diversicolor*. Environ. Sci. Technol. **45** (10): 4630-4636.
- Geranio, L., M. Heuberger, et al. (2009). "The Behavior of Silver Nanotextiles during Washing." Environmental Science & Technology **43**(21): 8113-8118.
- González, A. E., R. Hidalgo-Álvarez, et al. (2002) Concentration effects on two- and three dimensional colloidal aggregation. Phys. A (Amsterdam, Neth.) **314** (1-4): 235-245.

-
- Goss, K.-U., Schwarzenbach, R. P. (2001). Linear free energy relationships used to evaluate equilibrium partitioning of organic compounds. *Environ. Sci. Technol.* **35** (1): 1–9.
- Gottschalk, F., T. Y. Sun, et al. (2013). "Environmental concentrations of engineered nanomaterials: Review of modeling and analytical studies." *Environmental Pollution* **181**: 287-300.
- Grosse, S., L. Evje, et al. (2013). "Silver nanoparticle-induced cytotoxicity in rat brain endothelial cell culture." *Toxicology in Vitro* **27**(1): 305-313.
- Hahn, M. W., C.R. O'Melia, (2003) Deposition and reentrainment of Brownian particles in porous media under unfavorable chemical conditions: Some concepts and applications. *Environ. Sci. Technol.* **38** (1): 210–220.
- Hochella, M. F., B.S. Twining, et al. Nanominerals, mineral nanoparticles, and earth systems. *Science* 2008, 319 (5870), 1631–1635.
- Hoek, E. M. V., G.K. Agarwal, (2006). Extended DLVO interactions between spherical particles and rough surfaces. *J. Colloid Interface Sci.* **298** (1): 50–58.
- Huang, H. H., X. P. Ni, et al. (1996). "Photochemical Formation of Silver Nanoparticles in Poly(N-vinylpyrrolidone)." *Langmuir* **12**(4): 909-912.
- Hussain, S. M., K. L. Hess, et al. (2005). "In vitro toxicity of nanoparticles in BRL 3A rat liver cells." *Toxicology in Vitro* **19**(7): 975-983.
- Iqbal, P., J. A. Preece, et al. (2012). Nanotechnology: The "Top-Down" and "Bottom-Up" Approaches. *Supramolecular Chemistry*, John Wiley & Sons, Ltd.
- Jacobs, T. B., K. Ryan, et al. (2013). "The Effect of Atomic-Scale Roughness on the Adhesion of Nanoscale Asperities: A Combined Simulation and Experimental Investigation." *Tribology Letters* **50**(1): 81-93.
- Jang, J., M. Yang, et al. (2007). "Microscopic origin of the humidity dependence of the adhesion force in atomic force microscopy." *The Journal of Chemical Physics* **126**(17): 174705-6.
- Jain, P., T. Pradeep. (2005) Potential of silver nanoparticle-coated polyurethane foam as an antibacterial water filter. *Biotechnol. Bioeng.* **90** (1): 59–63.
- Jiang, Z.-J., C.-Y. Liu, et al. (2005). "Catalytic Properties of Silver Nanoparticles Supported on Silica Spheres." *The Journal of Physical Chemistry B* **109**(5): 1730-1735.
- Johnson, M., Hilpert, M. Upscaling Colloid Transport and Retention under Unfavorable Conditions. *Geophys. Res. Abstr.* 2013,15, EGU2013–6766.
- Johnson, P. R., M. Elimelech, (1995). Dynamics of colloid deposition in porous media: Blocking based on random sequential adsorption. *Langmuir* **11** (3): 801–812.
- Ju-Nam, Y. and J. R. Lead (2008). "Manufactured nanoparticles: An overview of their chemistry, interactions and potential environmental implications." *Science of The Total Environment* **400**(1-3): 396-414.
- Jung, J., K. Ha, et al. (2013). "Enhancing Light Trapping Properties of Thin Film Solar Cells by Plasmonic Effect of Silver Nanoparticles." *Journal of Nanoscience and Nanotechnology* **13**(12): 7860-7864.
- Kang, K., J. Wang, et al. (2011). "Fluorescence Manipulation by Gold Nanoparticles: From Complete Quenching to Extensive Enhancement." *Journal of Nanobiotechnology* **9**(1): 16.
- Kamat, P. V., G. V. Hartland, et al.(1998). Picosecond dynamics of silver nanoclusters. photoejection of electrons and fragmentation. *J. Phys. Chem. B* **102** (17): 3123–3128.
- Karakoti, A. S., L. L. Hench, et al. (2006). "The potential toxicity of nanomaterials-The role of surfaces." *JOM* **58**(7): 77-82.

-
- Katrin Kneipp and Harald Kneipp and Irving Itzkan and Ramachandra, R. D. a. M. S. F. (2002). "Surface-enhanced Raman scattering and biophysics." Journal of Physics: Condensed Matter **14**(18): R597.
- Kim, Y. T. and A. J. Bard (1992). "Imaging and etching of self-assembled n-octadecanethiol layers on gold with the scanning tunneling microscope." Langmuir **8**(4): 1096-1102.
- Kinniburgh, D. G. (1986). "General purpose adsorption isotherms." Environmental Science & Technology **20**(9): 895-904.
- Klapetek, P., M. Valtr, et al. (2011). "Atomic force microscopy analysis of nanoparticles in non-ideal conditions." Nanoscale Research Letters **6**(1): 514.
- Klavins, M. and L. Anson (2010). "Study of interaction between humic acids and fullerene C60 using fluorescence quenching approach " Ecological Chemistry and Engineering S **17**(3): 351-362.
- Klaine, S. J., J. R. Lead, et al. (2008). Nanomaterials in the environment: Behavior, fate, bioavailability, and effects. Environ. Toxicol. Chem. **27** (9): 1825–1851.
- Klar, T., M. Perner, et al. (1998). "Surface-Plasmon Resonances in Single Metallic Nanoparticles." Physical Review Letters **80**(19): 4249-4252.
- Ko, C. H., Elimelech, M. (2000). The shadow effect in colloid transport and deposition dynamics in granular porous media: Measurements and mechanisms. Environ. Sci. Technol. **34** (17): 3681–3689.
- Kumar, A., P. K. Vemula, et al. (2008). "Silver-nanoparticle-embedded antimicrobial paints based on vegetable oil." Nat Mater **7**(3): 236-241.
- Kruszewski, S., T. Wybranowski, et al. (2008). "Enhancement of FITC Fluorescence by Silver Colloids and Silver Island Films." Acta Physica Polonica A **113**(6): 1599.
- Landkamer, L. L., J.N. Ryan, et al. (2013). Colloid transport in saturated porous media: Elimination of attachment efficiency in a new colloid transport model. Water Resour. Res. DOI: 10.1002/wrcr.20195.
- Lara, H. H., N. V. Ayala-Nunez, et al. (2010). "Mode of antiviral action of silver nanoparticles against HIV-1." Journal of Nanobiotechnology **8**(1).
- LeBoeuf, E. J., Weber, W. J. A (1997). distributed reactivity model for sorption by soils and sediments. 8. Sorbent organic domains: Discovery of a humic acid glass transition and an argument for a polymer-based model. Environ. Sci. Technol. **31** (6): 1697–1702.
- Lee, H. J., S. H. Jeong, et al. Antibacterial effect of nanosized silver colloidal solution on textile fabrics. J. Mater. Sci. 2003, **38** (10), 2199–2204.
- Lee, J., P.J. Alvarez, et al. J. Nanomaterials in the construction industry: A review of their applications and environmental health and safety considerations. ACS Nano 2010, **4** (7), 3580–3590.
- Lentfer, C. J., W. E. Boyd, et al. (2003). Particle settling times for gravity sedimentation and centrifugation: A practical guide for palynologists. J. Archaeol. Sci. **30** (2): 149–168.
- Levard, C., E. M. Hotze, et al. (2012). "Environmental Transformations of Silver Nanoparticles: Impact on Stability and Toxicity." Environmental Science & Technology **46**(13): 6900-6914.
- Li, J.-F., Z. Q. Tian, et al. (2010). SERS and DFT study of water on metal cathodes of silver, gold and platinum nanoparticles. Phys. Chem. Chem. Phys. **12**, 10.
- Li, X., J. J. Lenhart, (2012). Aggregation and dissolution of silver nanoparticles in natural surface water. Environ. Sci. Technol. **46** (10): 5378–5386.
- Lim, L. T. W., A. T. S. Wee, et al. (2008). "Effect of Tip Size on Force Measurement in Atomic Force Microscopy." Langmuir **24**(6): 2271-2273.

-
- Lin, S., Y. Cheng, et al. (2012). "Polymeric Coatings on Silver Nanoparticles Hinder Autoaggregation but Enhance Attachment to Uncoated Surfaces." Langmuir **28**(9): 4178-4186.
- Lin, S. and M. R. Wiesner (2012). "Deposition of Aggregated Nanoparticles" A Theoretical and Experimental Study on the Effect of Aggregation State on the Affinity between Nanoparticles and a Collector Surface." Environmental Science & Technology **46**(24): 13270-13277.
- Litvin, V. A., R. L. Galagan, et al. (2012). "Kinetic and mechanism formation of silver nanoparticles coated by synthetic humic substances." Colloids and Surfaces A: Physicochemical and Engineering Aspects **414**(0): 234-243.
- Liu, J. Y. and R. H. Hurt (2010). "Ion Release Kinetics and Particle Persistence in Aqueous Nano-Silver Colloids." Environmental Science & Technology **44**(6): 2169-2175.
- Lin, S., M. R. Wiesner, et al. (2011) Deposition of silver nanoparticles in geochemically heterogeneous porous media: Predicting affinity from surface composition analysis. Environ. Sci. Technol. **45** (12): 5209–5215.
- Lowry, G. V., B. P. Espinasse, et al. (2012). "Long-Term Transformation and Fate of Manufactured Ag Nanoparticles in a Simulated Large Scale Freshwater Emergent Wetland." Environmental Science & Technology **46**(13): 7027-7036.
- Lowry, G. V., K. B. Gregory, et al. (2012). "Transformations of Nanomaterials in the Environment." Environmental Science & Technology **46**(13): 6893-6899.
- LuxResearch (2008). Nanomaterials State of the Market Q3 2008: Stealth Success, Broad Impact http://portal.luxresearchinc.com/research/document_excerpt/3735.
- Mafune, F., J.-y. Kohno, et al. (2000). "Structure and Stability of Silver Nanoparticles in Aqueous Solution Produced by Laser Ablation." The Journal of Physical Chemistry B **104**(35): 8333-8337.
- Malotky, D. L. and M. K. Chaudhury (2001). "Investigation of Capillary Forces Using Atomic Force Microscopy." Langmuir **17**(25): 7823-7829.
- Manoharan, V., A. Ravindran, et al. (2013). "Mechanistic Insights into Interaction of Humic Acid with Silver Nanoparticles." Cell Biochemistry and Biophysics: 1-5.
- Marambio-Jones, C. and E. V. Hoek (2010). "A review of the antibacterial effects of silver nanomaterials and potential implications for human health and the environment." Journal of Nanoparticle Research **12**(5): 1531-1551.
- Marciano, A., A. Gedanken, et al. (2008). Differential adsorption of silver nanoparticles to the inner and outer surfaces of the Agave americana cuticle. J. Phys. Chem. C 2008, **112** (46): 18082–18086.
- Marti, A. R.-Z. a. E. W. a. S. H. a. O. (1997). "The simultaneous measurement of elastic, electrostatic and adhesive properties by scanning force microscopy: pulsed-force mode operation." Measurement Science and Technology **8**(11): 1333.
- McNeil, S. E., J. Grobelny, et al. (2011). Size Measurement of Nanoparticles Using Atomic Force Microscopy. Characterization of Nanoparticles Intended for Drug Delivery, Humana Press. **697**: 71-82.
- Meyer, N., G. Marx, et al. (2000). Surface enhanced Raman spectroscopy on carbon filaments. Microchim. Acta **133** (1–4): 337–339.
- Moreno-Vega, A.I., V. Castano, et al. (2012). Polymeric and Ceramic Nanoparticles in Biomedical Applications. **2012**: 10.
- Mueller, N. C., Nowack, B. (2008) Exposure modeling of engineered nanoparticles in the environment. Environ. Sci. Technol. **42** (12): 4447–4453.

- Muller, D. J. and A. Engel (2007). "Atomic force microscopy and spectroscopy of native membrane proteins." Nat. Protocols **2**(9): 2191-2197.
- Mulfinger, L., S. D. Solomon, et al. (2007). "Synthesis and Study of Silver Nanoparticles." Journal of Chemical Education **84**(2): 322.
- Mulvaney, P. (1996). "Materials Mix. Optical properties of metal clusters By U. Kreibig, M. Vollmer, Springer Series in Materials Science, Vol. 25, Springer, Berlin 1995, XVII, 532 pp., Hardcover, DM 98.00, ISBN 3-540-57836-6." Advanced Materials **8**(8): 699-699.
- Nadworny, P. L., J. Wang, et al. (2008). "Anti-inflammatory activity of nanocrystalline silver in a porcine contact dermatitis model." Nanomedicine : nanotechnology, biology, and medicine **4**(3): 241-251.
- Nagarajan, R. (2008). Nanoparticles: Building Blocks for Nanotechnology. Nanoparticles: Synthesis, Stabilization, Passivation, and Functionalization, American Chemical Society. **996**: 2-14.
- Nagarajan, R. (2008). Nanoparticles: Synthesis, Stabilization, Passivation, and Functionalization, American Chemical Society.
- Nanny, M. A. and J. P. Maza (2001). "Noncovalent Interactions between Monoaromatic Compounds and Dissolved Humic Acids: A Deuterium NMR T1 Relaxation Study." Environ. Sci. Technol. **35**: 379-384.
- NanoAndMoreGMBH. "<http://www.nanoandmore.com/Functionalized-Chemical-AFM-Tips.html>."
- Nattich-Rak, M., M. Oc´wieja, et al. (2012). Hematite nanoparticle monolayers on mica: Characterization by colloid deposition. Colloids Surf., A **412** (0): 72–81.
- Navarro, E., A. Baun, et al. (2008). "Environmental behavior and ecotoxicity of engineered nanoparticles to algae, plants, and fungi." Ecotoxicology **17**(5): 372-386.
- Niazi, J., B.-I. Sang, et al. (2011). "Global Gene Response in *Saccharomyces cerevisiae* Exposed to Silver Nanoparticles." Applied Biochemistry and Biotechnology **164**(8): 1278-1291.
- Niemeyer, C. M. and C. A. Mirkin (2006). Nanobiotechnology: Concepts, Applications and Perspectives, John Wiley & Sons.
- Noguez, C.(2007). Surface plasmons on metal nanoparticles: The influence of shape and physical environment. J. Phys. Chem. C **111** (10): 3806–3819.
- Nowack, B., T. D. Bucheli, (2007). Occurrence, behavior and effects of nanoparticles in the environment. Environ. Pollut. (Oxford, U. K.) **150** (1): 5–22.
- Nowack, B., H. F. Krug, et al. (2011). "120 Years of Nanosilver History: Implications for Policy Makers." Environmental Science & Technology **45**(4): 1177-1183.
- Noy, A., Lieber, C.M. et al. (1997). "Chemical force microscopy." Annual Review of Materials Science **27**: 381-421.
- Noy, A. (2006). "Chemical force microscopy of chemical and biological interactions." Surface and Interface Analysis **38**(11): 1429-1441
- Oc´wieja, M., A. Michna, et al.(2011). High density silver nanoparticle monolayers produced by colloid self-assembly on polyelectrolyte supporting layers. J. Colloid Interface Sci. **364** (1): 39–48.
- Okabe, Y., U. Akiba, et al. (2000). "Chemical force microscopy of $-CH_3$ and $-COOH$ terminal groups in mixed self-assembled monolayers by pulsed-force-mode atomic force microscopy." Applied Surface Science **157**(4): 398-404.
- Pandey, P. A., G. R. Bell, et al. (2011). "Physical Vapor Deposition of Metal Nanoparticles on Chemically Modified Graphene: Observations on Metal–Graphene Interactions." Small **7**(22): 3202-3210.

-
- Paredes, J. I., A. Martínez-Alonso, et al. (2000). "Adhesion artefacts in atomic force microscopy imaging." Journal of Microscopy **200**(2): 109-113.
- Parimal, S., M. Prasad, et al. (2010). "Prediction of Equilibrium Sorption Isotherm: Comparison of Linear and Nonlinear Methods." Industrial & Engineering Chemistry Research **49**(6): 2882-2888.
- Park, J. J., A. Karim, et al. (2008). Langmuir adsorption study of the interaction of CdSe/ZnS quantum dots with model substrates: Influence of substrate surface chemistry and pH. Langmuir **25** (1): 443-450.
- Petosa, A. R., D. P. Jaisi, et al. (2010). "Aggregation and Deposition of Engineered Nanomaterials in Aquatic Environments: Role of Physicochemical Interactions." Environmental Science & Technology **44**(17): 6532-6549.
- Pillai, Z. S., Kamat, P. V. (2003) What factors control the size and shape of silver nanoparticles in the citrate ion reduction method? J. Phys.Chem. B **108** (3): 945-951.
- Pittenger, B., N. Erina, et al. "Quantitative Mechanical Property Mapping at the Nanoscale with PeakForce QNM ", from <http://www.veeco.com/pdfs/appnotes/quantitative-mechanical-property-mapping-at-the-nanoscale-with-peakforce-qnm-an128-lores.pdf>.
- Pletikapić, G., A. Berquand, et al. (2011). "Quantitative nanomechanical mapping of marine diatom in seawater using peak force tapping atomic force microscopy." Journal of Phycology **48**(1): 174-185.
- Poggi, M. A., P. T. Lillehei, et al. (2005). "Chemical Force Microscopy on Single-Walled Carbon Nanotube Paper." Chemistry of Materials **17**(17): 4289-4295.
- Quadros, M. E., R. Pierson, et al. (2013). "Release of Silver from Nanotechnology-Based Consumer Products for Children." Environmental Science & Technology **47**(15): 8894-8901.
- Quadros, M. E. and L. C. Marr (2011). "Silver Nanoparticles and Total Aerosols Emitted by Nanotechnology-Related Consumer Spray Products." Environmental Science & Technology **45**(24): 10713-10719.
- Rabani, E., L. E. Brus, et al. (2003). Drying mediated self-assembly of nanoparticles. Nature **426** (6964):271-274.
- Rao, C., R. Sen, et al. (1996). "Fullerenes and carbon nanotubes." Current Opinion in Solid State and Materials Science **1**(2): 279-284.
- Redman, J. A., S. L. Walker, et al. (2004). "Bacterial Adhesion and Transport in Porous Media: Role of the Secondary Energy Minimum." Environmental Science & Technology **38**(6): 1777-1785.
- Ren, X., X. Meng, et al. (2005). "Using silver nanoparticle to enhance current response of biosensor." Biosensors and Bioelectronics **21**(3): 433-437.
- Rodrigues, A., A. Brito, et al. (2009). "Quantification of humic acids in surface water: effects of divalent cations, pH, and filtration." Journal of Environmental Monitoring **11**(2): 377-382.
- Rogers, K. R., A. Williams, et al. (2012). Alterations in physical state of silver nanoparticles exposed to synthetic human stomach fluid. Sci. Total Environ. **420** (0): 334-339.
- Rosi, N. L. and C. A. Mirkin (2005). "Nanostructures in Biodiagnostics." Chemical Reviews **105**(4): 1547-1562.
- Rycenga, M., C. M. Cobley, et al. (2011). "Controlling the Synthesis and Assembly of Silver Nanostructures for Plasmonic Applications." Chemical Reviews **111**(6): 3669-3712.
- Sadezky, A., U. Poeschl, et al. (2005). Raman microspectroscopy of soot and related carbonaceous materials: Spectral analysis and structural information. Carbon **43** (8): 1731-1742.

-
- Sato, F., H. Okui, et al. (2003). "A study of topographic effects on chemical force microscopy using adhesive force mapping." Ultramicroscopy **97**(1&4): 303-314.
- Schwarzenbach, R. P.; Gschwend, P. M.; Imboden, D. M. Environmental Organic Chemistry; John Wiley: New York, 2003.
- Seog, J., D. Dean, et al. (2002). "Direct Measurement of Glycosaminoglycan Intermolecular Interactions via High-Resolution Force Spectroscopy." Macromolecules **35**(14): 5601-5615.
- Shateri Khalil-Abad, M., M. Nateghi, et al.(2009). Effect of cationization on adsorption of silver nanoparticles on cotton surfaces and its antibacterial activity. Cellulose (Dordrecht, Neth.) **16** (6): 1147-1157.
- Simpson, M. J., A. J. Simpson, et al. (2004). "Noncovalent interactions between aromatic compounds and dissolved humic acid examined by nuclear magnetic resonance spectroscopy." Environ Toxicol Chem. 2004 Feb;23(2):355-62.
- Song, J. E., G. V. Lowry, et al. (2011). Hydrophobic interactions increase attachment of gum arabic- and PVP-coated Ag nanoparticles to hydrophobic surfaces. Environ. Sci. Technol. **45** (14): 5988-5995.
- Song, J., J. Jang, et al.(2011). Adsorption of heavy metal ions from aqueous solution by polyrhodanine-encapsulated magnetic nanoparticles. J. Colloid Interface Sci. **359** (2): 505-511.
- Song, K., S. Lee, et al. (2009). "Preparation of colloidal silver nanoparticles by chemical reduction method." Korean Journal of Chemical Engineering **26**(1): 153-155.
- Song, L., P. R. Johnson, et al. (1994). "Kinetics of Colloid Deposition onto Heterogeneously Charged Surfaces in Porous Media." Environmental Science & Technology **28**(6): 1164-1171.
- Sotiriou, G. A. and S. E. Pratsinis. (2010) "Antibacterial Activity of Nanosilver Ions and Particles." Environmental Science & Technology **44**(14): 5649-5654.
- Struyk, Z. and G. Sposito (2001). "Redox properties of standard humic acids." Geoderma **102**(3-4): 329-346.
- Sugawara, Y., M. Ohta, et al. (1993). "Effects of humidity and tip radius on the adhesive force measured with atomic force microscopy." Wear **168**(1-2): 13-16.
- Tabor, D. (1977). "Surface forces and surface interactions." Journal of Colloid and Interface Science **58**(1): 2-13.
- Takei, K., Z. Yu, et al. (2013). Highly sensitive electronic whiskers based on patterned carbon nanotube and silver nanoparticle composite films.
- Taleb, A., M. P. Pileni, et al. (1997). Synthesis of highly monodisperse silver nanoparticles from AOT reverse micelles: A way to 2D and 3D self-organization. Chem. Mater. **9** (4): 950-959.
- Taurozzi, J. S.; Hackley, V. A.; Wiesner, M. R. CEINT/NIST Reporting Guidelines for the Preparation of Aqueous Nanoparticle Dispersions from Dry Nanomaterials; Duke University, Center for the Environmental Implications of NanoTechnology, 2010.
- Tiede, K., A. B. A. Boxall, et al. (2008). "Detection and characterization of engineered nanoparticles in food and the environment." Food Additives & Contaminants: Part A **25**(7): 795-821.
- Torkzaban, S., S. A. Bradford, et al. (2007). "Resolving the coupled effects of hydrodynamics and DLVO forces on colloid attachment in porous media." Langmuir **23**(19): 9652-9660.
- Tsai, D.-H.V. A. Hackley, et al. (2011) Quantitative determination of competitive molecular adsorption on gold nanoparticles using attenuated total reflectance-Fourier transform infrared spectroscopy. Langmuir **27** (15): 9302-9313.

-
- Tuelp, H. C., K. Fenner, et al. (2008). Experimental determination of LSER parameters for a set of 76 diverse pesticides and pharmaceuticals. *Environ. Sci. Technol.* **42** (6): 2034–2040.
- Tufenkji, N., M. Elimelech, (2003). Interpreting deposition patterns of microbial particles in laboratory-scale column experiments. *Environ. Sci. Technol.* **37** (3): 616–623.
- Tufenkji, N. and M. Elimelech (2004). "Deviation from the classical colloid filtration theory in the presence of repulsive DLVO interactions." *Langmuir* **20**(25): 10818-10828.
- Tufenkji, N. and M. Elimelech (2005). "Breakdown of Colloid Filtration Theory: Role of the Secondary Energy Minimum and Surface Charge Heterogeneities." *Langmuir* **21**(3): 841-852.
- Ukrainitsev, E., A. Kromka, et al. (2012). Artifacts in Atomic Force Microscopy of Biological Samples. *Atomic Force Microscopy Investigations into Biology - From Cell to Protein*. C. Frewin, InTech.
- Umadevi, M., S. R. Kavitha, et al. (2013). "Influence of Plasmonic Silver Nanoparticles on Fluorescence Quenching of 1,4-dihydroxy-3-methylanthracene-9,10-dione." *Plasmonics* **8**(2): 859-867.
- van Oss, C. J. (1993). Acid–base interfacial interactions in aqueous media. *Colloids Surf., A* **78** (0): 1–49.
- Vert, M., Y. Doi, et al. (2012). "Terminology for biorelated polymers and applications (IUPAC Recommendations 2012)." *Pure Appl. Chem.* **84**(2): 377-410.
- Verwey, E. J. W.; Overbeek, J. T. G. *Theory of Stability of Lyophobic Colloids*; Elsevier: Amsterdam, 1948.
- Vezenov, D. V., A. Noy, et al. (1997). "Force Titrations and Ionization State Sensitive Imaging of Functional Groups in Aqueous Solutions by Chemical Force Microscopy." *Journal of the American Chemical Society* **119**(8): 2006-2015.
- Vezenov, D. V., A. Noy, et al. (2005). "Chemical force microscopy: probing chemical origin of interfacial forces and adhesion." *Journal of Adhesion Science and Technology* **19**(3-5): 313-364.
- Wagener, P., S. Barcikowski, et al. (2012). How citrate ligands affect nanoparticle adsorption to microparticle supports. *Langmuir* **28** (14): 6132–6140.
- Walser, T., E. Demou, et al. (2011). "Prospective Environmental Life Cycle Assessment of Nanosilver T-Shirts." *Environmental Science & Technology* **45**(10): 4570-4578.
- Wang, T. C., M. F. Rubner, et al. (2002). "Polyelectrolyte Multilayer Nanoreactors for Preparing Silver Nanoparticle Composites: Controlling Metal Concentration and Nanoparticle Size." *Langmuir* **18**(8): 3370-3375.
- Wang, Y., R. L. McCreery, et al. (1990). Raman spectroscopy of carbon materials: Structural basis of observed spectra. *Chem. Mater.* **2** (5): 557–563.
- Wen, H.-C., Y.-N. Lin, et al. (2007). "Observation of Growth of Human Fibroblasts on Silver Nanoparticles." *Journal of Physics: Conference Series* **61**(1): 445.
- Wijnhoven, S. W. P., R. E. Geertsma, et al. (2009) Nano-silver: A review of available data and knowledge gaps in human and environmental risk assessment. *Nanotoxicology*, **3** (2): 109–138.
- Wilbur, J.L., Whitesides, G. M. et al. (1995) "Scanning Force Microscopies can image Patterned Self- Assembled Monolayers". **11** (3):825-831.
- Wilkinson, K. J., E. Balnois, et al. (1999). "Characteristic features of the major components of freshwater colloidal organic matter revealed by transmission electron and atomic force microscopy." *Colloids and Surfaces a-Physicochemical and Engineering Aspects* **155**(2-3): 287-310.

-
- Wu, F. and B. Xing (2009). Natural Organic Matter and Its Significance in the Environment. Beijing, China, Science Press.
- Xia, Y. and N. J. Halas (2005). Shape-Controlled Synthesis and Surface Plasmonic Properties of Metallic Nanostructures, Cambridge Journals Online. **30**: 338-348.
- Xing, B., Pignatello, J. J. (1997). Dual-mode sorption of low-polarity compounds in glassy poly(vinyl chloride) and soil organic matter. Environ. Sci. Technol. **31** (3): 792–799.
- Xing, B., Pignatello, J. J. (1996). Time-dependent isotherm shape of organic compounds in soil organic matter: Implications for sorption mechanism. Environ. Toxicol. Chem. **15**: 1282–1288.
- Xu, J., J. Wu, et al. (2013) Interactions Between Silver Nanoparticles and Dissolved Natural Organic Matter Under Estuarine Conditions. Functions of Natural Organic Matter in Changing Environment, Springer Netherlands: 805-809.
- Yang, Y., J. E. Saiers, et al. (2013). "Impact of Interactions between Natural Organic Matter and Metal Oxides on the Desorption Kinetics of Uranium from Heterogeneous Colloidal Suspensions." Environmental Science & Technology **47**(6): 2661-2669.
- Yang, Y., J. Zhang, et al. (2002). "Toward the Chemistry of Carboxylic Single-Walled Carbon Nanotubes by Chemical Force Microscopy." The Journal of Physical Chemistry B **106**(16): 4139-4144
- Yao, K.-M., M. T. Habibian, et al. (1971). "Water and waste water filtration. Concepts and applications." Environmental Science & Technology **5**(11): 1105-1112.
- Yin, Y., Y. Xia, et al. (2001). Template-assisted self-assembly: A practical route to complex aggregates of monodispersed colloids with well-defined sizes, shapes, and structures. J. Am. Chem. Soc. **123** (36): 8718–8729.
- Young, T. J., M. A. Monclus, et al. (2011). "The use of the PeakForce™ quantitative nanomechanical mapping AFM-based method for high-resolution Young's modulus measurement of polymers." Measurement Science and Technology **22**(12): 125703.
- Yuan, Z., R. J. Puddephatt, et al. (1995) Chemical vapor deposition of silver. Chem. Mater. **7** (9): 1696–1702.
- Yu, S.-j., Y.-g. Yin, et al. (2012). "Silver nanoparticles in the environment." Environmental Science: Processes & Impacts **15**(1): 78-92.
- Yuan, B., M. Pham, et al. (2008). "Deposition Kinetics of Bacteriophage MS2 on a Silica Surface Coated with Natural Organic Matter in a Radial Stagnation Point Flow Cell." Environmental Science & Technology **42**(20): 7628-7633.
- Zhang, W., T. S. Steenhuis, et al. (2010). Colloid transport and retention in unsaturated porous media: Effect of colloid input concentration. Environ. Sci. Technol. **44** (13): 4965–4972.
- Zhang, W., Y. Chen, et al. (2011). Modeling the primary size effects of citrate-coated silver nanoparticles on their ion release kinetics. Environ. Sci. Technol. **45** (10): 4422–4428.
- Zhao, C.M., W. X. Wang, (2010) Biokinetic uptake and efflux of silver nanoparticles in *Daphnia magna*. Environ. Sci. Technol. **44** (19): 7699–7704.
- Zhao, Y. P., D. X. Ye, et al. (2002). "Novel Nano-Column and Nano-Flower Arrays by Glancing Angle Deposition." Nano Letters **2**(4): 351-354.
- Zhu, J., S. Liu, et al. (2000). "Shape-Controlled Synthesis of Silver Nanoparticles by Pulse Sonoelectrochemical Methods." Langmuir **16**(16): 6396-6399

Annex I

List of abbreviations

AFM	Atomic Force Microscopy
BET	Brunauer–Emmett–Teller
CFT	colloid filtration theory
CFM	Chemical force microscopy
DLVO	Derjaguin-Landau-Verwey-Overbeek
DLS	Dynamic light scattering
EDX	Energy dispersive X-ray scattering
ENP	Engineered nanoparticles
f_{whm}	full width at half maximum
HA	Humic acid
HPLC	High performance liquid chromatography
ICP-MS	Inductively coupled plasma mass spectrometry
K_L	Langmuir coefficient
K_F	Freundlich coefficient
n	Freundlich exponent
$n\text{Ag}$	Silver nanoparticle
$n\text{Ag-HA}$	Humic acid coated silver nanoparticle
$n\text{Ag-citrate}$	Citrate coated silver nanoparticle
NOM	Natural organic matter
PSD	Power spectral analysis
PFQNM	Peak force quantitative nanomechanical mapping

Q_{\max}	Absorption maximum
SEM	Scanning electron microscopy
TEM	Transmission electron microscopy
TOC	Total organic carbon

Curriculum Vitae

Contact

Name: Priya Mary Abraham

Address: Westbahn strasse 13, Landau- 76829, Germany.

Email: priya10mary@gmail.com

Telephone: 0049 6341 280 31579

Personal data

Date of birth: 19.01.1986

Place of birth: Kerala, India

Nationality: Indian

Marital Status: Married

Employment history

Date: May 2010 - present

Position: Scientific Staff

Employer: Universität Koblenz-Landau, Landau, Germany

Date: December 2008 - April 2010

Position: Project Assistant

Employer: National Chemical Laboratory, Pune, India

Education

Date: 2006 – 2008

Qualification: MSc. (Inorganic Chemistry)

University: School of Chemical Sciences, Mahatma Gandhi University, Kerala, India

Date: 2003 –2006

Qualification: BSc. (Chemistry)

University: Vimala College, Calicut University, Kerala, India

Publications

- “Interaction of silver nanoparticles with environmental and model surfaces.” P.M.Abraham, S. Barnikol, T. Baumann, M. Kuehn, N.Ivleva, G.E. Schaumann Environmental Science Technology 2013, 47 (10): 5083-5091.
- “Role of grain water repellency in transport and retention of negatively charged hydrophilic colloids in saturated sand matrices ” M. Göbel, S. K. Woche, P. M.Abraham, G. E. Schaumann, J.Bachmann Colloids and Surfaces A. 2013 431 150-160.
- “In Situ Synthesis and Surface Functionalization of Gold Nanoparticles with Curcumin and their Antioxidant Property: An Experimental and Density Functional Theory Investigation” D.K.Singh, R.Jagannathan, P.K. Khandelwal, P. M. Abraham, P. Poddar, Nanoscale. 2013. 5 1882-1893.
- “Modes of interaction between inorganic engineered nanoparticles and biological and abiotic surfaces ” G.E. Schaumann, P. M.Abraham, A. Dabrunz, Geophysical Research Abstracts. 2012, 14 EGU2012-1357.
- “Temperature-Dependent Spectroscopic Evidences of Curcumin in Aqueous Medium: A Mechanistic Study of Its Solubility and Stability” R.Jagannathan, P. M. Abraham, P. Poddar, The Journal of Physical Chemistry B. 2012. 116 (50): 14533-14540.
- “A robust, particle size independent, method for quantifying metal(loid oxide) nanoparticles and their agglomerates in complex environmental matrices by electrothermal vaporisation coupled to ICP-MS” Duester, L., Rakcheev, D., Bayer, J.V., P. M. Abraham, Dabrunz, A., Schulz, R., Schaumann, G.E. 2011. Journal of Analytical Atomic Spectrometry. 26 450-455.
- “Magnetic and dielectric properties and Raman Spectroscopy of GdCrO₃ nanoparticles ”, A. Jaiswal, R. Das, K. Vivekanand, T. Maity, P. M. Abraham, S. Adyanthaya, P. Poddar Journal of Applied Physics 2010, 107, 013912-013912-7
- “Effect of Reduced Particle Size on the Magnetic Properties of Chemically Synthesized BiFeO₃ Nanocrystals”, A.Jaiswal, R. Das, K. Vivekanand, P.M. Abraham, S. Adyanthaya, and P. Poddar J. Phys. Chem. C, 2010, 114 (5), 2108–2115

Poster presentations

- P.M. Abraham, T. Baumann, G.E. Schaumann. Sorption of untreated and humic acid treated silver nanoparticles to environmental and model surfaces. Internano workshop, March 2014 in Landau, germany
- P.M. Abraham, S. Barnikol, A. Grün, G.E. Schaumann. Effect of Silver nanoparticles on surface properties of bacterial biofilm - An AFM study. 3rd Biohydrology conference on water for life, may 2013 in Landau, germany
- P.M. Abraham, G.E. Schaumann. Interaction of bare and humic acid coated silver nanoparticles to environmental and model surfaces. European Geosciences Union General Assembly, April 2012 in Vienna, Austria

-
- P. M. Abraham, G. E. Schaumann. Sorption of engineered silver nanoparticles to environmental and model surfaces. Goldschmidt conference, August 2011 in Prague, Czech Republic.
 - P. M. Abraham, G. E. Schaumann. Sorption of engineered silver nanoparticles to environmental and model surfaces. 16 th Annual meeting of Society of Environmental Toxicology and Chemistry (SETAC), September 2011 in Landau, germany.
 - P. M. Abraham, L. Duester, J.V. Vogel, G. E. Schaumann. Interaction of engineered nanoparticles with environmental surfaces. WG4 Norman working group meeting on Engineered nanomaterials in the Environment, 2010 in Koblenz, germany.

Oral presentations

- P. M. Abraham, R. Jagannathan, P. Poddar. In-situ synthesis of gold nanoparticles using antibiotics. National Conference on Nanoscience and Nanotechnology (NCNN). January 2010 in Nagpur, India